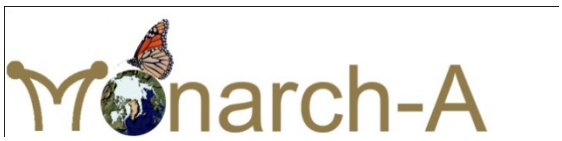

Seventh Framework Programme
Theme 9 Space FP7-SPA.2009.1.1.02
Monitoring of climate change issues (extending core service activities)

Grant agreement for: Collaborative Project (generic).
Project acronym: **MONARCH-A**
Project title: **MONitoring and Assessing Regional Climate change in High latitudes and the Arctic**
Grant agreement no. 242446
Start date of project: 01.03.10
Duration: 39 months
Project coordinator: Nansen Environmental and Remote Sensing Center, Bergen, Norway

D4.1 - Synthesis Report of the state and variability of changes in high latitudes and Arctic Region

Due date of deliverable: 31.05.2013

Actual submission date: 08.07.2013

Organization name of lead contractor for this deliverable: NERSC

Authors (order per partner):
J.A. Johannessen, K.Lygre, J. E. Nielsen, R. Raj, K. Khvorostovsky (NERSC)
S. Quegan, E Kanzas, M. Lomas (USFD)
D. Stammer, N. Koldunov (UHAM)
A. Cazenave, O. Henry, A. Kouraev, A-L Dhomps, N. Mognard (CNRS)
L. Bobylev, D Pozdnyakov, E Shalina, E.A. Zakharova (NIERSC)
O.B. Andersen, V. Barletta, R. Forsberg, P. Knudsen, H. Skourup, L. S. Sørensen, Y. Cheng (TUD)
C. Heinze, N. Goris, T. Johannessen, S.K. Lauvset (UiB)
B Chapron, F. Ardhuin, E. Maximova (Ifremer)

Project co-funded by the European Commission within the Seventh Framework Programme, Theme 6 Environment		
Dissemination Level		
PU	Public	X
PP	Restricted to other programme participants (including the Commission)	
RE	Restricted to a group specified by the consortium (including the Commission)	
CO	Confidential, only for members of the consortium (including the Commission)	

ISSUE	DATE	CHANGE RECORDS	AUTHOR
1	31/05/2013	Report 1st version	K. Lygre
2	08/07/2013	Report 2nd version	J.A. Johannessen

Table of Contents

1 Introduction

The MONARCH-A project is based on a cross-cutting activity in which an Earth System approach is adopted in order to quantify combined and interrelated changes in terrestrial carbon and water fluxes (Theme I), sea level and ocean circulation (Theme II) and the marine carbon cycle (Theme III) in the high latitude and Arctic regions. The ultimate goal is to generate a dedicated information package tailored to a subset of multidisciplinary Essential Climate Variables (ECVs) and their mutual forcing and feedback mechanisms associated with changes within both the terrestrial and oceanic domains In particular the generation of refined and consistent multidisciplinary time series of:

- river discharge, snow cover, ice sheet mass balance and permafrost;
- sea ice drift and sea ice volume, sea level, current, ocean color and CO2 partial pressure;
- near surface wind field

integrated and extended with tailored information on land cover, fire, sea ice extent and concentration they will provide tailored information and products to assist climate change research to incorporate the refined and consistent ECVs.

The synthesis (Theme IV) includes combining selected time series of ECVs generated in the project together with other existing time series, checked and assessed for consistency. In so doing, variability and trends in these ECVs together with 3D fields from reanalyses will be synthesized to establish a more comprehensive quantitative understanding of the climate changes in the high latitude and Arctic region over the last 50-60 years. In particular, this includes:

- New and more accurate characterization of the state and variability of river discharge, snow cover and snow water equivalent, permafrost extent and seasonal variability of frozen ground; sea level and Greenland ice sheet mass loss, ocean currents and sea ice drift as well as ocean mass and heat transport, CO2 partial pressure, and near surface wind field.
- New and better quantification of mutual forcing and feedback mechanisms of the high latitude and Arctic climate system, including natural and anthropogenic contributions;
- New knowledge and support to the attribution of the causes of high latitude and Arctic climate change;
- New knowledge and support to interannual-to-decadal prediction of high latitude climate change, in particular through generation of more accurate initial conditions;
- New knowledge and support to advanced understanding of the two-way connections between global and regional climate change.

The integrated science and technology achievements from the three main research themes together with the results of the synthesis and interaction with the scientific climate change community have contributed to advancing the knowledge base that, in turn, can feed into an overall assessment of priorities, design and implementation of a high latitude and Arctic monitoring system for climate change. This is reported in this synthesis reports and is essential for future advances in operational decadal scale prediction and services targeted the high latitude and Arctic regions.

2 Theme I: Changes in terrestrial carbon and water fluxes

The overarching aims of Theme I are:

a) To provide a coherent and consistent view of changes that have occurred in the carbon and water cycles of the Arctic over the last two decades, by amalgamating measurements of ECVs and other relevant variables that describe changes in key high latitude land processes;

b) To assess how these changes relate to climate change, both as indicators and drivers;

c) To devise improved methods to interface models with new datasets developed in MONARCH-A and already existing data, in order to improve climate predictions.

The land components dealt with are hydrological processes, the soil-vegetation–atmosphere complex and the cryosphere, as represented by the dynamics of snow and permafrost. These components interact strongly at high latitudes and hence datasets gathered to investigate the behaviour of each of them affects the others. Quantitative understanding of these interactions has been addressed using several state-of-the-art land surface models that estimate the stores and fluxes of carbon and water. However, several of the ECVs investigated are also important for land-atmosphere transfers of energy and momentum, and there is an important land-ocean interaction through fresh water discharge into the Arctic Ocean from river run-off.

The ECVs considered are:

(i) ***Snow cover:*** Decadal change in snow properties as snow cover extent and period (start and end dates), snow depth and snow water equivalent provide indicators of climate change, but also have strong effects on water availability for plant growth, vegetation growing periods, albedo and flow of fresh water into the Arctic Ocean.

(ii) ***Runoff*** *and high latitude water bodies:* The decadal dynamics of huge numbers of lakes forming in the summer season at high latitudes are important for greenhouse gas exchange, evapo-transpiration, runoff and groundwater.

(iii) ***Permafrost:*** Permafrost location and depth are strong indicators of climate change and have important consequences for greenhouse gas emissions (both methane and carbon dioxide), water availability in the root zone (hence affecting land cover) and energy transfer between the land and atmosphere.

(iv) ***Land cover*** *and fire regimes*: land cover is a crucial determinant of land-atmosphere fluxes and affects momentum transfer because of its strong effects on surface roughness, while changes in fire regimes are both indicators of climate change and likely to be strongly affected by climate change, with consequences for carbon emissions and sequestration.

2.1 The modelling framework

A key aim of the Theme was to investigate the interactions between ECVs by amalgamating the observations in a modelling framework. Single land surface models are inappropriate for this synthesis, as each has its own process representations and parameterisations, making it hard to draw robust conclusions. As a result, we exploited several state-of-the-art Dynamic Vegetation Models (DVMs), most of which are embedded in IPCC-class climate and Earth system models (ESMs):

- the Lund-Potsdam-Jena (LPJ) model, used in the Bergen Climate Model (BCM);
- CLM4, used in the Norwegian Earth System Model (NorESM);
- JULES, used in the Hadley Centre climate model;
- ORCHIDEE, which is the land surface model in the Institut Pierre Simon Laplace ESM;
- the Sheffield Dynamic Global Vegetation Model (SDGVM), which is a stand-alone DVM.

These models are used here in uncoupled mode, in which climate is an input driving set of variables. From climate and data on soil texture, the models calculate carbon and water stocks and fluxes using parameterised process representations that do not depend on any external data sources. This is because they are meant to be *predictive*, hence require only climate projections in their calculations.

This formulation of the models means that ECV and other data can only affect their calculations in the four ways, all of which are investigated in this project. These are illustrated in Figure 1, where the DVM is shown converting the current state, S_n, into the state at the next time-step, S_{n+1}:

1. Data can be used to modify the *current state*, e.g. several DVMs allow the land cover to be constrained, normally using information derived from satellite data;
2. Internal *parameters* may be derived or optimised from observations, e.g. the degree-day algorithm for the date of bud-burst in boreal forests (Picard et al. 2005);
3. *Processes*, such as fire activity, may be observed from space and used to modify model functioning;
4. The predictions of the models can be *tested*, offering the possibility of assimilating the data into the models by a feedback loop.

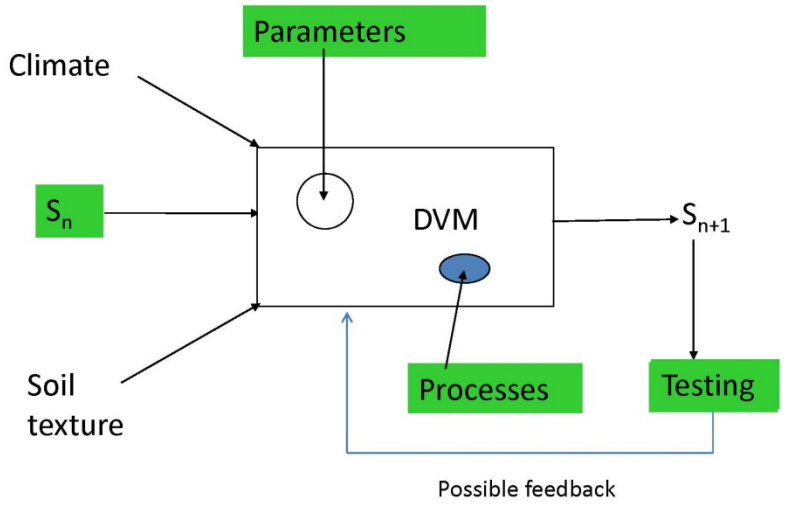

Figure 1 *Schematic illustrating the possible interactions between data and a DVM.*

The models play a central role in synthesising the ECV data since they make explicit connections between different quantities. For example, land cover, fire and climate interact in generating the net land surface carbon balance; the dynamics of permafrost are found to be intimately connected to land cover and the properties of fire; and snow dynamics, precipitation, permafrost, land cover and climate are all involved in surface run-off. At an even higher level, the models explicitly connect the water and carbon cycles through their representations of carbon and water exchanges by vegetation canopies and soils.

2.2 Decadal changes in snow properties

2.2.1 Snow cover extent

The snow extent over the period 1987-2009 was calculated using the Adaptive Threshold Algorithm for Snow detection (ATAS) for four sub-regions: North America, Europe (up to 60° E), Western/Central Siberia (60° to 120° E) and Eastern Siberia (East of 120°E) and for the whole Northern Hemisphere in the latitudinal band 28°- 80°N.

The general decrease in snow duration in the Northern Hemisphere (see Section 2.2.2) is accompanied by a statistically significant (p-value < 0.05) decrease in snow extent in spring (March-May) in Europe (1.3% yr^{-1}), Western-Central Siberia (1-2.5% yr^{-1}) and Eastern Siberia (0.2-1.7% yr^{-1}): see Figure 2. In North America, although a decreasing trend is observed for April and May, this is not significant because of its low value in April (< 0.5% yr^{-1}) and high inter-annual variability in May. Taken as a whole, the spring trends in the Northern Hemisphere are statistically significant and are -0.04% yr^{-1}, -0.4% yr^{-1} and -0.13% yr^{-1} respectively for March, April and May (Figure 2b).

Similar overall behaviour is seen in autumn. For the whole Northern Hemisphere a decline in snow extent of around -2% yr^{-1} is observed for September (Figure 3). There is a small but statistically significant increasing trend in October, but November again shows a decrease. The region suffering the largest changes is Western/Central Siberia (-3% yr^{-1} in September). In Europe the average September snow covered area increases by 2% yr^{-1}, but due to the high variability and relatively short period of observation (21 years) this trend is not statistically significant. For all sub-regions, the trends in the winter months are very small and statistically insignificant.

As expected, the inter-annual variability of snow extent is highest at the beginning (September) and end (May) of the snow season. In Europe and Northern America it reaches ±50%. In these two regions, the intermediate season with unstable snow cover extends up to October and back to April. Surprisingly, high inter-annual variability of snow extent (±70%) is observed in September in Eastern Siberia, where the snow cover is very stable during other months. In Europe, the winter inter-annual variability of snow covered area is around ±20%, but is smaller in all other sub-regions, varying from ±5% in Eastern Siberia to ±10% in North America.

It is worth noting that in all sub-regions the maximal extent of snow cover does not decline over time, and even rises slowly at the Northern Hemisphere scale at the 15% confidence level (Figure 4).

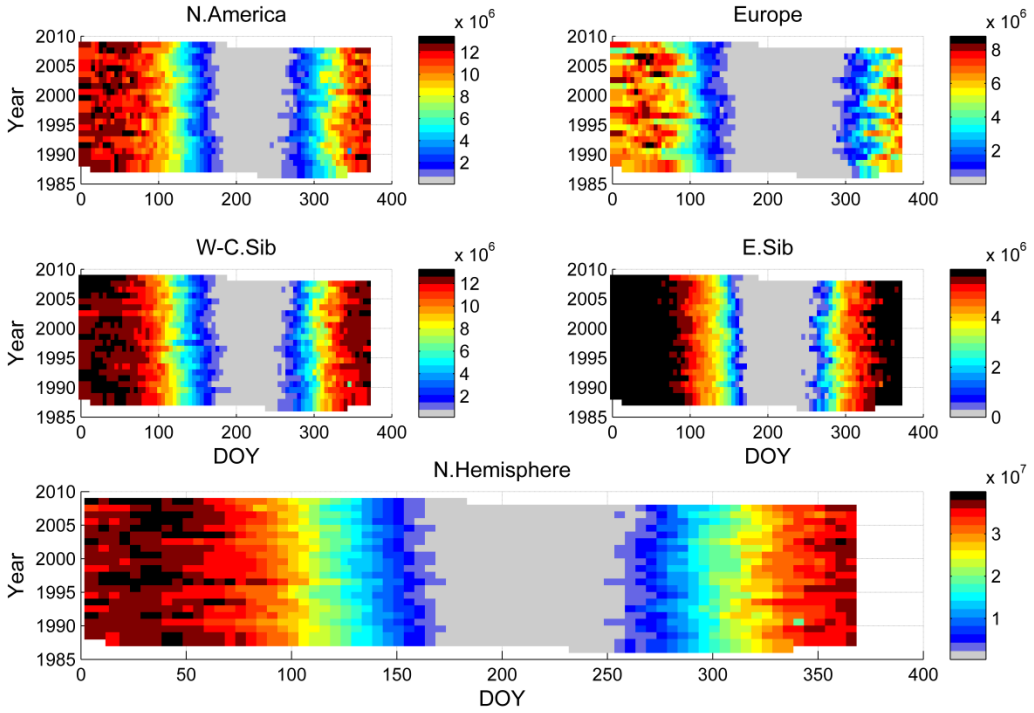

Figure 2 *Snow covered area (km^2) as a function of day of the year over the period 1987-2009 for N. America, Europe, West & Central Siberia and Eastern Siberia, and the whole Northern Hemisphere.*

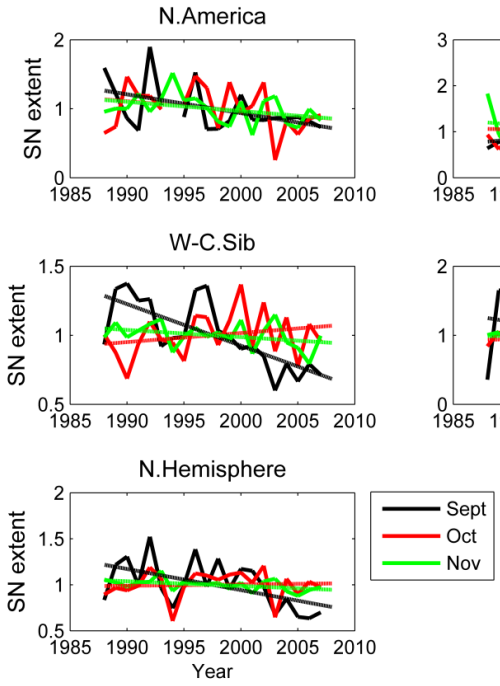

(a)

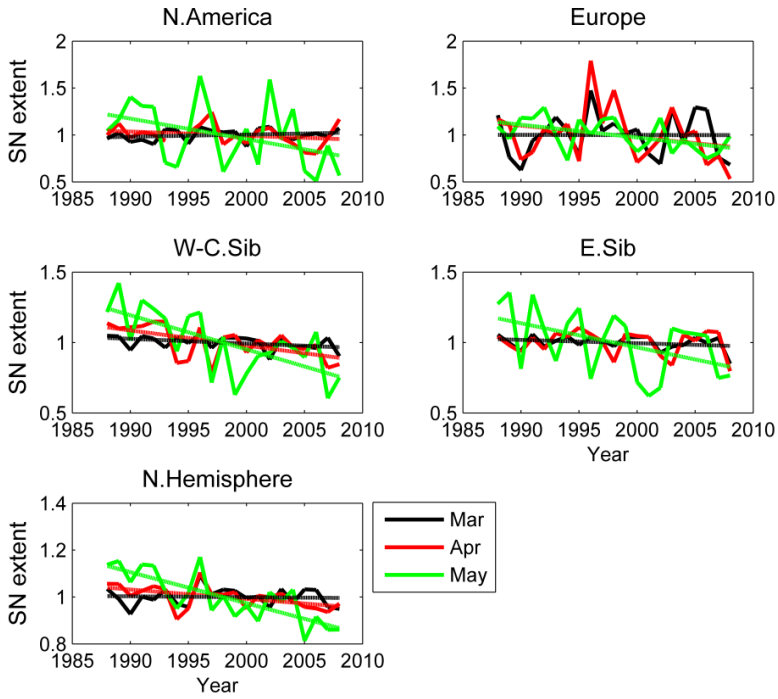

(b)

Figure 3. *Normalised snow extent in (a) autumn and (b) spring for the four sub-regions and the whole Northern Hemisphere.*

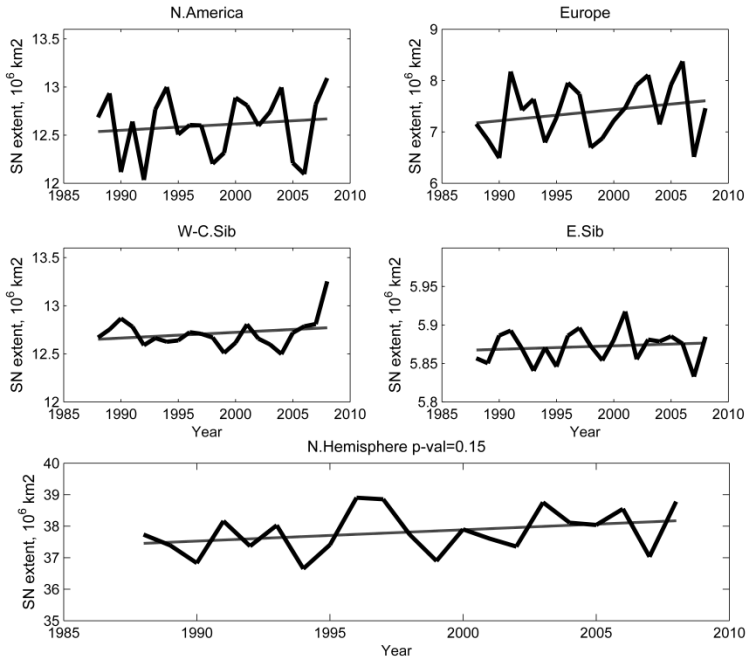

Figure 4 *Maximal snow extent, in units of 10^6 km^2, over the period 1987-2009 for the four sub-regions and the whole Northern Hemisphere.*

2.2.2 Trends in snow start and end dates, snow duration and days with snow cover

The dates of snow appearance and disappearance over the period 1987 to 2008 were calculated from SSM/I data with a new Adaptive Threshold Algorithm. This was shown to be much superior to the Chang et al. (1987) algorithm, giving very good agreement with historical data both in terms of absolute values (little or no bias) and spatial homogeneity. For each EASE-Grid pixel, linear trends in these two dates and also in continuous snow duration (difference between these dates) and the number of days with snow (taking account of discontinuous snow events, such as snowfall followed by subsequent melting before the formation of stable snow cover, etc.) were estimated; only trends that are statistically significant (p-value < 0.05) are reported.

No consistent overall trend is apparent in the date of appearance of stable snow cover (Figure 5; the units are pentads/yr, i.e., a trend of 1 pentad/yr indicates a change of 5 days over the year). Later dates (warming) are observed in North America for Northern Quebec, Victoria Island & Northern Alaska, and in Eurasia for the Volga and Severnaya Dvina basins, the Middle Ob' region, the Altai mountains, the southern parts of the Yenisey and Lena river watersheds and Chukotka. Cooling trends (earlier dates) are apparent for regions south of the Great Lakes, the Rockies and the Northern part of the Northwest Territories in North America, and north of Lake Baikal, the Verkhoyanskiy ridge (east of the Lena river) and in North-Eastern China in Eurasia.

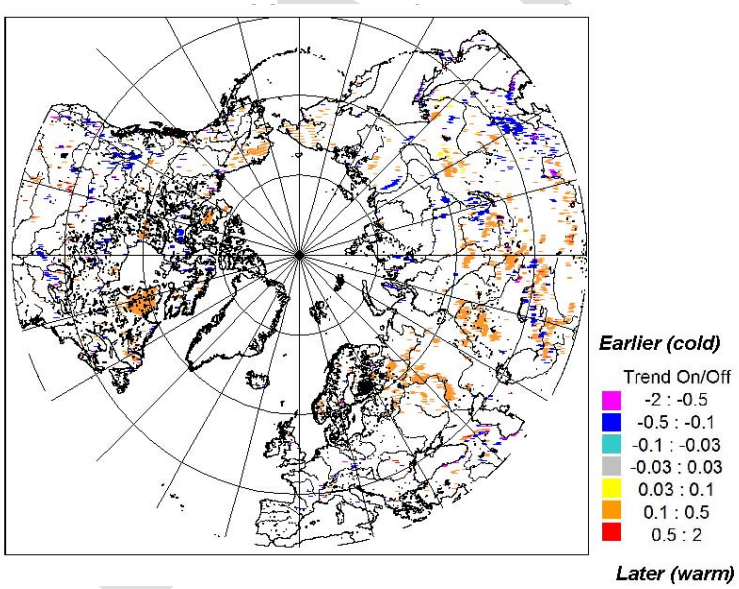

Figure 5. *Trends in date of appearance of stable snow (in pentads/yr) over the period 1987-2008.*

Regions exhibiting statistically significant trends in the date of snow disappearance are much more widespread (Figure 6), and mainly indicate warming trends (earlier snow disappearance). Among the most prominent in North America are Northern Quebec, a region north of the Great Lakes, and a large part of Eastern Canada and the USA, while in Europe and Eurasia warming is observed in the Pyrenees, the Alps, Norway, the Upper Volga region, the Putorana mountains, a large band around 50°N extending from Kazakhstan to the Khingan mountain east of the Lake Baikal, and the Chukotka and Kamchatka regions. Some isolated regions with cooling trends are observed in central and south-eastern North America, south of St Petersburg and around the Novosibirsk and Krasnoyarsk reservoirs.

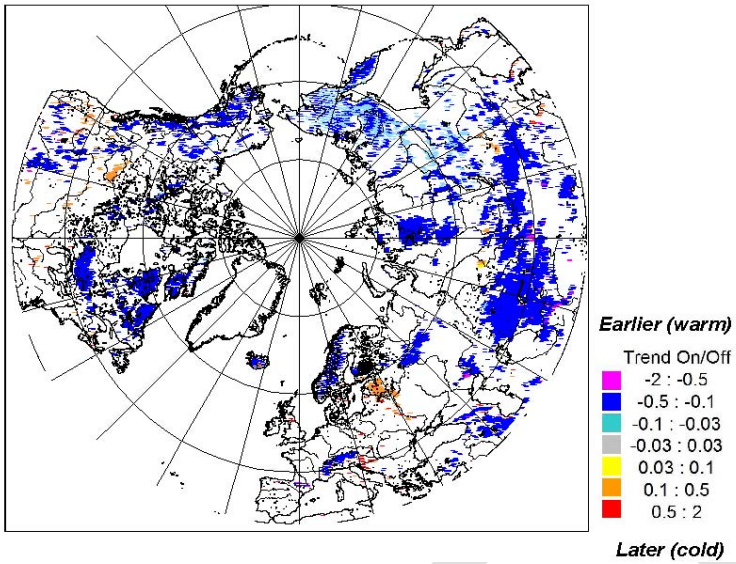

Figure 6. *Trends in date of disappearance of snow (in pentads/yr) over the period 1987-2008.*

Trends in snow duration and the number of days with snow are very similar (

Figure **7** & Figure 8). Warming trends (reduction of snow duration and fewer days with snow) occur in parts of Northern Quebec, the Northwest Territories and Alaska in North America, and in a broad band extending from Norway to the Severnaya Dvina and Volga watersheds, and then to Kazakhstan and mountain ranges south of Kazakhstan. Cooling trends are seen in the central parts of Canada, north-east of Lake Baikal, Mongolia and North-Eastern China.

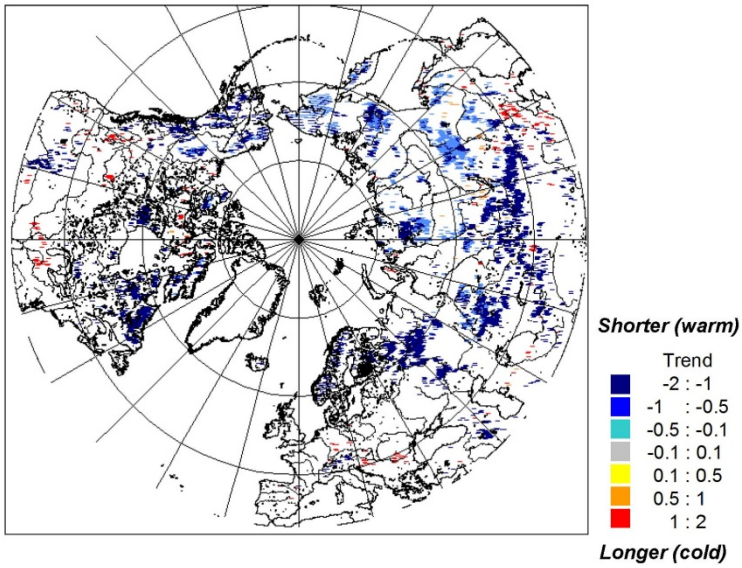

Figure 7. *Trends in snow duration (d/yr) over the period 1987-2008.*

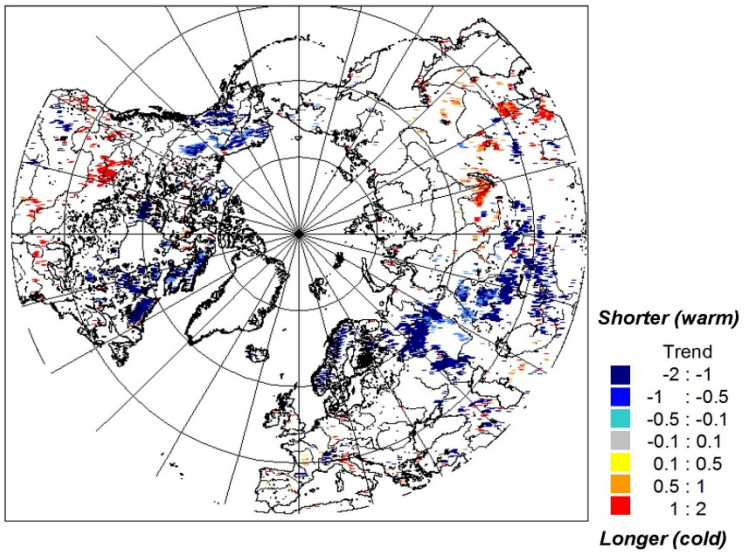

Figure 8. *Trends in days with snow (d/yr) over the period 1987-2008.*

2.2.3 Snow water equivalent (SWE)

In order to evaluate temporal trends in SWE, for each 1° grid-cell we extracted the maximum value of monthly SWE in each year from 1980 to 2010 from the GlobSnow dataset; this is denoted Smax(lat,lon,t), with 90°N ≤ lat ≤ 40°N, -180°W ≤ lon ≤ 180°E and 1980 ≤ t ≤ 2010. Other descriptors, such as aggregated monthly SWE over the year, provided similar results.

The linear trend in the evolution of Smax at each grid-cell, normalised by the average value of Smax during the whole period, is shown in the top row of Figure 9. Those grid-cells with statistically significant change (i.e. 95% CI that the slope of the regression is positive or negative) are marked in the middle row. Relatively small but statistically significant decreases occur around Hudson Bay and in the Ob and Lena Basins, and larger decreases are seen in the Altai Mountains in Mongolia, central Europe and the Baltic. Regions where Smax increases include the central plains of Siberia and the Bering Sea coastal region. However, the aggregated annual values of Smax over all northern Latitudes, Eurasia and N. America shown in the three plots in the bottom row exhibit no statistically significant changes, which is in agreement with [*Takala et al.*, 2011]).

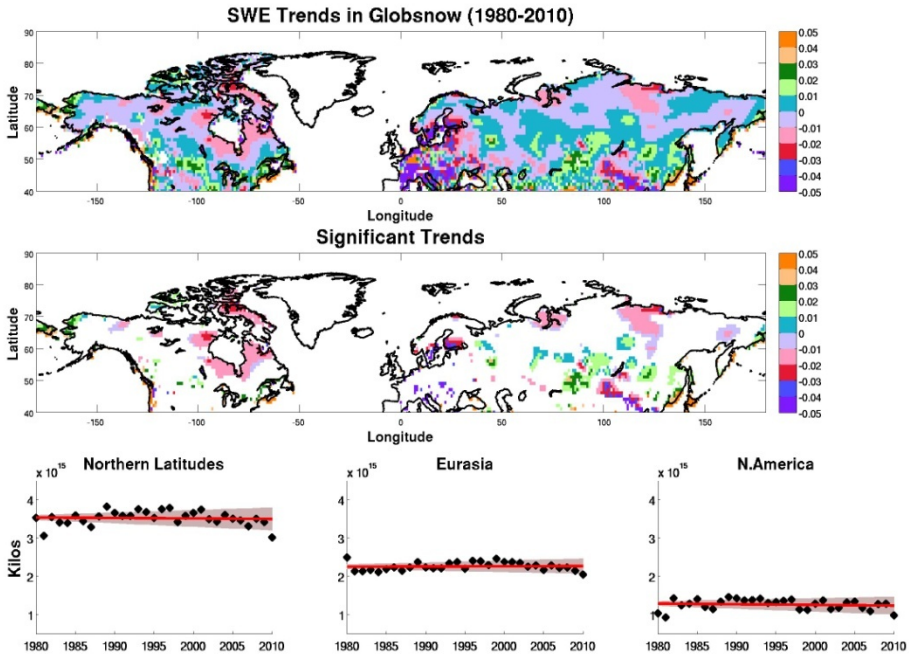

Figure 9. *Trends in GlobSnow Smax for 1980-2010. Top: slope of the regression coefficient normalised by the average value of Smax. Middle: grid-cells with significant trends. Bottom: aggregated values of Smax for all northern Latitudes, Eurasia and N. America.*

Figure 10 and Figure 11 have the same format but with the temporal range divided into two periods, 1980-1999 and 2000-2010 respectively; the colour scale has also doubled to accommodate larger changes than occur in Figure 9. For the earlier period, Smax has a statistically significant increase at northern latitudes driven mainly by the central regions of Eurasia and N. America. For the later period, Smax exhibits a significant decrease, mainly driven by the regions in Central Eurasia that showed an increase during 1980-1999. Western Europe follows the opposite behaviour, with a large decrease in Smax during 1980-1999 which is compensated by an increase of equal magnitude during 2000-2010.

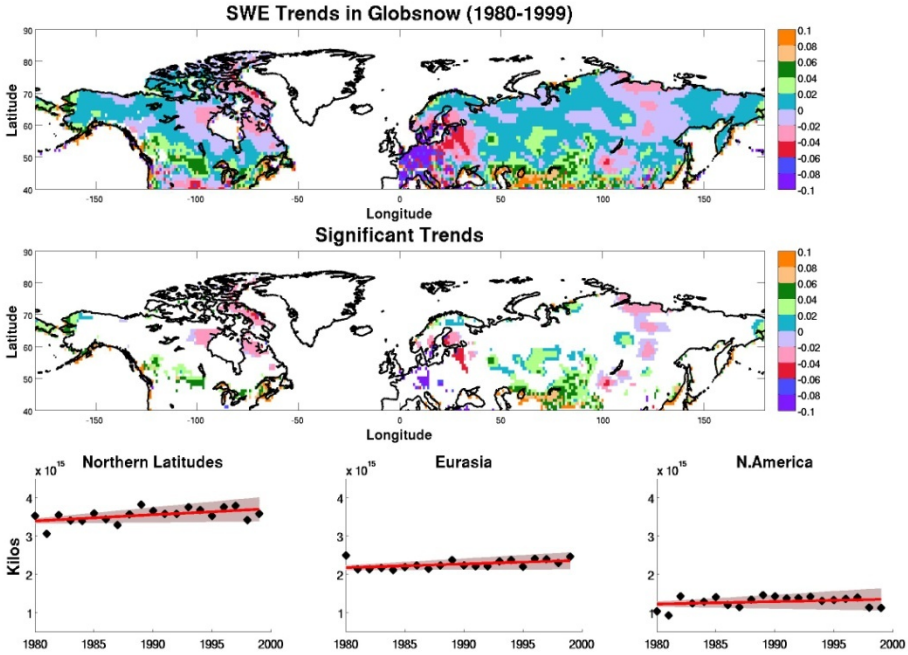

Figure 10. *As Figure 9, but for 1980-1999.*

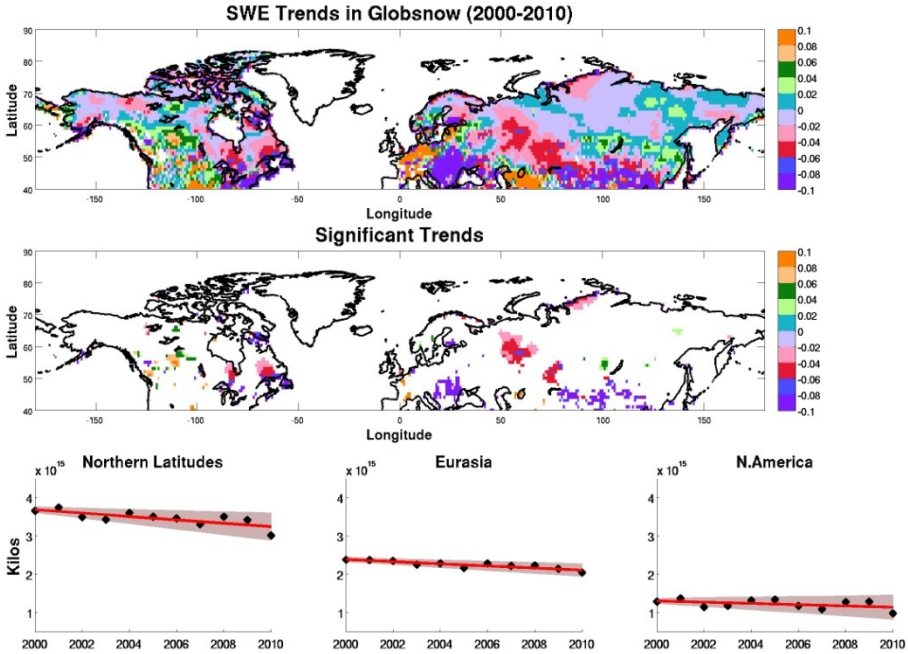

Figure 11. *As Figure 10, but for 2000-2010.*

2.3 Decadal dynamics of high latitude water bodies

2.3.1 Wet zones changes 1988-2008

A specific feature of the arctic regions is extensively developed wet zones occurring as lakes, bogs and floodplain fens. These wet zones substantially alter the vertical water and heat exchange in the atmospheric boundary layer, as well as transforming the runoff regime. Like arid zones, their water balance and water storage is expected to vary with climate change. One of the indicators of this variation is the change in surface extent of the wet zones. For deep boreal lakes located outside the zone of modern permafrost the variability in water surface is not important, but for shallow arctic lakes on permafrost-affected ground, variation in surface extent can indicate not only the wetness conditions of a given year, but also mark permafrost erosion (thermokarst processes). The spatial extent of bogs and fens is more stable, and would respond only to major long-term changes in water regime and vegetation. However, the water abundance within the existing bogs and fens is a good signature of current climatic conditions. The volume and extent of the wet zones in arctic regions have seasonal variations. In spring they fill up from snowmelt and then release this water during the summer. The wet zone extent usually has a minimum in July and, by choosing this period, it is possible to trace its inter-annual variability and detect morphological changes in land properties.

We have used two remote sensing products. For global analysis we use wet zone surface (WZS, in km^2) from the passive microwave observations from the SSM/I (Special Sensor Microwave/Imager) for 1987-2008. For regional validation of WZS, we use the wet zone fraction (FWZ, in %) from the altimetric missions TOPEX/Poseidon (1992-2002) and ENVISAT (2002-2012). This product was calibrated on historical data of fraction of lakes and bogs in 20 middle-sized watersheds in the Western Siberia plain.

Both products agree in FWZ estimates in lake-dominated basins, but diverge in rising bog, flat bog and fen-dominated landscapes where the SSM/I product underestimates the fraction of wet zones, particularly in highly forested basins. In sparse forest and tundra basins the inter-annual variability of the FWZ of both products is similar. Hence the SSM/I WZS dataset is satisfactory for global analysis in most northern territories (forest-tundra and tundra zones) as well as lake regions (Canada, Scandinavia, Northern Siberia).

Figure 12 presents a global map of trends in fraction of wet surface obtained from SSM/I. It shows a strong rise of WZS along the South-West coast of Hudson Bay and in central Western Siberia. The North-West Canadian Territories and Quebec, and the north part of Central Siberia have a negative trend.

A

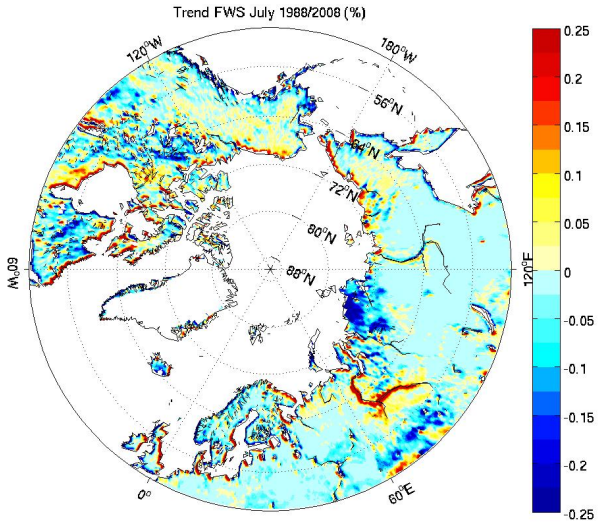

B

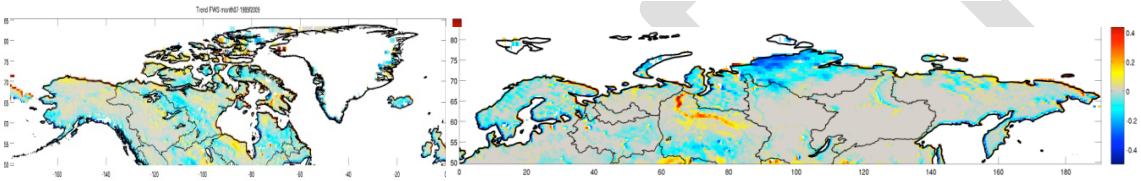

Figure 12. *Global trends in July fraction of wet zone surface from SSM/I sensor for 1988-2008. A: all trends, B: significant trends.*

A

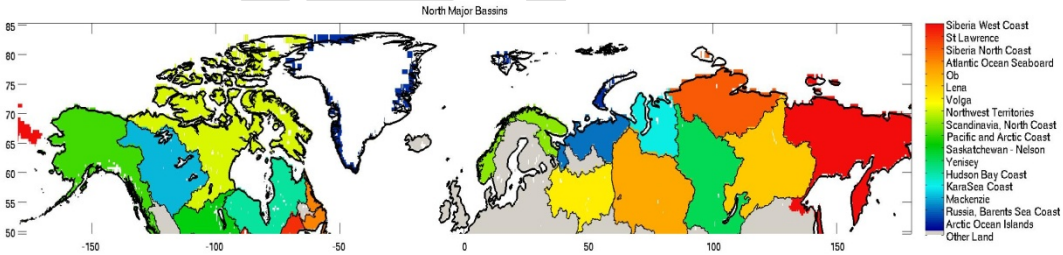

B

Figure 13 *Map of major drainage basins (A) and FWZ time series for basins with significant trends (B)*

In most part of the Arctic the trends in FWZ are insignificant. Of the large American and Eurasian drainage basins, only the Yenisey, North Siberian Coast and Pacific and Arctic Coasts have significant negative FWZ trends (Figure 13b). In some watersheds, like the Ob', different parts can exhibit opposite trends (Figure 12b). As a result, the average Ob' basin FWZ trend is insignificant. Also it should be noted that in the southern part of the Arctic basins the SSM/I signal is strongly affected by dense forest vegetation and the product indicates mostly the variations in lake surface fraction, while bogs and fens are not well sensed.

2.3.2 Decadal changes in runoff

Climate drivers. At northern latitudes, runoff is largely determined by precipitation and to a lesser extent by temperature, which impacts runoff through evapotranspiration. For long time-scales, the effect of changing CO_2 should also be considered. Increase in CO_2 results in higher water use efficiency with regard to carbon production, which produces increases in carbon productivity and potentially decreases in transpiration leading to increased runoff.

For latitudes above 50°N the CRU data set shows:

(a) an increase of 1.5°C in average temperature over the period 1900-2005 (Figure 14). This alone would lead to increased evapotranspiration and thus reduced runoff. A similar temperature increase is observed for North America and Asia.

(b) A gradual increase in precipitation of ~10% over the same period (Figure 15). A reduction occurs in North America during 1900-1920 but Eurasia is consistent with the global Northern trend.

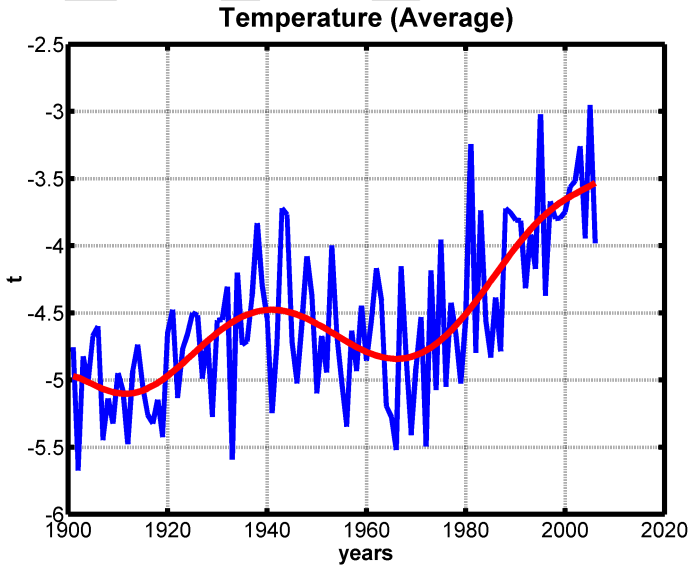

Figure 14. *Mean annual temperature from 1900-2005 for latitudes above 50° N from the CRU dataset*

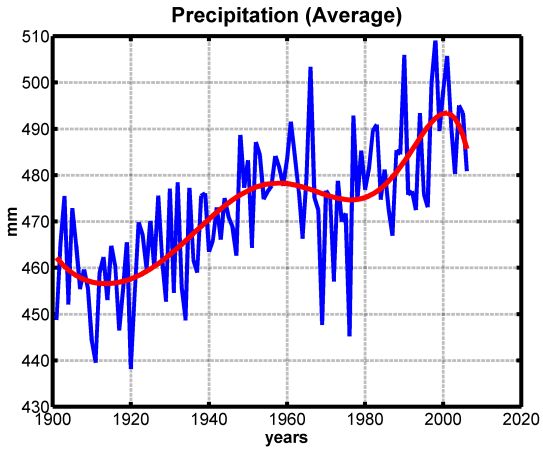

Figure 15. *Mean annual precipitation from 1900-2005 for latitudes above 50° N from the CRU dataset. Note that the y-axis is not scaled to zero.*

Observed runoff. Runoff data from GRDC and Arctic Rims are in very good agreement. There is evidence of increasing runoff over the latter half of the twentieth century, particularly in the Ob, Yenisey, Volga and Mackenzie basins (Figure 16).

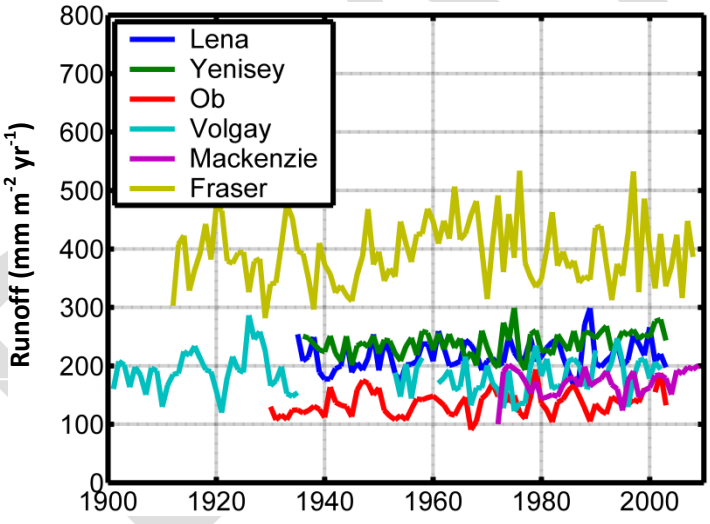

Figure 16. *Observed runoff from GRDC data over the period 1900-2006 for several large high latitude basins.*

2.4 Decadal changes in permafrost location and depth

2.4.1 Active Layer Depth

Permafrost, or permanently frozen ground, is soil, sediment or rock that remains at or below 0°C for at least two years. Frozen ground data are critical to understanding environmental change and ground water system transformation, validating models, and building and maintaining structures in permafrost regions. Permafrost is covered by an active layer that freezes and thaws on an annual basis. Climatic warming could lead to an increase in the thickness of the active layer. This, in turn, can cause damage to roads, structures and utility lines. Thaw subsidence can also alter local hydrological

patterns and lead to profound ecological changes. An additional consequence of increased active layer thickness is that carbon sequestered in the uppermost permafrost reservoir can be released to the atmosphere in the form of greenhouse gases.

We evaluated trends in active layer depth and permafrost temperature using data from the Circumpolar Active Layer Monitoring (CALM) and Thermal State of Permafrost (TSP) projects. Only sites where at least a decade of continuous data are available are considered. Unfortunately, records and data for many permafrost regions are incomplete or of short duration, with the exception of a few dozen sites with relatively long-term permafrost monitoring and some sites with really long-term data records. Additionally, the spatial distribution of the measurement sites is irregular, making it impossible to give any substantiated conclusion about changes in the distribution of permafrost parameters. During the International Polar Year 2007-2008, the permafrost monitoring network in the Polar Regions was enhanced and new information on permafrost thermal state is now available for some undersampled territories. Although data from these new sites cannot be used to evaluate trends in the permafrost over recent decades, they form a basis for deeper understanding of future permafrost changes.

The permafrost temperature is observed to be increasing at most sites where we have long records, but there are only a few such sites, so we instead focus on active layer depth (ALD), the permafrost parameter with the best available spatial distribution and temporal duration of data. The sites where ALD observations were made are shown in Figure 17, with sites showing an increase in ALD over the last (more than 10) years marked as red, those showing a decrease in blue, and those with insufficient data to make any conclusion about the trend shown in grey.

Active layer depth has tended to increase in the Russian sub-arctic zone, Mongolia and China over the last decade(s). The strongest trends have been observed in the Russian European North and Chukotka. Different parts of Alaska and Canada exhibit different trends. Increases in ALD are observed at sites in the interior, but both increasing and decreasing trends have been detected in areas close to the ocean.

Drawing general conclusions from these data is hampered by the sparse, non-uniform spatial sampling of the observations and the fact that ALD has substantial spatial variability, since it depends on soil composition and very different values of ALD can be measured at points several kilometers apart. The trends in ALD observed at these sites can also be different.

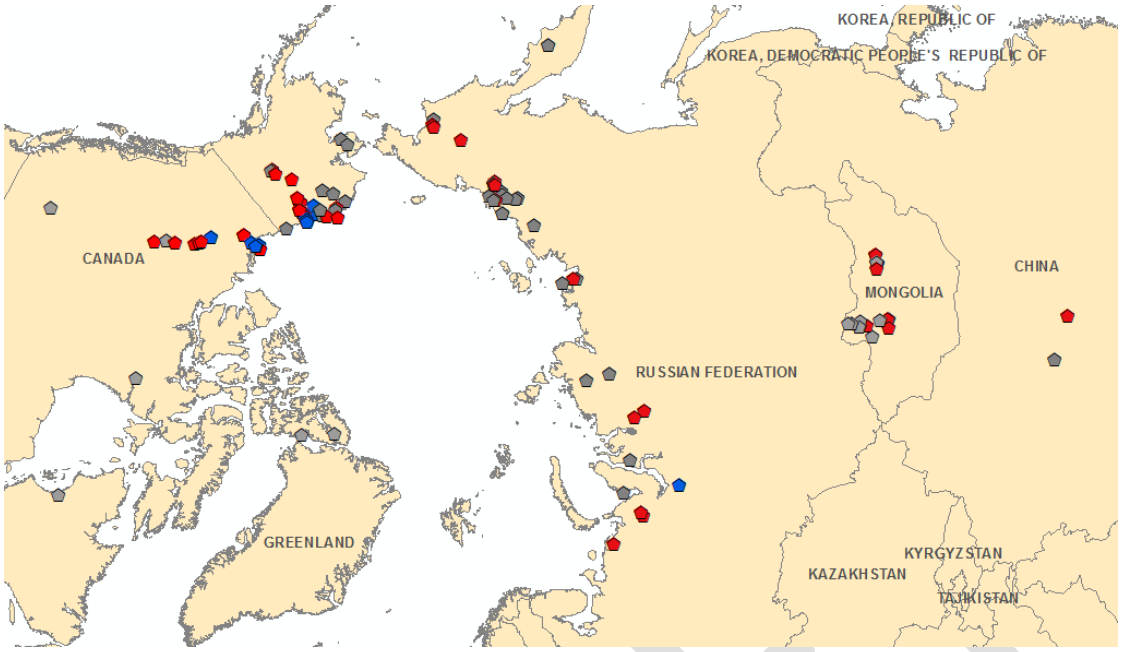

Figure 17 *Sites with active layer depth (ALD) measurements. Sites where ALD trends are positive are shown in red, sites with negative trends are shown in blue, and sites where there is insufficient data to calculate trends are shown in grey.*

2.5 Fire regimes

2.5.1 Burned area

Global circulation models driven by emissions scenarios show an increase in fire activity in boreal forests [*Stocks et al.*, 1998] caused by the predicted increase in air temperature embedded in the climate drivers of these models. However, analysis of the last 15 years of active fire data [*Arino et al.*, 2012] as well as burned area products, such as the Global Fire Emission Database [*Giglio et al.*, 2010], shows no statistically significant increase over the Northern latitudes. Inventory studies of the Canadian forests over a longer period, 1960s to 1990s, also failed to reach a conclusive result [*Krezek-Hanes et al.*, 2011]. It should be noted that the periods examined are substantially smaller than the Fire Return Interval at boreal latitudes, which usually exceeds 100 years [*Kasischke et al.*, 1995], so at present these methodologies do not allow a safe conclusion regarding trends in fire activity at Northern Latitudes.

3 Theme II: Changes in sea level and ocean circulation.

The overall goal within Theme II is to improve our understanding of the role the high latitude and Arctic plays in water mass formation, in contributing to the global circulation and in changing sea level on regional and global scale. More specific objectives include:

1) Improve climate-quality data base for the Arctic Ocean
2) Provide a reanalysis of the Arctic Ocean over the last 50 years, connecting especially also the IPY era to long-term Arctic variability.
3) Jointly through the above two points improve ECVs (sea ice drift and sea ice volume, ocean currents, and sea level) for the high-latitude Atlantic and the Arctic Ocean.

In the following, we will describe in detail several improved data sets obtained in the framework of Theme II and provide a systematic view of the main changes in the Arctic Ocean during the beginning of the 21st century.

3.1 Improving the climate-quality historical data base

One of the sub-objectives was to reprocess historical data, and by combining them with newly available observations provide longer, quality controlled record of ECVs for the Arctic Ocean. Data sets of several parameters observed in and around the Arctic have been reprocessed and improved, including:

i) tide gauge data

ii) altimetric sea surface height observtions

iii) sea ice motion

iv) land ice

v) wind

Important results that emerged in this respect are:

- Reprocessed sea level records from the coastal tide gauges (1950-2009) and satellite observations (1993-2009)
- Gridded time series of steric sea level from in situ hydrography and from “altimetry minus GRACE ocean mass”
- Greenland ice sheet elevation from merged ERS-1, ERS-2 and Envisat satellite radar altimeter data (1992-2010)
- Sea ice freeboard heights and dynamic topography of the Arctic Ocean observed from ICESat altimetry 2003-2008.
- QuikSCAT, CERSAT/IFREMER blend and PO.DAAC blend seem to be quite successful in storm detection

3.1.1 Sea surface height

Tide gauge records: Starting from the monthly RLR (Revised Local Reference) tide gauge records from the Permanent Service for Mean Sea Level (PSMSL Woodworth and Player 2003), tide gauge data around the Arctic rim were reprocesses and improved. Data have been downloaded from http://www.pol.ac.uk/psmsl and corrected for the inverted barometer response of sea level to atmospheric loading using surface pressure fields from the National Centers for Environmental Prediction (NCEP; Kalnay et al., 1996, http://www.ncep.noaa.gov/) and for GIA using the Peltier model ICE-5G VM2, (http://www.psmsl.org/train_and_info/geo_signals/gia/peltier/). As we focus here on interannual to multidecadal time scales, we removed the seasonal cycles from the monthly sea level time series, by fitting sinusoids with periods of 12 and 6 months.

Figure 18 shows individual corrected tide gauge time series over 1950-2009 along the Norwegian and Russian coasts. Figure 19 shows mean sea level evolution for 1950-2009 for the Arctic sector. The figure reveals that the Arctic coastal mean sea level (CMSL) displays high interannual variability but almost no trend until the end of the 1970s. On average over the whole 60-year time span (1950-2009), we find a positive Arctic CMSL trend of 1.62 +/- 0.11 mm/yr (after correcting for GIA and IB). Our results indicate that between 1950 and the mid-to-late 1990s, Arctic CMSL was mostly driven by internal climate modes, in particular the AO, possibly through changes in wind-stress and associated ocean circulation (although quantitative analyses of the latter effects remain to be performed), as well as ocean mass changes. Since the mid-to-late 1990s, Arctic CMSL shows a marked rise of 4.07 +/- 0.65 mm/yr.

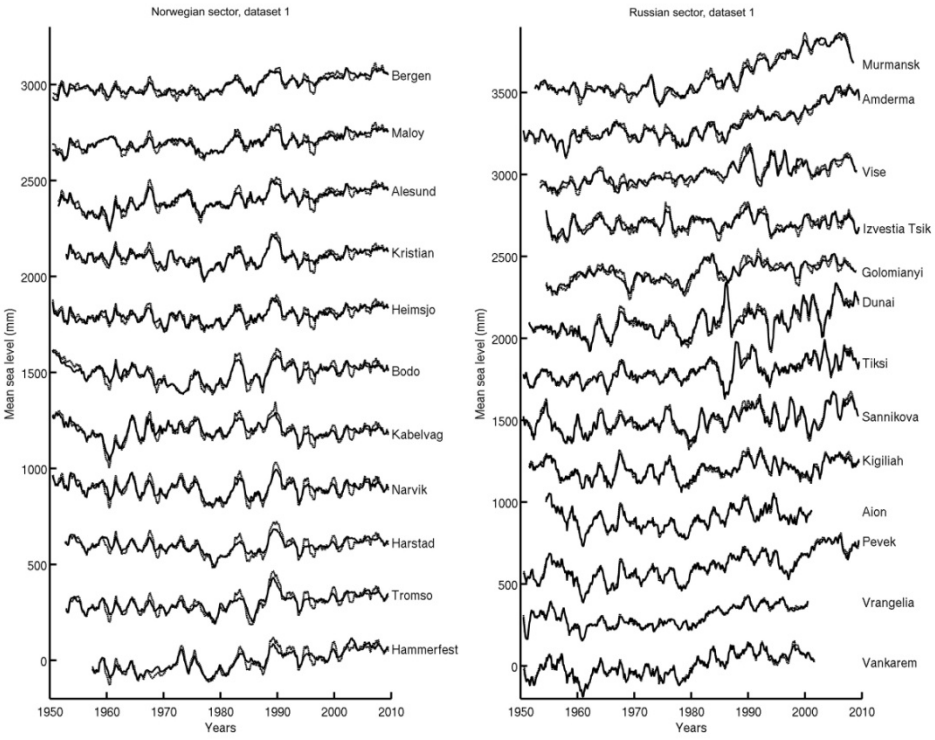

Figure 18 *Plots of individual tide gauge time series over 1950-2009 for the Norwegian sector (11 tide gauges; left panel) and Russian sector (13 tide gauges; right panel).*

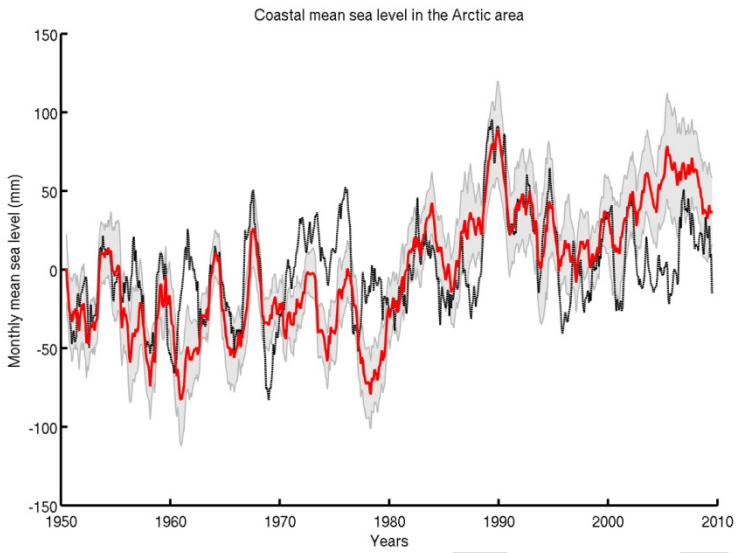

Figure 19. *Coastal mean sea level from tide gauge records over 1950-2009 for the Arctic sector (Russian and Norwegian) (red curve: coastal mean sea level; black dashed curve: Arctic Oscillation index).*

Satellite altimetry: For the altimetry data, we use the DT-MSLA "Ref" series provided by Collecte Localisation Satellite (CLS; http://www.aviso.oceanobs.com/en/data/products/sea-surface-heightproducts/global/msla/ index.html). This data set is used over the time span from January 1993 to December 2009. It is available as 1/4°×1/4° Mercator projection grids at weekly interval. The DT-MSLA "Ref" series are based on the combination of several altimetry missions, namely: Topex/Poseidon (T/P), Jason-1 and 2, Envisat and ERS 1 and 2. It is a global homogenous inter-calibrated dataset based on a global crossover adjustment (Le Traon and Ogor, 1998) using T/P and then Jason-1 as reference missions.

One main limitation results from the low data availability due uncovered high latitudes areas by most altimetry missions and the presence of sea ice. T/P, Jason-1 and Jason-2 share the same ground track and have an orbit inclination of 66°. As a consequence there is no data available from these missions at latitudes higher than 66°N. Parts of high latitudes are sampled up to 82°N by the ERS-1, ERS-2 and Envisat altimetry missions. However, north of 82°N, no satellite altimeter data is available. Any satellite altimetry-derived SSH dataset leaves uncovered large portions of the Arctic Ocean. In order to generate a new dataset suitable to study sea level variability and trend in the Arctic Ocean, we reprocessed satellite altimetry data from the T/P, ERS-1, ERS-2, GFO, Envisat, Jason-1 and Jason-2 missions. The aim of this reprocessing was to address some of the limitations previously described. We focused on the specific limitations discussed above, namely the low data quality and the uneven sampling of the ocean. The improvements concern: (1) the mean sea surface, (2), the ocean tide model, (3) the regional multi-mission merging, (4) the sea level grid computation using the objective analysis approach. These improvements lead to a much larger availability of the sea level data in the Arctic region. The details of these improvements are described in Prandi et al. (2011). The spatial trend patterns in sea level over 1993-2009 of the original and reprocessed data are presented in Figure 20a,b.

We constructed an altimetry-based CMSL along the Norwegian coast averaging individual time series at the 11 Norwegian tide gauge sites of our dataset. The tide gauge and altimetry-based CMSL curves in the Norwegian sector for 1993-2009 are shown in Figure 21. Both curves are highly correlated and show an increasing sea level trend of 3.32 +/- 0.65 mm/yr (from tide gauges) and 4.23 +/- 0.23 mm/yr (from satellite altimetry) over the altimetry period (1993-2009). The trend difference (0.9 mm/yr) is only slightly larger than the tide gauge trend uncertainty. Thus the altimetry data clearly confirm the recent sea level increase in that particular region. We note in passing that the rate of sea level rise in this region is very similar to the global mean rate (of 3.3 mm/yr over 1993-2009, e.g., Cazenave and Llovel, 2010), a result confirmed by Prandi et al. (2012) for the whole Arctic region (Figure 20).

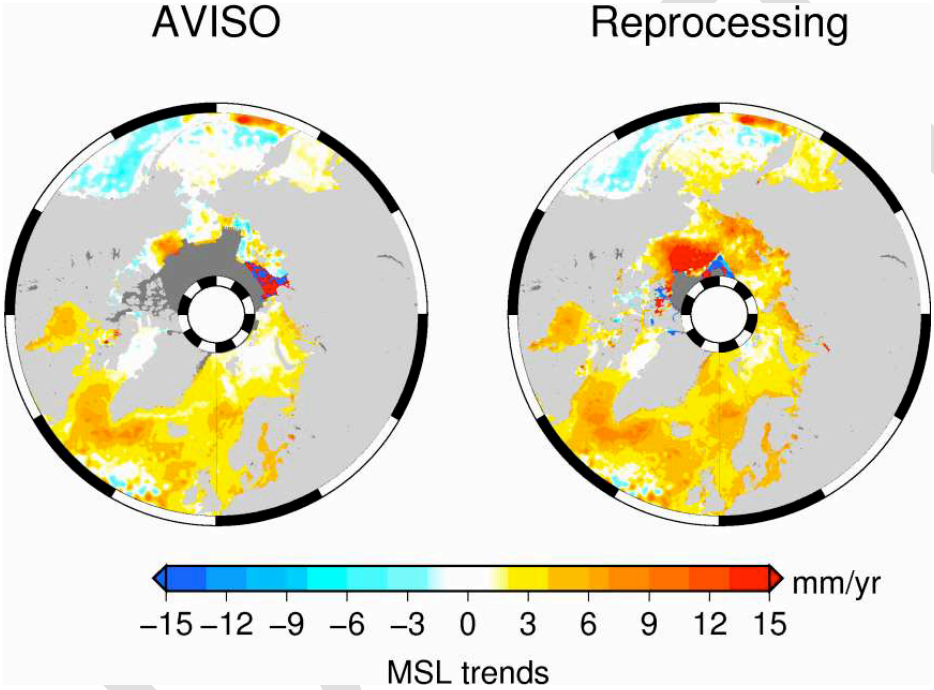

Figure 20. *Map of altimetry-based sea level trends (mm/yr) between 1993 and 2009 in the Arctic Ocean from SSALTO/Duacs grids (left panel) and from the reprocessed grids (right panel).*

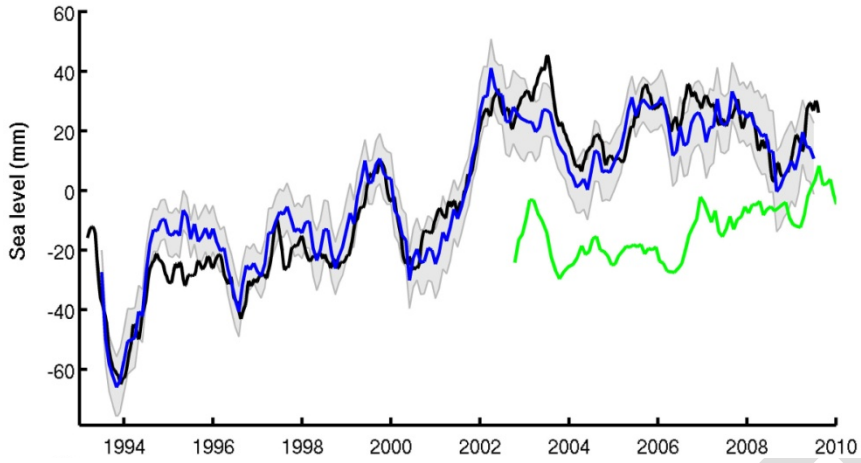

Figure 21 *Coastal mean sea level from tide gauge records over 1993-2009 for the Arctic sector (Russian and Norwegian, blue curve) and from altimetry (interpolated to each TG sites, black curve), the green curve is the coastal mean ocean mass from GRACE/CSR (interpolated at each TG sites).*

Gridded time series of ocean mass variations from GRACE: About 7 years of gravity data from the GRACE mission are now available. This satellite mission was launched in March 2002 to measure temporal change of the earth gravity field at monthly interval. On land, GRACE mainly measures change in land water storage while over the oceans GRACE provides variations of the mass of the oceans (Wahr et al. 2004). At regional scale, ocean mass change results from redistribution of sea water by the ocean circulation plus local exchange of water with the atmosphere (through precipitation and evaporation). Here, we have explored the latest releases (RL04) from three groups: CSR, GFZ and GRGS solutions (1°×1° ocean grids at monthly interval) and selected CSR data. This new data set includes an implementation of the carefully calibrated combination of destripping and smoothing, with different half-width Gaussian filters (the solutions need to be smoothed because errors increase with wavelength; Swenson and Wahr 2002). Compared to earlier products (contaminated by north– south strips due to aliasing by the GRACE coverage of high frequency signals of atmospheric and oceanic origin), the latest release is less noisy, mostly because of the destripping procedure applied to the data. The gridded ocean GRACE products are corrected for post-glacial rebound (the solid earth response to last deglaciation, also sensed by GRACE) using Paulson et al. (2007) model, and for the leakage due to land hydrology (Chambers 2006). The gridded time series we use in this study are based on the 300-km Gaussian smoothing and cover the following time spans: August 2002 to December 2010 (Figure 22). GRACE solutions are expressed here in terms of equivalent sea level.

For our studies, we interpolated monthly GRACE-ocean mass grids at the 11 Norwegian tide gauge sites, removed the seasonal signals as for the other data sets and then averaged the 11 individual ocean mass time series. Corresponding GRACE-based averaged ocean mass curve is superimposed to the CMSL curve in Figure 21. Over 2003-2009, the GRACE ocean mass trend is positive and equal to 2.9 +/- 0.66 mm/yr.

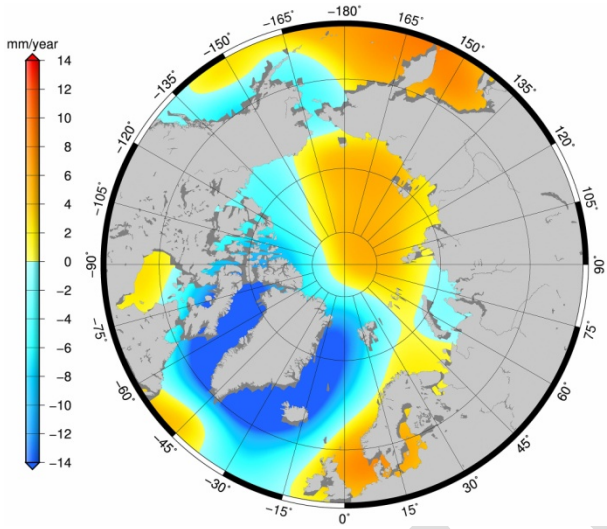

Figure 22. *Map of Ocean mass trends (mm/yr) between August 2002 and December 2010 in the Arctic Ocean from CSR GRACE data.*

Improved Mean Sea Surface and Mean Dynamic topography using GOCE and GRACE

The mean sea surface and mean dynamic topography are critical reference surface for sea level and circulation studies as well as for the assimilation of sea level data into the models. With the launch of the ESA GOCE and nearly 2 decades of satellite altimetry we were able to derive new consistent set of Mean Sea Surfaces and Mean Dynamic Topographies from satellites independent of the hydrodynamic models. When deriving the quantities from satellite the fundamental relationship between the mean sea surface (MSS), geoid (G) and mean dynamic topography (MDT) MSS = G + MDT is used where geostrophic circulation is manifested through the MDT. New Geoid estimates from the first year of GOCE were ingested into the EIGEN6C and together with the DTU10MSS it was used to derive the DTU12MDT and Monarch-A MDT (Figure 23)providing the absolute reference surface for improved mean ocean circulation determination.

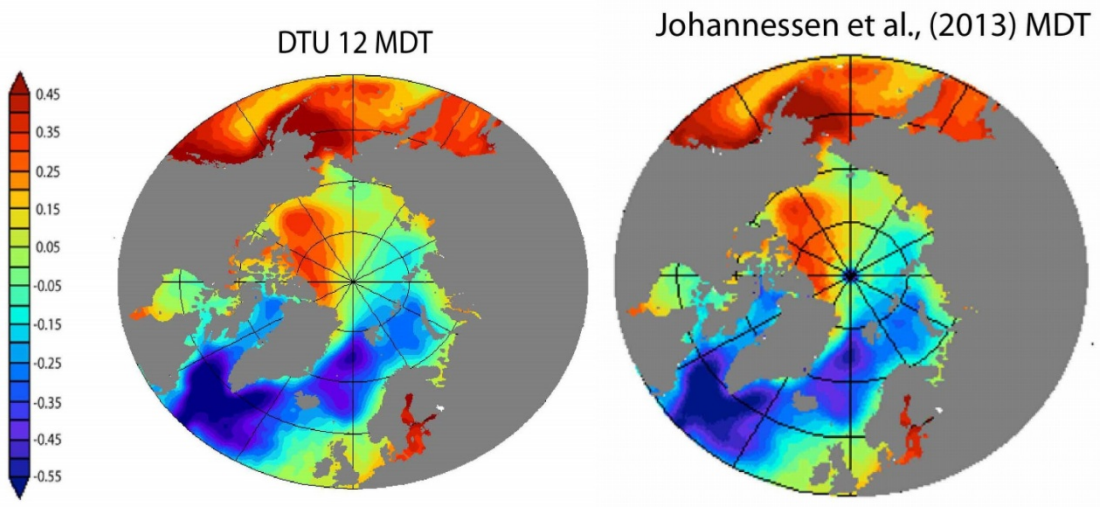

Figure 23. *The DTU12MDT used for Monarch-A together with the MDT derived at the Nansen center by Johannesen et al.*

The mean sea surface height model derived from satellite altimetry is determined as the mean over the altimetry era (1993-2009). In order to get the altimetric mean sea surface to coincide with 50 years period used in Monarch-A, it was initially thought to use the reconstructed sea level (Figure 25) to estimate a mean sea surface representing the last 50 years. However, as the reconstruction did not cover the entire Arctic Ocean it was decided to use ocean model output instead. An initial investigation indicated that trend estimated from both DRAKKAR and SODA (Figure 24) agrees reasonably well with trend estimates interpolated to the tide gauges over the identical period. However, the two models disagree by more than 1 mm/year in the trend for large parts of the interior of the Arctic Ocean, where no tide gauge data are available, so it is currently impossible to determine which is the most correct.

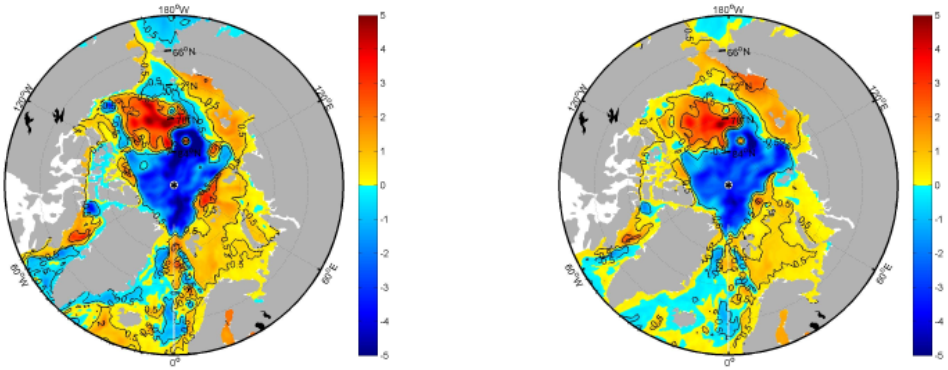

Figure 24. *Sea level trend from the DRAKKAR model (left) and the SODA (right) for the (1970 -2007) period.*

As the tide gauge data suffers from a very biased spatial distribution towards the Russian and Norwegian sector of the Arctic Ocean, it was decided to use a constant mean value as determined from the tide gauges for the entire Arctic Ocean for the correction of the mean sea surface to cover the 60 years period of 1950-2009. This value of 1.4 mm/year was subsequently used to adjust the DTU10MSS model to create the Monarch-A MSS model for the 1950-2010 period. Integrating the 1.4 mm/year sea level change over the difference in period between the models yielded a correction of 3 cm being applied to derived the 50 year MSS used for Monarch-A.

Sea level reconstruction: Satellite altimetry data provide information about regional variability in sea level since the beginning of the 1990's. But if we want to study sea level in the past we must reconstruct sea level. Prior to the altimetry era, we do not have such information but past sea level reconstruction methods can be developed to construct gridded sea level time series in the past. The reconstruction process is described by Meyssignac et al (2012) and consists of 2 steps. In the first step an EOF (Empirical Orthogonal Function) decomposition of 2-D sea level grids (satellite altimetry or numerical ocean models) is done (Fig. WP2.11). This decomposition separate sea level signal (matrix H) into spatial modes (U(x,y)) and temporal amplitudes (α(t)): $H(x,y,t) = U(x,y)\alpha(t)$. Assuming that spatial modes are stationary with time, the reconstructed sea level in the past (called here $H_R(x,y,t)$) has an EOF decomposition as follow: $H_R(x,y,t) = U(x,y)\alpha_R(t)$, where $\alpha_R(t)$ is the new temporal amplitudes of the EOFs. The second step consists of computing these new $\alpha_R(t)$ amplitudes through a least squares adjustement that minimizes the reconstructed field and the tide gauge data at the tide

gauges locations. Combining spatial modes and new temporal amplitudes gives a reconstruction of past sea level in 2-dimension.

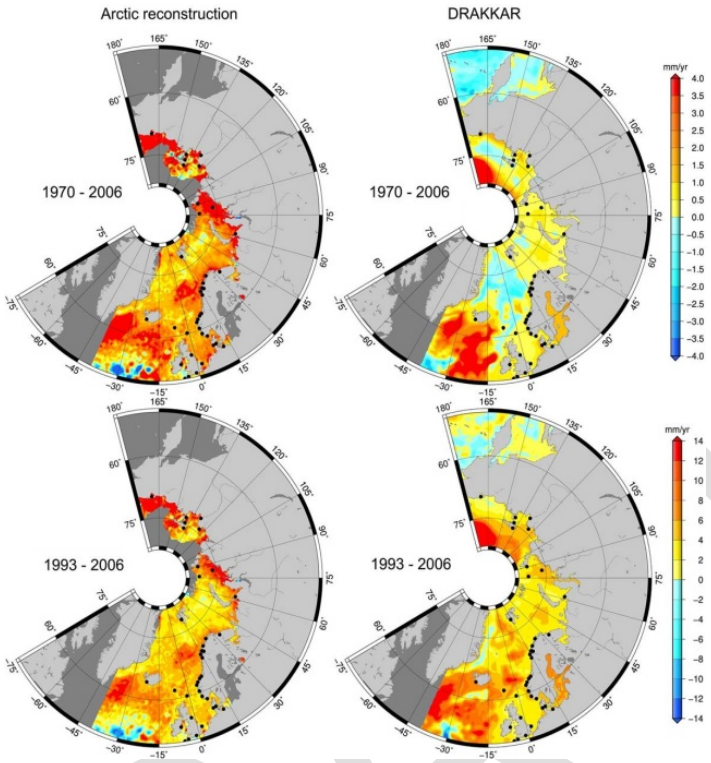

Figure 25 *F1: Past 2-D sea level reconstruction from 1970 to 2006 (left panel) and from 1993 to 2006 (right panel) in the Arctic region.*

The reconstruction covers the period 1958 – 2006 and concerns North Atlantic, Nordic Seas, Greenland Sea, Barents Sea, Kara Sea and Siberian Sea. It has been validated by comparing reconstructed and observed sea level at tide gauge sites not used in the reconstruction (Figure 25).

Gridded time series of steric sea level from in situ hydrography and from "altimetry minus GRACE ocean mass": In this section we estimate the contribution of the steric (effect of ocean temperature T -thermosteric component- and salinity S -halosteric component- variations) sea level to Arctic MSL. For that purpose, we use T and S data from 3 data bases: the WOD09 (Levitus et al., 2009), the Ishii and Kimoto (2009, called after IK09), and EN3 data bases (from Hadley Center). The depth and time coverage of these temperature and salinity data is very inhomogeneous in the studied region, leaving much of the Arctic Ocean uncovered (Figure 26). The coverage during the 1960s and earlier is far too sparse and limited to the near surface layers, preventing us to quantify the steric contribution in the whole Arctic and even along the Russian coasts. Before the 1990s, we also note that the S data coverage is poorer than for T data. This leads us to : (1) not consider data prior to 1970, (2) compute the thermosteric sea level as of 1970 and the halosteric sea level as of 1993 (the beginning of the altimetry era), and (3) only consider a limited geographical sector bounded by the 75°W-45°E longitudes and the 50°N 80°N parallels.

For each database, we computed the thermosteric/halosteric sea level on a 1°x1° grid at monthly interval since 1970, integrating T/S anomalies down to 700 m. Figure 27 shows steric trend patterns computed over 1970-2009 with the EN3 and Ishii et Kimoto 2009 data over the limited region

described above. We further compare the altimetry-based with thermosteric and halosteric spatial patterns over the 1993-2009 time span over the North Atlantic and Nordic Seas regions (**Figure 28**). In several areas the spatial trend patterns of altimetry-based and thermosteric sea level show very similar behaviour. In Figure 28 is also shown the residual (altimetry minus steric –sum of thermosteric plus halosteric-) trend map. Comparing thermosteric and halosteric trends indicates that the patterns appear anticorrelated (with higher magnitude for the thermosteric trends). This anticorrelation between the trend patterns in thermosteric and halosteric sea level suggests simultaneous increase of both temperature and salinity in the area of the North Atlantic and Nordic Seas sector during the past 17 years (the two factors having opposite effects on sea level).

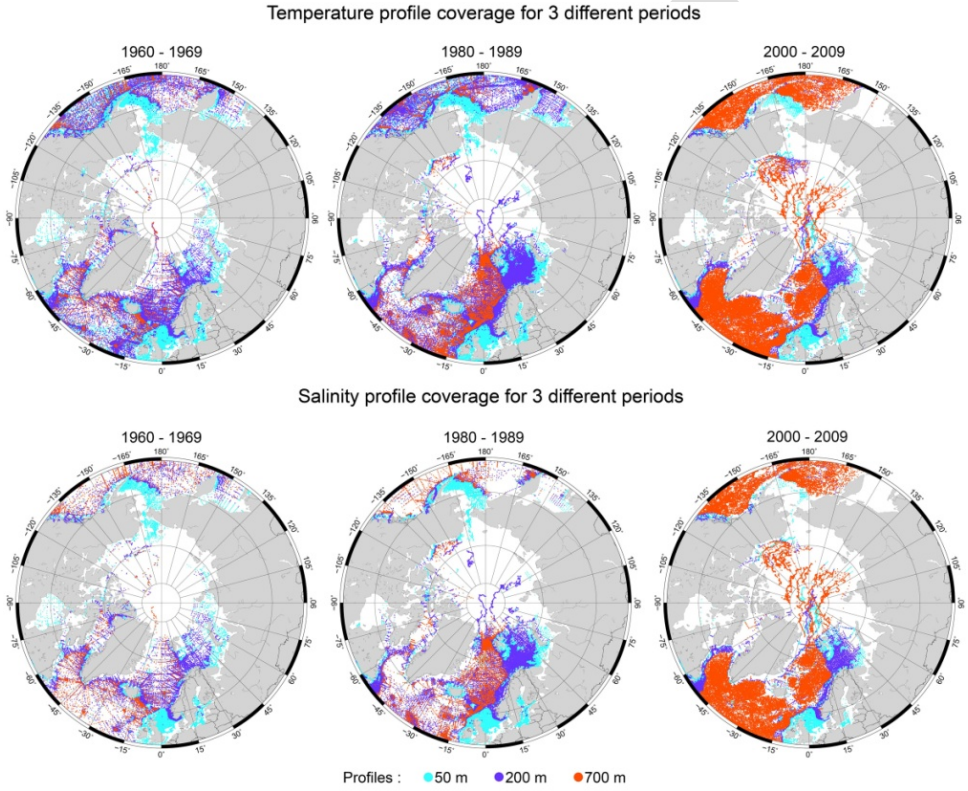

Figure 26. *Spatial and temporal distribution of the temperature and salinity profiles included in the EN3 database.*

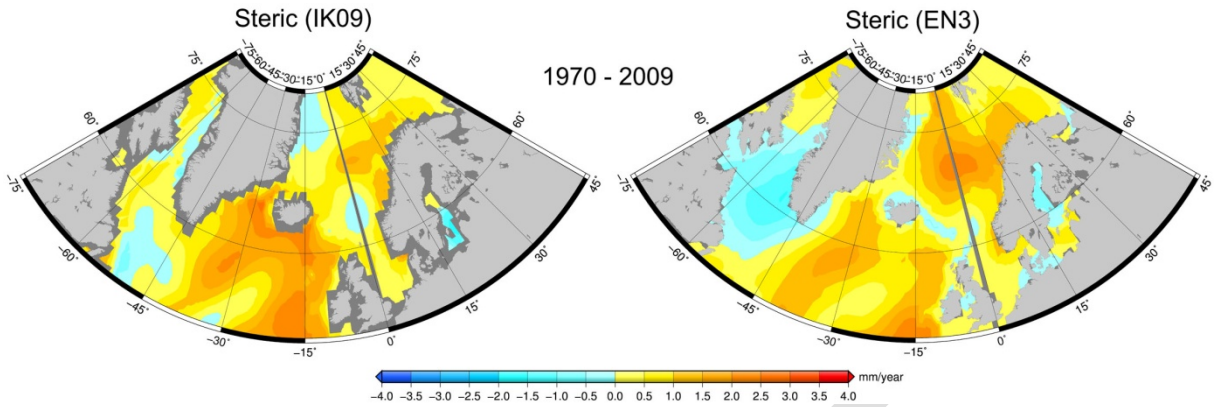

Figure 27. *Spatial trend patterns in thermosteric sea level for 1970-2009 over the North Atlantic and Nordic sea; IK09 (left panel); EN3 (right panel).*

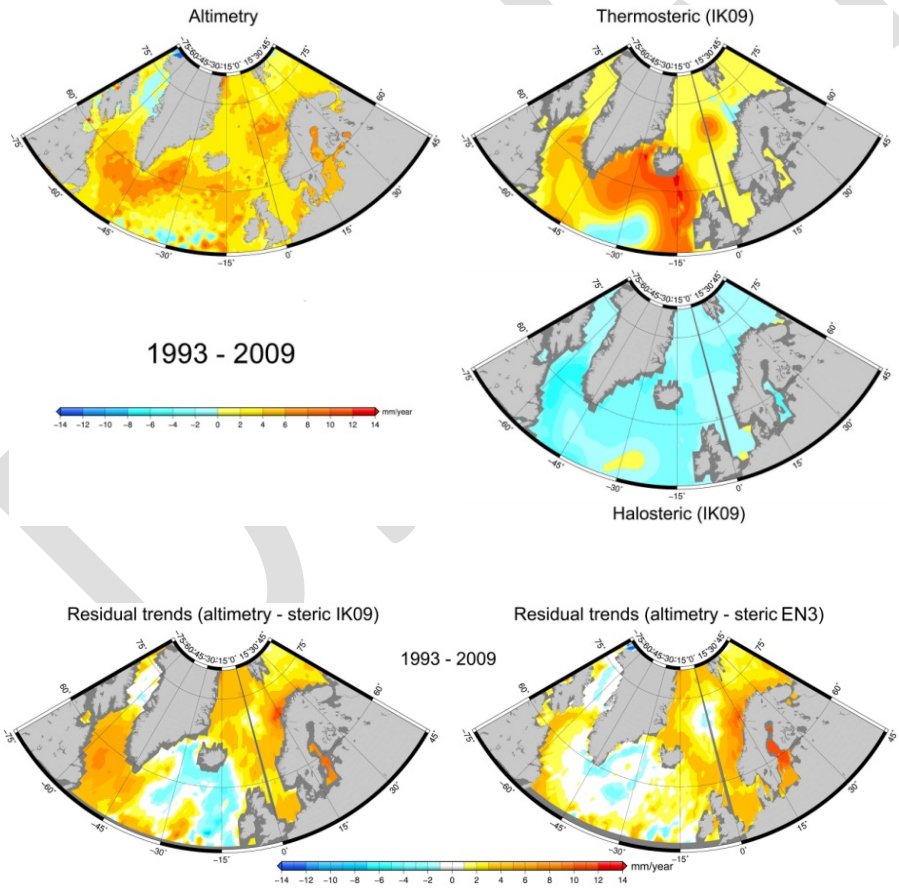

Figure 28. *a) Altimetry-based and thermosteric/halosteric (from IK09) sea level, b) residual (altimetric minus steric) sea level trend patterns (lower panel, Altimetry – IK09 and altimetry – EN3) in the North Atlantic and Nordic Seas region over 1993-2009.*

We also computed the steric sea level (thermosteric plus halosteric components) using the IK09 and EN3 data since 1970 at the 11 Norwegian tide gauge sites by interpolating the steric grids at the tide gauge locations (averaging the gridded data within a 1° radius around the tide gauge). Corresponding

curves are shown in Figure 29 superimposed to the Norwegian CMSL curve. We first note that both IK09 and EN3 curves are in general good agreement (as previously noticed between IK09 and WOD09 thermosteric components). Although smoother, they correlate also well between 1970 and 2006 with the CMSL curve (correlation of 0.65). However as of 2006, the steric sea level curves show a downward trend not seen in the CMSL curve. The steric sea level trends over 1970-2006 amounts to 1.63 +/- 0.14 mm/yr and 1.9 +/- 0.17 mm/yr for IK09 and EN3 respectively, a value quite comparable to the CMSL trend over the same time span (of 1.73 +/- 0.23 mm/yr). This suggests that, at least over this time span (1970-2006), observed CMSL rise along the Norwegian coast has a steric origin. However the interannual variability in steric sea level and Norwegian CMSL are not well correlated, suggesting that the latter is influenced by other factors on such time scales, e.g., wind stress-driven ocean circulation and ocean mass changes.

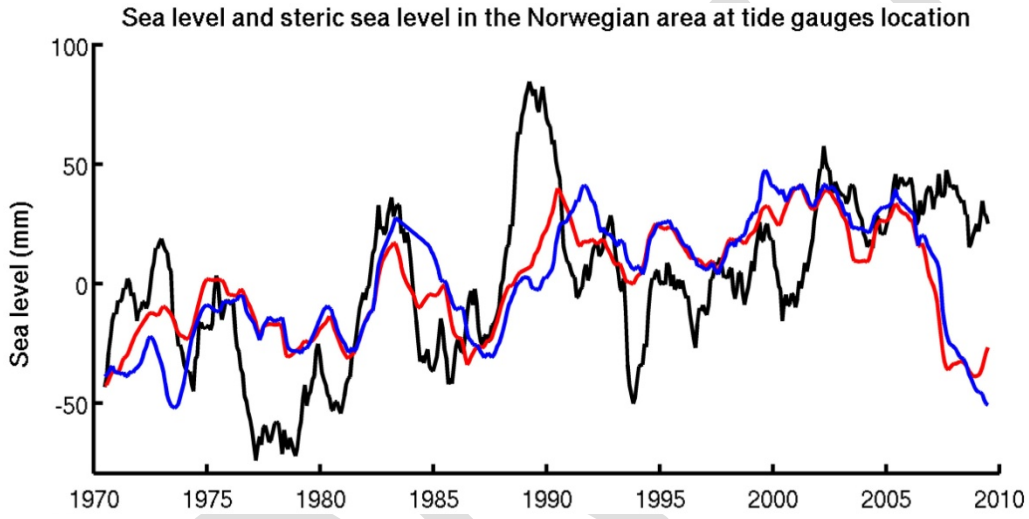

Figure 29. *Coastal mean sea level from Norwegian tide gauge records (11 stations, black curve), steric sea level computed from EN3 (blue curve) and IK09 (red curve) database (interpolated at each tide gauge sites).*

In Figure 30 is shown the difference over 2003-2009 between CMSL and GRACE-based ocean mass averaged at the Norwegian tide gauges. This difference should primarily reflect the steric component. The coastal steric sea level from the IK09 data is also shown over 1993-2009. While both curves show a downward trend over their overlapping time span (2003-2009), the highly negative observed steric trend seems somewhat suspect. This highly negative steric trend may not be real and may simply reflect lack of data in the very recent years. Besides considering the 2003-2006 time span during which there are some T data, we note that the "CMSL minus GRACE ocean mass" curve closely follows the steric curve, and both trends (equal to 1.41 +/- 0.7 mm/yr and 1.36 +/-0.4 mm/yr for "CMSL-GRACE ocean mass" and steric sea level respectively over 2003-2006) agree quite well.

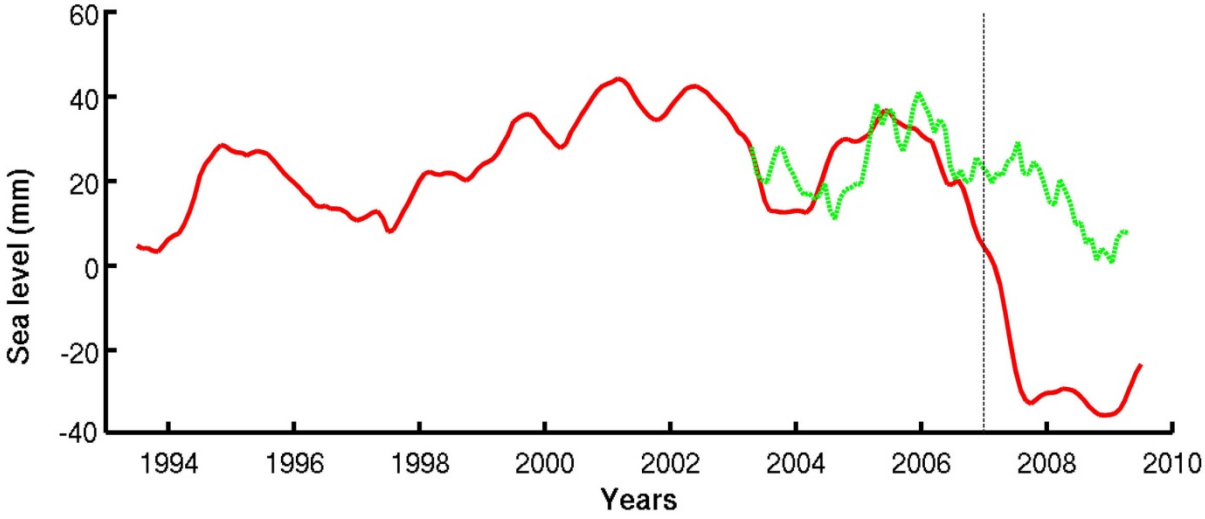

Figure 30. *Coastal steric sea level from IK09 database (interpolated at each tide gauge sites, red curve), "CMSL – GRACE ocean mass" residual curve (green curve).*

Sea level variability along the Russian and Norwegian coasts. Over the past ~60 years along the Norwegian and Russian coasts there are good quality tide gauge data that have been reprocessed in the framework of the MONARCH-A project. Between 1950 and 1980, coastal sea level did not rise significantly but beyond 1980, it shows a significant upward trend. Estimate of the thermosteric and halosteric sea level since 1970 in a limited sector including the North Atlantic subpolar gyre and the Nordic Seas indicates a strong change around 1995, with simultaneous increase in temperature and salinity. Along the Norwegian coast, a similar behaviour is noticed with an increasing trend of observed sea level (from tide gauges and satellite altimetry) since the mid-1995s (note that the downward trend observed in the mean coastal steric sea level as of 2007 is likely an artefact due to a lack of data in this region over the very recent years). We also observe an increase in the GRACE-based averaged ocean mass at the Norwegian coast since 2003. Its positive trend (of 2.9 +/- 0.66 mm/yr over 2003-2009) is somewhat larger than the global mean ocean mass increase due to total land ice melt over about the same time span (of 1.5-2 mm/yr) (e.g., Church et al., 2011). It thus includes a regional ocean mass trend component (due to ocean circulation-driven mass redistribution), in addition to the global mean mass trend. Anyway, this ocean mass increase at least partly reflects the recent acceleration reported in ice mass loss from glaciers and ice sheets (e.g., Steffen et al., 2010, Rignot et al., 2011).

Between 1950 and 1995, sea level along Norwegian and Russian coasts does not display any significant upward trend, while being highly correlated to the AO. On the other hand, since the mid-to-late 1990s, coastal sea level in the Norwegian and Russian sectors has been rising faster during the previous decades. This coincides with strong changes affecting thermosteric and halosteric sea level in the North Atlantic and Nordic Seas, with simultaneous increase in temperature and salinity over the past 15 years.

Moreover, subdecadal variability in RSL along the Norwegian coast has been examined by comparing tide gauge observations of RSL with hydrographic measurements (steric height), atmospheric surface pressure (IBE) as well as land uplift rates (GIA) for the period 1960– 2010 as presented in Richter et al., (2012). They found that these components account for 30–85% of the observed variability on

monthly to interannual time scales, depending on location, and that the largest contribution to variability comes from IBE. For the steric effects, there are large regional differences along the coast. Linear trends in RSL are positive in southwestern and northern Norway. The most prominent contributions to the trend are the land uplift and a positive thermosteric contribution from a warming in the coastal waters (e.g. -1.7 and 0.9 mm/yr, respectively, for Bergen). Other contributions not taken into account, might be connected with wind effects, melting of land based ice as well as ocean mass redistribution due to hydrographic changes in the deep ocean. While the large scale winds are not expected to contribute to a positive trend through the last two-three decades, the accelerating rates of loss of land-based ice may explain part of the remaining residual. In addition, changes in hydrology may contribute to the residual trend, but are also related to large uncertainties.

3.1.2 Ice sheets and glaciers

The focus of ice sheet research has been to assess the overall Greenland mass balance by comparison and synthesis of different satellite-based data and estimation methods to provide improved estimates of the total freshwater input to the ocean from the ice sheet melt, as well as the contribution of Greenland ice mass loss to sea level rise. Spatial–temporal variability and changes of Greenland ice sheet elevation from 1992 to 2012 have been analyzed from merged ERS-1, ERS-2 and Envisat satellite radar altimeter data. A methodology for determining inter-satellite biases was developed and applied, in order to merge measurements from these different satellites and to create continuous and consistent time series of ice sheet elevations (Khvorostovsky, 2012). Adjustment of elevation time series for its dependence on backscatter coefficient and other waveform parameters substantially reduced the amplitude of elevation seasonal variations and locally corrected elevation change-rate estimates by up to several cm/year (Khvorostovsky, 2012). An average elevation change rate of 1.9±0.3 cm/year from 1992 to 2010 over 81% of the Greenland ice sheet area (Figure 31, left) was found on the basis of the methods described in Khvorostovsky, 2012. However marginal areas are not completely measured by radar altimetry and substantial thinning rates over these areas could offset the observed average elevation change. At the same time spatio-temporal analysis reveals large inter-annual elevation variability over western and south-eastern regions. Ice sheet elevation evolution for the high and low elevation areas respectively from 1992 to 2012 are indicated in Figure 31, right). Temporal variations show that increases in surface elevation from 1995 observed over the high-elevation regions of Greenland were followed by an elevation decrease from 2006 (Johannessen et al., 2005; Khvorostovsky, 2012). In contrast, over low-elevation areas below 1500 m the surface elevation decrease that started from 2000 has continued.

Surface heights for the Greenland Ice Sheet based on NASA's laser altimetry satellite mission ICESat has also been derived by L. S. Sørensen (2011) for the time span October 2003 – March 2008. The mean surface elevation changes are presented in Figure 32, left. A distinct thinning of the ice sheet is found along the southeast and west coasts, and a smaller but consistent thickening is found in the interior part of the ice sheet. This is in agreement with the trends derived from ERS/ENVISAT, Figure 31, right.

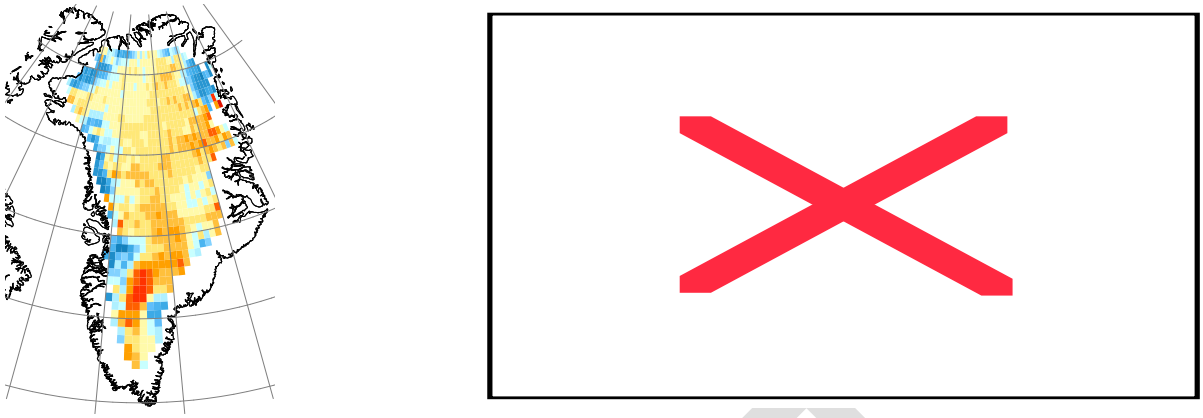

Figure 31. *Elevation changes from ERS/ENVISAT 1992-2012 (left) and corresponding elevation time series over the areas above (blue curve) and below (red curve) 1500m.*

The joint American-German GRACE gravity satellite mission has measured the Earth gravity field, since 2002. A generalized inversion method has been used to estimate the Greenland Ice Sheet mass changes Figure 32(middle). The GRACE estimate of the total mass changes for the entire ICESat period (October 2003-March 2008) is -204 +/- 21 Gt/yr. Conversion of the ICESat heights into mass changes using firn densification and snow density models, results in a larger estimate of -240 +/- 28 Gt/yr. Work to estimate the freshwater contribution to the Arctic Ocean from GRACE data is ongoing (Barletta and Sørensen, 2010??). The contribution from the Greenland Ice Sheet will be estimated for each of the seven major basins presented in Figure 32 (right), adapted from Hardy et al, 2000. Examples of mass changes for basin 4 and 7 are given in Figure 33 both showing a negative trend/mass balance.

.

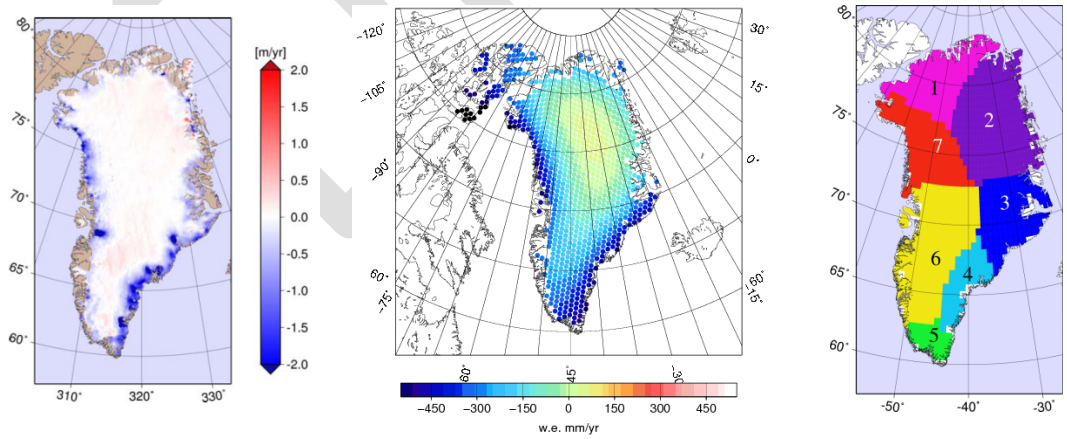

Figure 32. *Observed mean elevation changes from ICESat (left) and GRACE-derived mass changes (Barletta et al. 2012) with an inversion method (middle) over the period 2003-2008. Definition of seven major drainage basins (right)*

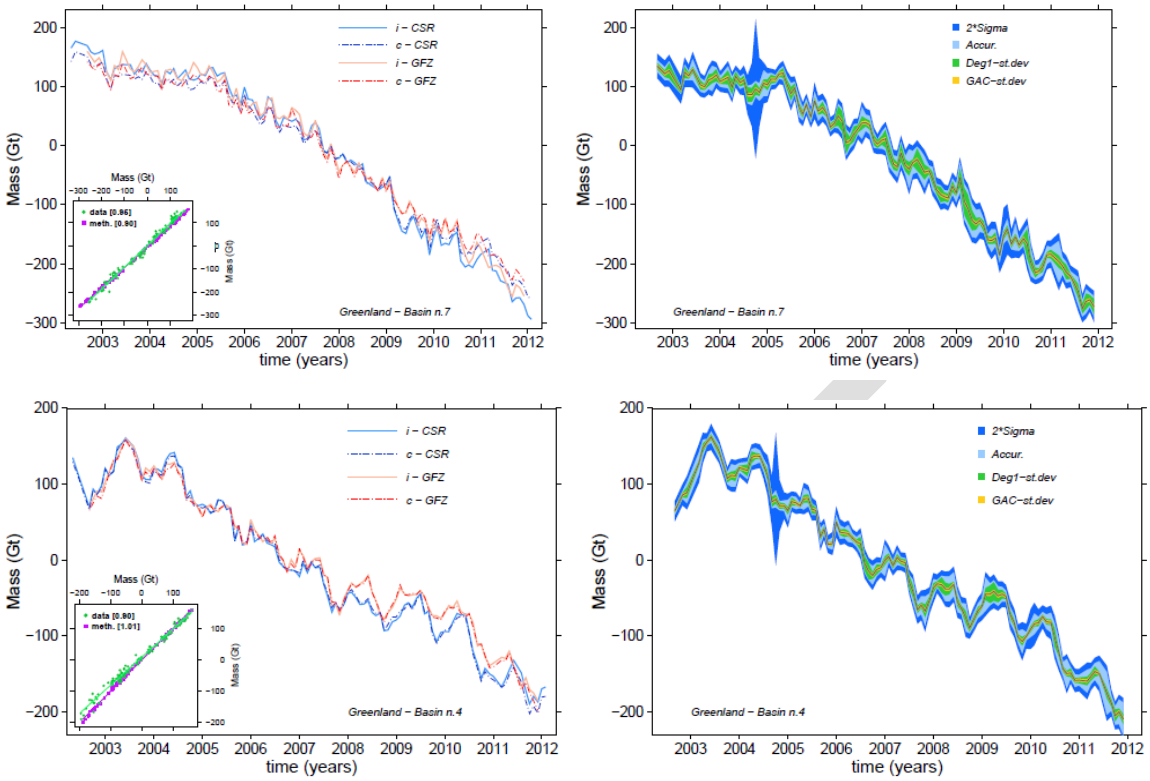

Figure 33. *From Barletta et al. (2012), here the RL04 monthly solution for Greenland. Basin number is indicated in each plot. Left column represents the comparison between the two methods and two data sets (CSR and GFZ). Right column represents the monthly average solution where each color in the band around the average represents a contribution to the error estimate*

First results, of near-coincident CryoSat-2 (level 2) and airborne laser scanner data over the Greenland Ice Sheet (Sørensen et al, 2011) is not consistent and show biases between the two data sets by up to 50m. This is believed to improve with the reprocessed data using the updated ground processor, which are about to be implemented at the time of writing

3.1.3 Sea ice

Sea ice thickness: Sea ice freeboard heights and dynamic topography of the Arctic Ocean observed from ICESat altietry 2003-2008 have been updated to release 33 and are available in grids of resolution 0.1°x0.2°. The sea ice freeboard heights (Figure 34) show good spatial correlation between the distribution of first year ice and multiyear ice observed by QuikSCAT scatterometer data (Skourup, 2010). Overall, a decrease in the Arctic Ocean mean freeboard heights of approximately 10-15 cm is observed, since the beginning of the ICESat observations in 2003 (***Figure 35***). These are realistic values and can be explained by a combination of a decrease in the perennial sea ice extent together with a general decrease in the ice thickness due to an increased heating of the atmosphere and ocean. The freeboard (f) to thickness (t) conversion is debated in many papers and is highly variable (R = 1-10) depending on sea ice type, settings and snow conditions. Recent studies (Doble et al, 2011) of the relation between freeboard heights and thickness at the dimension of the ICESat footprint size (~70m in diameter), finds a conversion value of 4.4 for level ice and 5.2 for deformed ice in the central Arctic Ocean.

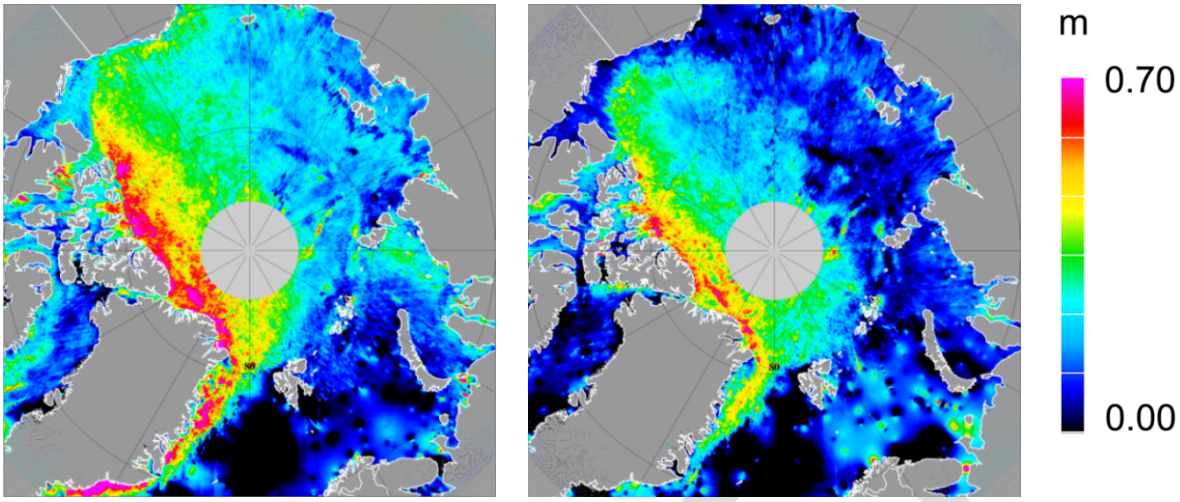

Figure 34. *Sea ice freeboard maps February-March 2006 (left) and October-November 2005 (right)*

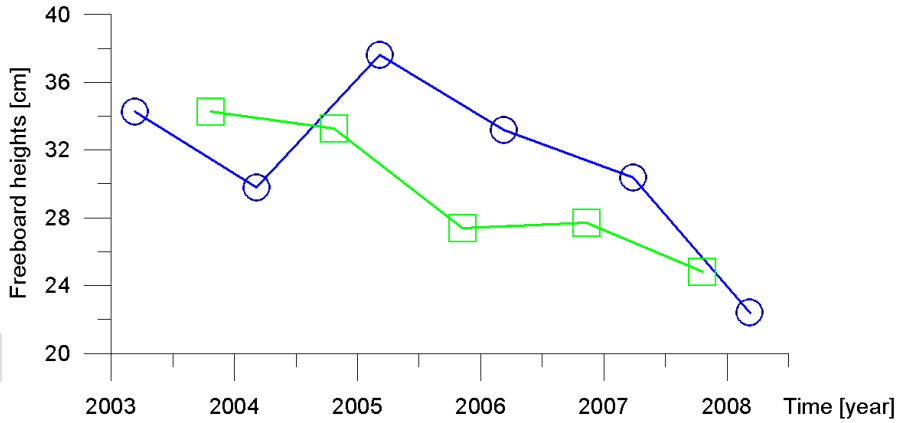

Figure 35. *Mean sea ice freeboard heights in the Arctic. Blue circles February-March and green rectangles October-November. From Kwok*

3.1.4 Wind

Sea surface wind stress strength and its direction can be deduced from near-surface wind time series. Reanalyzed wind fields derived from numerical models are in common use, like ECMWF (ERA Interim) or NCEP (MERRA and CFSR) products, all continuously updated and physically consistent. Other products include those deduced from various satellite measurements. Scatterometer is a wind dedicated sensor, in operation since 1991 on several platforms. The deduced wind fields have been processed, archived, and disseminated at CERSAT/IFREMER. Their spatial resolution is 12.5 to 50 km, i.e better than the best available reanalyses of 0.5-degree latitude/ longitude. Near-surface winds in the marginal ice seas between 60°N and 80°N during winter are investigated here for the 20-year period 1992-2012 (Bentamy et al., 2013). Four products are considered: Winds from the individual sensors (ASCAT and QuikSCAT, both produced at CERSAT/FREMER) the satellite merged product by

PO.DAAC, and the ERA-Interim reanalysis (ERAI). Marginal Arctic seas were schematically regrouped into five subregions: (1) Baffin Bay (80°W-45°W), (2) Greenland-Norwegian Seas (45°W-25°E), (3) Barents-Kara Seas (25°E-100°E), (4) Laptev-East-Siberian Seas (100°E-180°E), (5) Chukchi-Beaufort Seas (120°W-180°W).

Wind measurements are of strong interest along the sea ice edge, where the storms develop and (re-) generate. However, difficulties arise when sea ice edge evolves from day-to-day, and that various remotely sensed and model sea ice products seem to locate the ice edge differently. Applying a common sea ice mask, the CERSAT/IFREMER sea ice concentration product, from 12.5 km SSM/I, was found to produce best results. Wind values are removed (masked) if there exists at least some ice (>0%) within 15 km radius around each regular 0.25^{o} grid location.

Wind speed distribution during four seasons and within the 5 subregions is compared in ***Figure 36***. In winter (Dec-Feb) averaged wind velocities are around 10-11 m/s (median) +- 3.5 m/s (std) according to the remote sensed records, and 8-9 +- 3-4 m/s according to the ERAI model product. The maximum likelihood wind speed (the peak of each curve) is shifted towards weaker wind velocities (5-7 +- 2.5-3 m/s) during June-August months (***Figure 36***). This is consistent with weaker surface thermal gradients along the sea ice margin during the melt season, oppressing storm (re-) generation. If comparing panels in ***Figure 36***, the shapes of the spatial distribution curves over all look very similar in all panels and between four data sets, except Dec-Feb season in the Laptev – East Siberian and the Chukchi - Beaufort Seas. Below 5 m/s, though, large differences are found, e.g. for ERAI and PO.DAAC weak winds comprise as much as 18-25% of the data, while only 4-7% for QuikSCAT and ASCAT.

Storm events are schematically determined as those single grid points exceeding 20 m/s during one day. It is found that satellite-derived wind products have a higher spatial resolution, and has much better performance with regard to detection of strong (storm) wind patterns. However, the model wind is also a first guess estimate and hence a constraint for the satellite-based wind procedure. Further combination of multiple remotely-sensed wind products and the general model wind field (blended multi-sensor wind product) is a considerable improvement, especially for the remote areas where ship and buoy observations are limited. A comparison between several wind products shows that the remotely sensed winds when assimilated in ERA Interim, can no longer resolve the small scale (100-200 km) storm tracks and wind speeds. QuikSCAT, CERSAT/IFREMER blend and PO.DAAC blend seem to be quite successful in storm detection, whereas ASCAT and ERAI fail in detection of the wind speeds exceeding 20 m/s. For operational needs a *StormWatch* tool is under development at CERSAT/IFREMER with an aim to detect storm activity, and to locate its track based on the weather model output and constrained by the scatterometer wind velocity retrievals

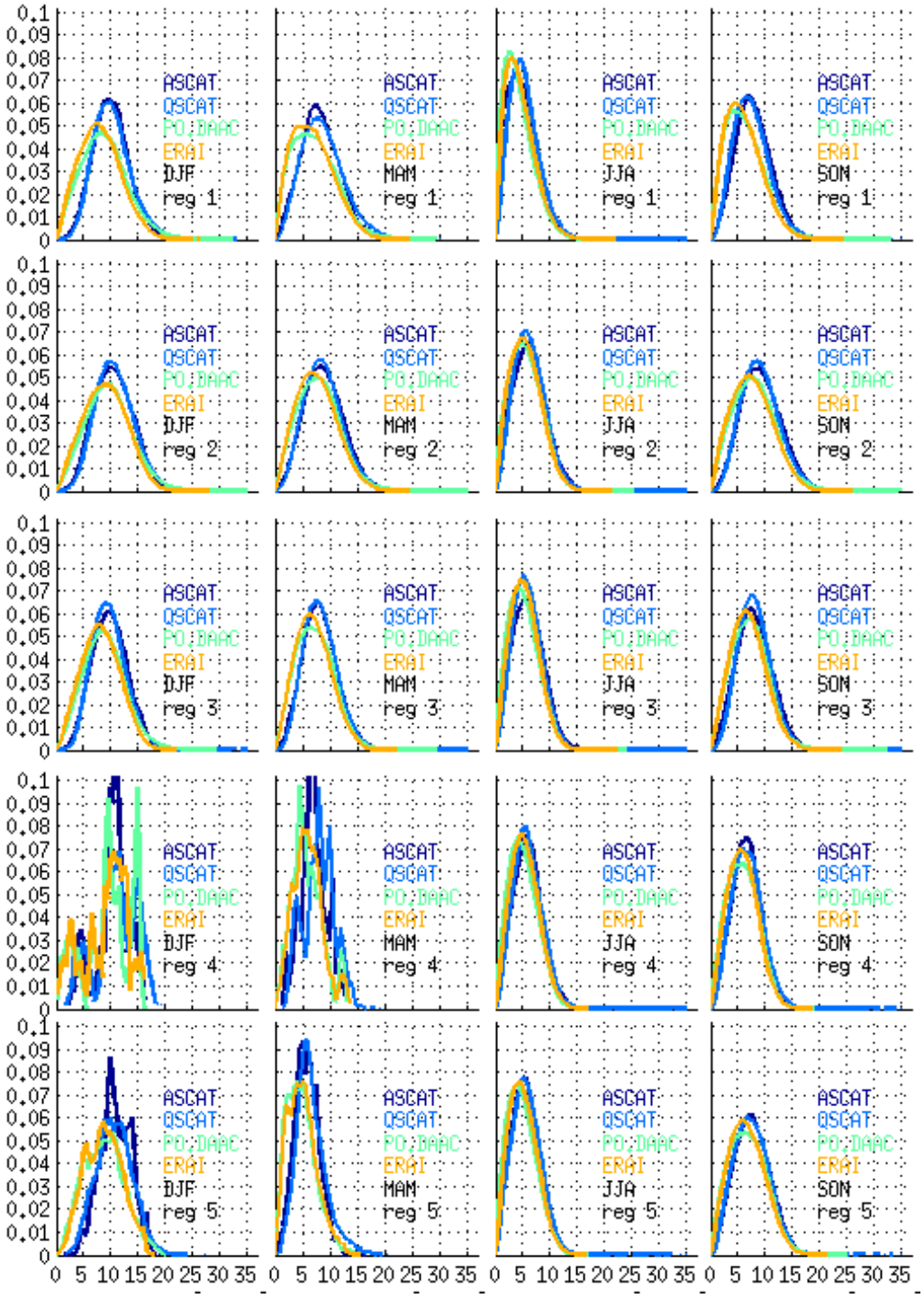

Figure 36. *Probability density plots of the daily mean wind velocities, 1992-2011 period. The panels from left to right: (a) December-February, (b) March-May, (c) June-August, and (d) September-November months. From the upper panel to the lower panel: (1) Baffin Bay, (2) Greenland-Norwegian Seas, (3) Barents-Kara Seas, (4) Laptev-East-Siberian Seas, (5) Chukchi-Beaufort Seas.*

3.1.5 Circulation

As part of the MONARCH-A project we compared several state of the art models against observational data generated ether by groups working in the MONARCH-A or obtained from other sources (see below). Results show that many models reasonably well reproduce variability of SSH, temperature, salinity, sea ice and currents. The existing level of resemblance between models and available observations allows drawing realistic conclusions about variability of the Arctic Ocean parameters, at least on decadal scale, and revealing underlying mechanisms.

One way to further improve the skill of ocean model of the Arctic Ocean is to use data assimilation approaches. Dynamically consistent assimilation techniques can provide a better understanding of the mechanisms responsible for observed changes, and, as a side effect, improves estimates atmospheric forcing fields. Moreover reliable decadal predictions are possible only with good initial conditions, and this is what data assimilation can provide. Within the framework of MONARCH-A we created an assimilation system for the Arctic Ocean, and performed assimilation experiments with medium resolution model for the first decade of the 21st century. This period characterized, as mentioned before, by significant changes in the Arctic Ocean, and, likely enough, by increased amount of observations. This makes it a good test ground for assimilation system, and promise valuable scientific outcome. Among assimilated parameters are: in situ TS profiles from the EN3 and NISE data sets, mean and daily SSH from satellite measurements and sea ice concentration.

Central parts of the Arctic Ocean suffer from serious undersampling of currents and other ECVs while variability of ocean characteristics here determine in large the behavior of the whole ice-ocean system in the Arctic. Our knowledge about the variability in this region can be increased by utilizing models and reprocessed observational data. This allows us to reveal the state of observations in the central Arctic, and determine what information is necessary from an observational point of view in order to understand pan-Arctic and regional processes and trends. Here, results are shown in terms of data-based and model-based syntheses of changes observed over the Arctic Ocean, including

1. Circulation patterns derived from GOCE MDT
2. Model based simulations of changes of the Arctic Ocean
3. Sea level variability along the Russian and Norwegian coasts

The main changes of the Arctic Ocean during the last decades are discussed.

Circulation patterns derived from GOCE MDT. The GOCE based MDT spatial pattern representing the mean from 1993-2009 for the North Atlantic, Nordic Seas and the Arctic Ocean is shown in Figure 37 (lower right). The total MDT elevation range from the high in the Arctic Ocean to the low in the sub-polar gyre in the North Atlantic reaches about 0.9 m. The regional shape of the MDT with the orientation of the dominant slopes in the different sub-domains reveals the presence of the circulation pathways in: (i) the sub-polar gyre south of Greenland; (ii) the inflow of Atlantic Water respectively between Iceland and the Faroe Islands and between the Faroe and Shetland Islands; (iii) the continuous northward flowing Atlantic Water towards the Arctic Ocean; (iv) the southward flowing East Greenland Current; (v) the Beaufort Gyre; and (vi) the transpolar drift in the Arctic Ocean. Note that as neither the GOCE nor the altimeter data cover the Arctic Ocean entirely, e.g. within 300-400 km from the pole, the data coverage is insufficient to calculate a reliable MDT. Also,

the presence of sea ice may hamper the computation of the MSS and hence the MDT. Though care is taken to avoid erroneous data, some of the data that have been used to calculate the MSS may represent the top of the sea ice flow rather than the sea surface. Especially off the coasts of the Canadian Archipelago and northern Greenland the high values of the GOCE MDT may be caused by the influence of the permanent and thick sea ice cover.

The Arctic Ocean displays an elevation change reaching up to about 0.45 m associated with the high in the Beaufort Gyre, and with the corresponding dominant orientation of the slope mostly aligned from Siberia to the northern shores of Greenland. In the Nordic Seas the general shape of the MDT favors the cyclonic circulation pattern displaying steepest MDT slopes of 0.4 m/100 km between the Faroe and Shetland Islands, along the northwest coast of Norway and in the northern part of the East Greenland Current. As further discussed and analyzed in Johannessen et al., (2013) this spatial pattern in the MDT agrees well with the spatial pattern in the mean steric height (Figure 37) derived from hydrographic data (Nilsen et al., 2008) for the period 1950-2010 referenced to a maximum depth of 1500m.

In the Nordic Seas the total range in the MDT derived from the combined GOCE and altimetry data is around 0.50 – 0.55 m as seen in Figure 37a. In comparison, the range of the mean steric height of 0.30 m (Figure 37b) suggests that there might be a significant contribution to the MDT pattern from the large-scale atmospheric pressure field as well as deep barotropic currents in some of the sub-basins. By subtracting the GOCE based MDT from the hydrographic based steric height associated with the baroclinic structure in the water masses in the Nordic Seas an estimate of the barotropic contribution to the MDT is derived as shown in Figure 37c. The barotropic contribution contains distinct elevation changes of about 10 cm with pattern consistent with the known barotropic cyclonic circulations in the Greenland Sea, the Lofoten Basin and in the Norwegian Sea (Nøst and Isachsen, 2003). Evidence of this cyclonic barotropic circulation in the Norwegian Sea has also been observed from Argo floats in the intermediate waters below the Norwegian Atlantic Current (Søiland et al., 2008). In conclusion the assessment of the GOCE derived MDT for the Nordic Seas and the Arctic Ocean is promising.

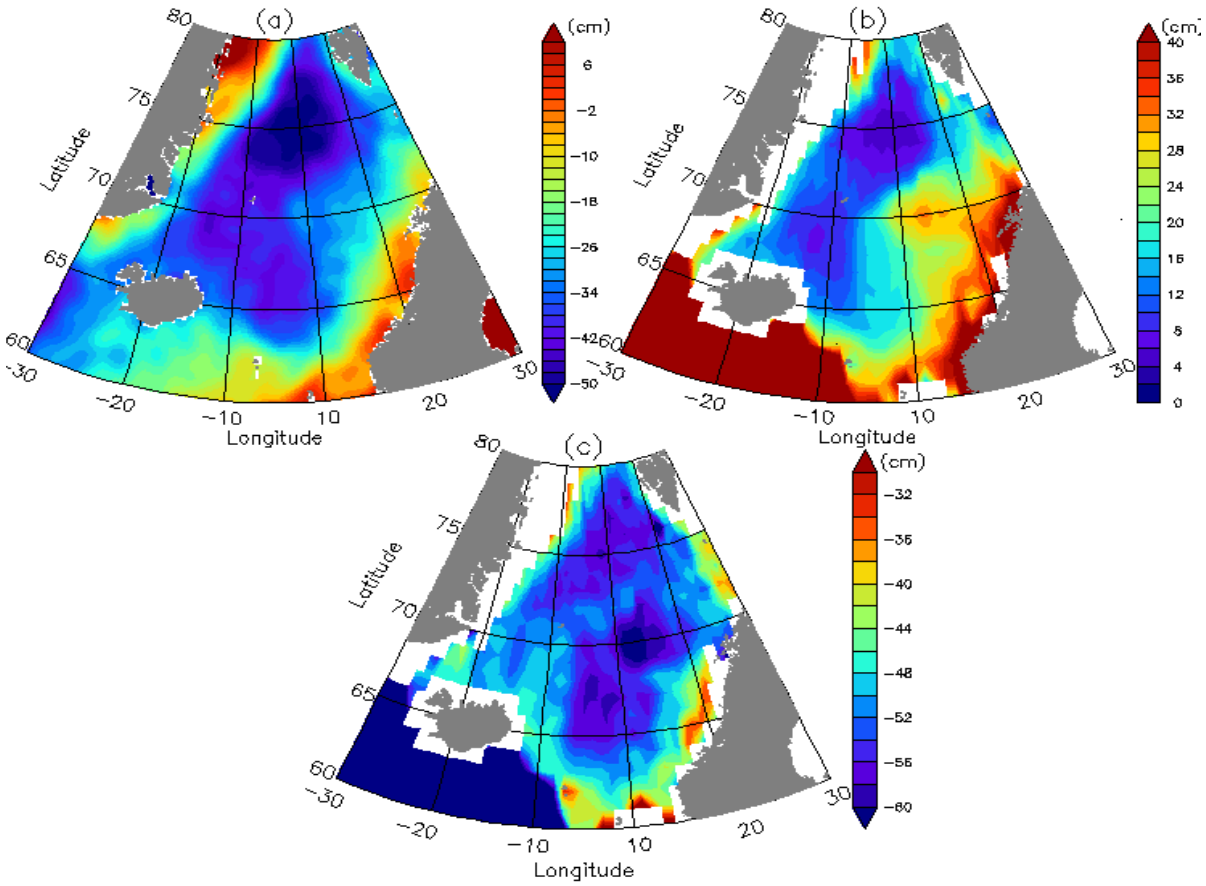

Figure 37. *(a) MDT derived from combined GOCE and altimetry, (b) steric height derived from the in-situ hydrographic database where the white areas in the 1500 m reference steric height (see Figure 4) is filled with steric height values representing every 100 m from 1400 m to 500 m, and (c) difference between (a) and (b). The color bars represent the height contours in unit of cm. Note the different colour ranges.*

Model Simulations of the Arctic Ocean Circulation. During MONARCH-A several model solutions of the Arctic Ocean were produced, analyzed, intercompared and assessed against the GOCE MDT retrieval. The model experiments include:

- Regional setup of MITgcm model ATL (Serra et al., 2010) in three different resolutions from the Institute of Oceanography, University of Hamburg
- Regional setup of MICOM model (Hátún et al., 2005) from the Nansen Environmental and Remote Sensing Center.
- Global setup of MPIOM model (project STORM https://verc.enes.org/community/projects/national-projects/german-projects/storm/) from the Max Planck Institute for Meteorology.

Model/data intercomparison show, that there is a large spread among models, however the different models appear to have distinct strengths and weaknesses in simulating different parameters. Combined analysis of ocean surface and intermediate water circulation, distribution of temperature and salinity, sea ice and SSH extent (Figure 38) and variability reveal that ATL12 version of the ATL model better describes the Arctic Ocean as a system. This means that spatial distribution and

temporal variability of all ocean characteristics in consideration correlate well with observations, and neither of them deviate too far away from in situ or satellite measurements. In conclusion, ATL12 is used in the remaining analysis.

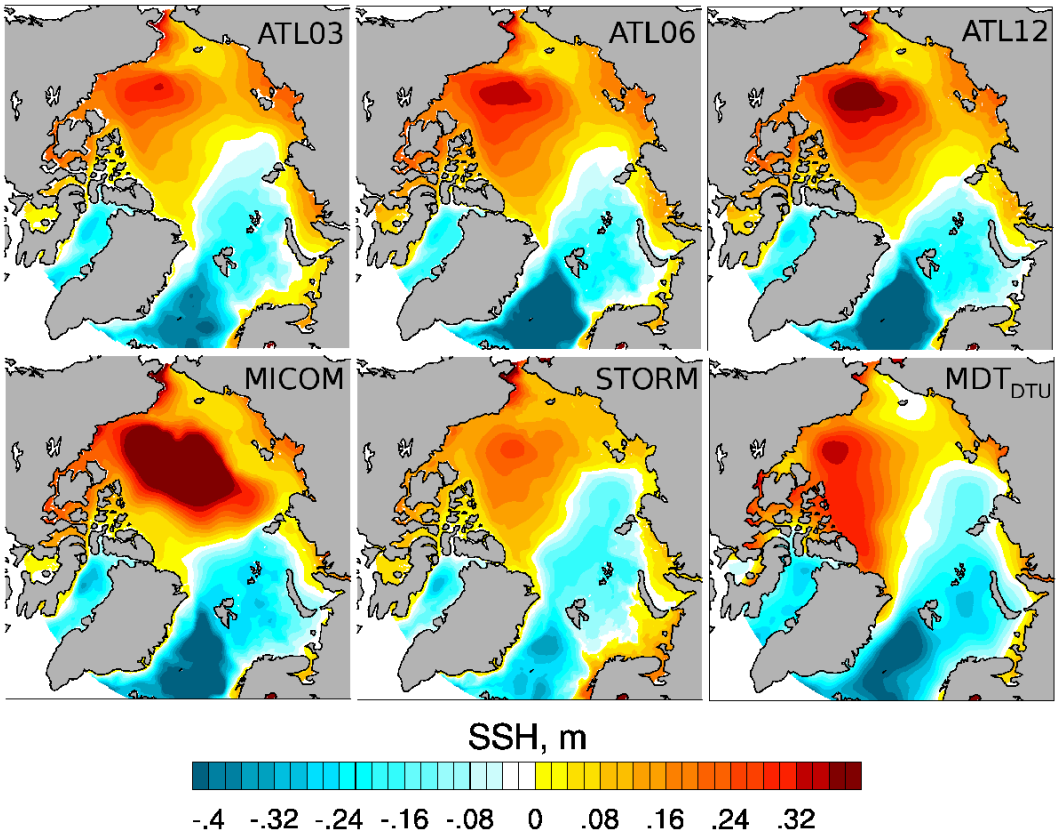

Figure 38. *Example of model/observations intercomparison. Mean sea surface height for the period 1993-2009 as simulated by several models and measured by satellites. Satellite data are reprocessed in the framework of the MONARCH-A.*

Due to sparseness and limited availability of direct current measurements in the Arctic Ocean, we still have limited understanding of Arctic Ocean circulation at intermediate depths and at the deep layers. Ocean surface currents are better known, since sea ice to some extent can be used as their proxy. We do not assimilate directly characteristics of the currents, but it is expected that they improve in the model as a consequence of assimilation of other parameters. There are two large scale surface currents in the Arctic Ocean. Beaufort gyre – anticyclonic current with center close to the Beaufort Sea. It rotates water and ice in the Amerasian Basin of the Arctic Ocean. Transpolar Drift Current transports water and ice from East Siberian and Laptev seas, across the Arctic through the North Pole towards the Fram Strait.

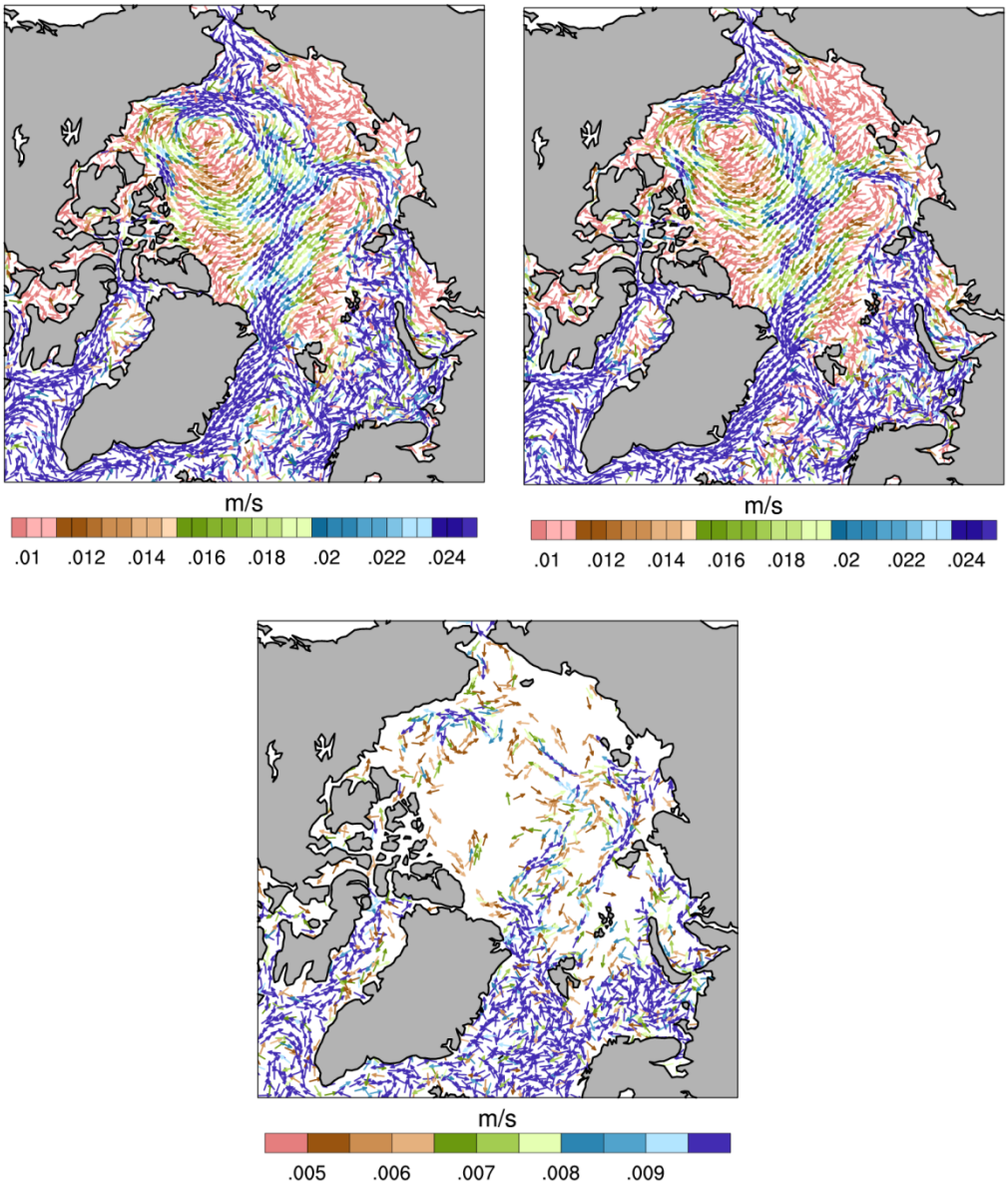

Figure 39 *Mean surface ocean currents for the period 2000-2009. (top left) First iterations, (top right) last iterations, (bottom) difference between last and first iterations.*

Figure 39 shows that the model reproduce both large-scale patterns of surface ocean circulations in the Arctic Ocean. Mean difference between first guess and last iterations indicate, that assimilation of the data lead to slow down of the surface circulation. In particular currents along Siberian shelf and part of the Transdrift current that flows over the Lomonosov ridge become weaker. Another region, were currents become slower is to the north of Alaska. The main feature of intermediate water circulation in the Arctic Ocean, that is mostly responsible for redistribution of relatively warm Atlantic water, is cyclonic movement of water along the shelf break. Proper simulation of this circulation for a long time was (and to some extend still is) a challenge for regional and global circulation models. Atlantic water enters the Arctic Ocean trough the Fram Strait and St. Anna

Trough, and then distributed along the Siberian shelf towards Amerasian Basin. There is relatively well-known recirculation flow of Atlantic water over the Lomonosov Ridge.

To assess the volume budget, the following straits were analysed: the Fram Strait, were warm salty Atlantic Water coming in to the Arctic along eastern flank of the strait and cold and fresher Arctic waters flow southward with the East Greenland Current. The Davis Strait integrates the entire outflow through Canadian Archipelago. The Barents Sea Opening (BSO) – another way for warm Atlantic waters to enter the Arctic. And the St. Anna Trough through which Atlantic Waters modified in the Barents Sea transported further to the Arctic Ocean.

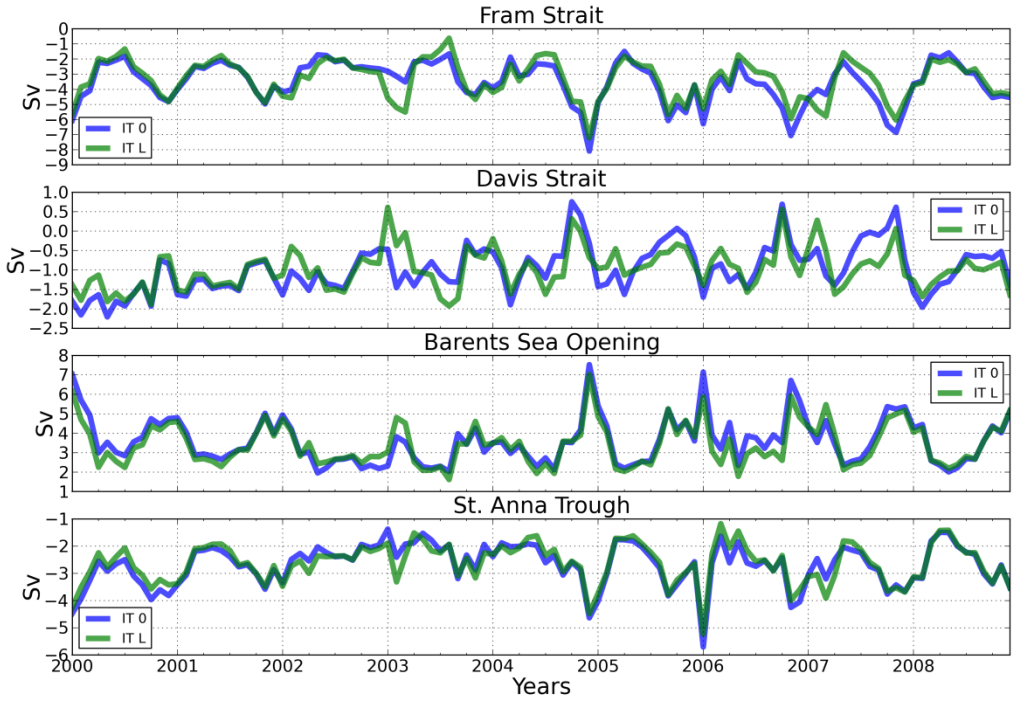

Figure 40 *Volume transport through Arctic Ocean straits. (blue) – model before data assimilation, (green) – model after data assimilation.*

Differences in volume transport between the runs with and without data assimilation (Figure 40) overall are not large, but episodically can reach several Sv. A striking example is the year 2003, when transport through the Fram Strait increased by about 2 Sv. Simultaneously there is also a large change in volume transport through BSO and Davis Strait. There is no defined pattern of change for any of the straits, so that for the differences can be both positive and negative.

Changes in the central parts of the Arctic Ocean. As shown in the literature and what has become clear from the model simulations and observations obtained during MONARCH-A, among the central parts of the Arctic Ocean the region with most pronounced changes is the Beaufort Gyre. In the following we will use it for illustration of the variability, trends and interactions between ECVs, while also making broader conclusions about Arctic Ocean as a whole. The area of the Beaufort Gyre region

(BGR) used in the further analysis, is shown in Figure 41. Data from the ATL12 model presented in Figure 42 is either averaged or integrated over this region.

The most striking and relatively easily observable trend in the Arctic Ocean characteristics is the change of the sea ice extent (SIE). Atmospheric temperature increase of the northern Hemisphere, caused by increase of CO2 concentration in the air, is likely the main driver of the SIE decrease (Notz and Marotzke, 2012), while changes in the wind circulation is mostly responsible for interannual changes, but do not define the trend (Vihma, Shpreen 2012). September SIE shrinks mostly in Amerasian Basin, which is, at least in part, determined by the distribution of the ocean currents. The Transpolar Drift Current move sea ice from the Laptev and East-Siberian Seas towards Fram Strait, and Beaufort Gyre current also transport thin ice westward in the Siberian part of the Amerasian Basin. Before mid 1990s sea ice in September almost completely cover BGR (Figure 42a), but since about 1997 there is decrease in SIE, that is more obvious in observations than in the model. For the whole Arctic Ocean total Arctic SIE experience negative trend since mid 1970s (Walsh and Chapman, 2001, Meier et al., 2012). In the 2000s this trend become stronger and the SIE reach two record minimums in 2007 and 2012.

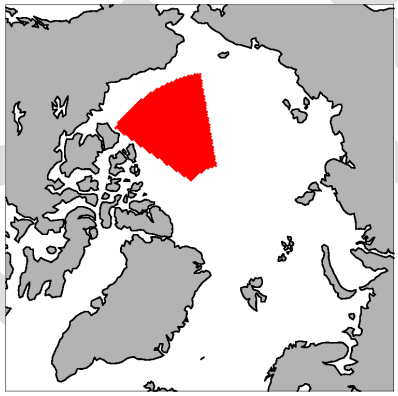

Figure 41. *Beaufort Gyre Region (BGR) area.*

Decrease in SIE is accompanied by thinning of the sea ice. In the model sea ice thickness (SIT) steadily decrease since the mid 1970s (Figure 42b), with a large outlier in the year 1982. Contrary to the SIE, of which we have continues satellite record since 1978, data on SIT changes are sporadic and discontinuous. Only recently measurements from ICESat satellite allow estimates of SIT with good spatial resolution, while temporally it is only covers two months a year and represents monthly mean values (Kwok). Comparison of model results with satellite observations (Figure 42b) show large offset, but model result is still within uncertainty of observations. Unfortunately the short duration of ICESat record does not allow us to make any robust conclusions about trends in the SIT. Submarine and airborne measurements do provide information about overall trend, but their lack of spatial resolution make regional analysis difficult. In our estimates of spatial SIT and sea ice volume change we still have to rely on indirect methods (Maslanik et al., 2007) or models. It is of great importance that missions like ICESat, Cryosat 2 and SMOS continue to collect information about sea ice thickness.

Less abundant and thinner sea ice means, that for the wind it is easier to move it. Model data demonstrate (Figure 42c) that since 1970 there is an increase of the mean ice drift speed (IDS) in BGR

that become stronger since the mid 1990s. Hakkinen et al., 2008 have found that since 1950s sea ice move faster over the whole Arctic Ocean and IDS increase related to increased wind stress. However, for shorter time period of 1989-2009 Vihma et al., 2012 found that increased trends in IDS cannot be explained by changes in the wind field, and Spreen et al., 2011 noted that ice drift trends are much larger than wind speed trends. In the model SIT and IDS seems to be anticorrelated for the BGR (Fig. Figure 42b,c), in a way that generally IDS increases with thinning of the sea ice in this region. A good example of such a behavior is the sudden increase in IDS together with thinning of sea ice in the beginning of 1980s. One should note, that there is nothing unusual in the SIE record in the model and in observations, which means that without proper SIT observations we can totally miss events like this one.

Sea ice not only complicates the ocean-atmosphere heat flux, but it also controls most of the atmosphere-ocean momentum transfers. Increase in sea ice mobility and larger ice free areas during summer season should have consequences for the surface ocean currents. Wind-driven convergence drives Ekman pumping in the BGR and to a large extent controls amount of fresh water (FW) stored in the upper part of this region. Giles et al., 2012 have found steadily increasing wind stress curl over the BGR, however this increase alone cannot explain the sudden increase in sea surface high (SSH), that is observed in satellite records since the year 2002. They conclude that one possible explanation is more effective transport of momentum from the atmosphere to the ocean due to changes in sea ice cover.

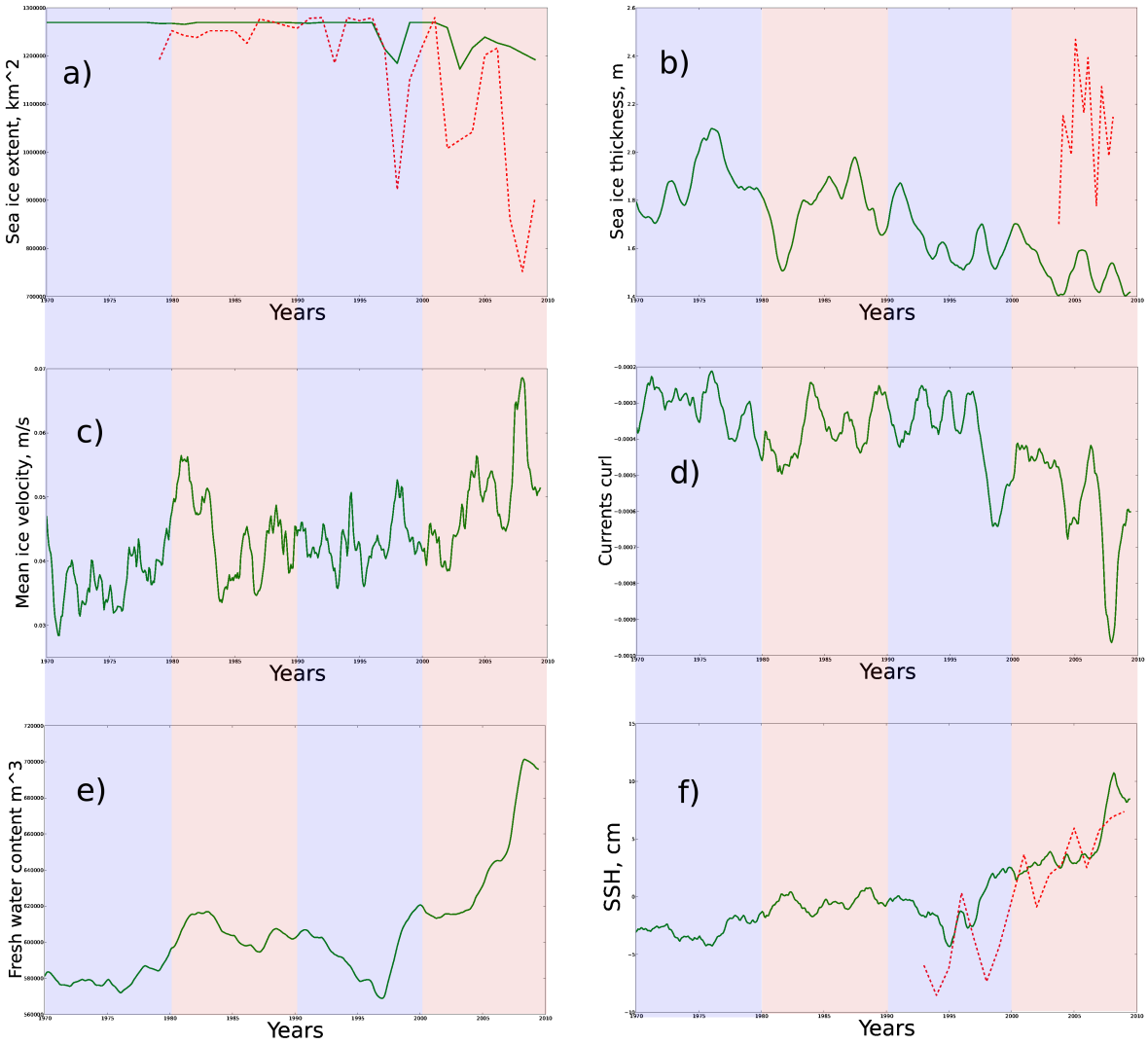

Figure 42. *Time series of climate variables in BGR from ATL12 model (green) and observations (red, dotted). a) Mean September sea ice extent. Observations are from Cavalieri et al. (1996) (NASA Team algorithm) b) Mean sea ice thickness. Model data are smoothed with 12 month window. Observations are from ICESat data and available only for two month per year (October, March). c) Mean sea ice velocity. d) Mean curl of surface currents. e) Fresh water content. f) Mean sea surface hight. Observations are taken from Prandi et al., 2012 (contribution to MONARCH-A).*

4 Theme III: Changes in the marine carbon cycle

In this Theme 3 the focus has been two-fold and targeting the following:

(i) exploitation and (re-) processing of the relevant EO-data sets (EO=Earth Observations) of two ECVs including ***surface ocean CO_2 partial pressure*** and ocean ***colour/primary productivity*** based on up-to-date algorithms and calibration-validation corrections.

(ii) integration and merging of the individual calibrated data sets for each of these ECVs to constitute comprehensive and well-characterized long term records for the high latitude and Arctic regions for the last 30-50 years that in turn can be assessed in the context of changes in marine carbon cycle.

4.1 General motivation

Why is the marine carbon cycle important for climate and the Earth system in general? There are three major relevant areas:

1. Integrated over time the ocean has been so far the main sink for human produced CO_2 emitted into the atmosphere through human activities (fossil fuel burning, land use change, cement manufacturing, e.g. *Raupach et al., 2007*). How does this sink change over time?
2. The uptake of human-produced excess CO_2 from the atmosphere by the ocean changes the chemical state of the ocean, in particular, it reduces in parallel the pH value and the carbonate saturation of seawater, a process generally termed "ocean acidification" (e.g. *Raven et al., 2005; Gattuso and Hansson, 2011*). How do these changes impact on marine ecosystem functioning (and possibly marine food resources)?
3. The ocean carbon cycle and the cycling of related elements (nutrients, oxygen) provide a multi-component system of passive tracers which can give important information on the combined physical and biogeochemical functioning of the ocean. It reflects in particular, the synchronous action of ocean circulation, gas exchange, biological particle production, and degradation of marine biogenic particulate matter (see, e.g., *Broecker and Peng, 1982; Sarmiento and Gruber, 2006*).

We will look here mainly at issues 1 and 2. For the high latitudes, a thorough monitoring of the marine carbon cycle is important, as the general "polar amplification" of climate change also translates into the biogeochemical realm. As compared to the global ocean, the sink for human-produced CO_2 is fairly small in the Arctic Ocean itself (e.g., *Lundberg and Haugan, 1996*) and of intermediate importance in the Greenland-Iceland Sea (e.g., *Jeansson et al., 2011*), in any case much less relevant than the Southern Ocean sink in total (e.g., *Tjiputra et al., 2010b*). Nevertheless, it is important to follow up this Arctic sink as a further control of regional carbon budgets (as relevant for control of emission reduction goals for specific nations/regions) and to record changes in nutrient/cycling and biological carbon cycling on the way towards a "*blue Arctic*". Especially interesting is the change in carbon uptake due to the high solubility of CO_2 at low temperatures (*Weiss, 1974*), but on the other hand low buffer capacity for excess CO_2 (*Sabine et al., 2004*). Uptake reductions due to rising CO_2 partial pressure in surface ocean and atmosphere will lead to a potentially accelerated decrease in ocean CO_2 uptake in the Arctic. Such a trend will, however, also

depend on the development of the seaice cover, of the hydrography (temperature, salinity), and the deep-water production mode (potentially away from shelf-plume induced deep-ventilation to more open ocean ventilation, see e.g. *Aagaard et al., 1985*).

Any change in air-sea CO_2 flux will also alter the atmospheric CO_2 concentration and hence the radiative budget of the atmosphere through the greenhouse effect. Due to the feedbacks between climate change and the carbon cycle and between rising CO_2 itself, the carbon cycle needs to be included in monitoring as well as prediction of climate change.

The decrease in Arctic ocean buffer capacity has its corresponding counterpart in strongly enhanced ph-reduction and carbonate-saturation reduction in the ocean surface layer at cold temperatures (e.g., *Orr et al., 2005; Steinacher et al., 2009*). During the past million years, the saturation for aragonite (the metastable polymorph of calcium carbonate $CaCO_3$) and for calcite (the less soluble $CaCO_3$ polymorph) has never become negative (undersaturation) (e.g., *Caldeira and Wickett, 2003*). This changes now quickly, and the first appearance of aragonite undersaturation is projected already for year 2016 (*Steinacher et al., 2009*). This progressing ocean acidification can potentially have severe impacts on marine ecosystem functioning. Especially, *pteropods* (small snails which produce aragonitic shell material) may be affected as well as cold water corals (e.g. *Guinotte and Fabry, 2008*), which both have important roles in the marine foodweb. Potential regional extinction of marine key species together with a projected decrease in oceanic primary (plant) production (e.g. *Steinacher et al., 2010*) can have severe implications for the standing stock biomass in the ocean and respective food production also for human societies.

It would be desirable to measure a series of multi-tracer variables in the ocean in order to follow-up the changing carbon cycle. We are still far away from such capabilities. In order to make at least an attempt to include key variables, we focus here on four essential variables for marine carbon cycling: 1. Surface-water CO_2 partial pressure, 2. atmospheric CO_2 partial pressure, 3. primary production (plant production, derived from remotely sensed chlorophyll), and 4. suspended calcium carbonate.

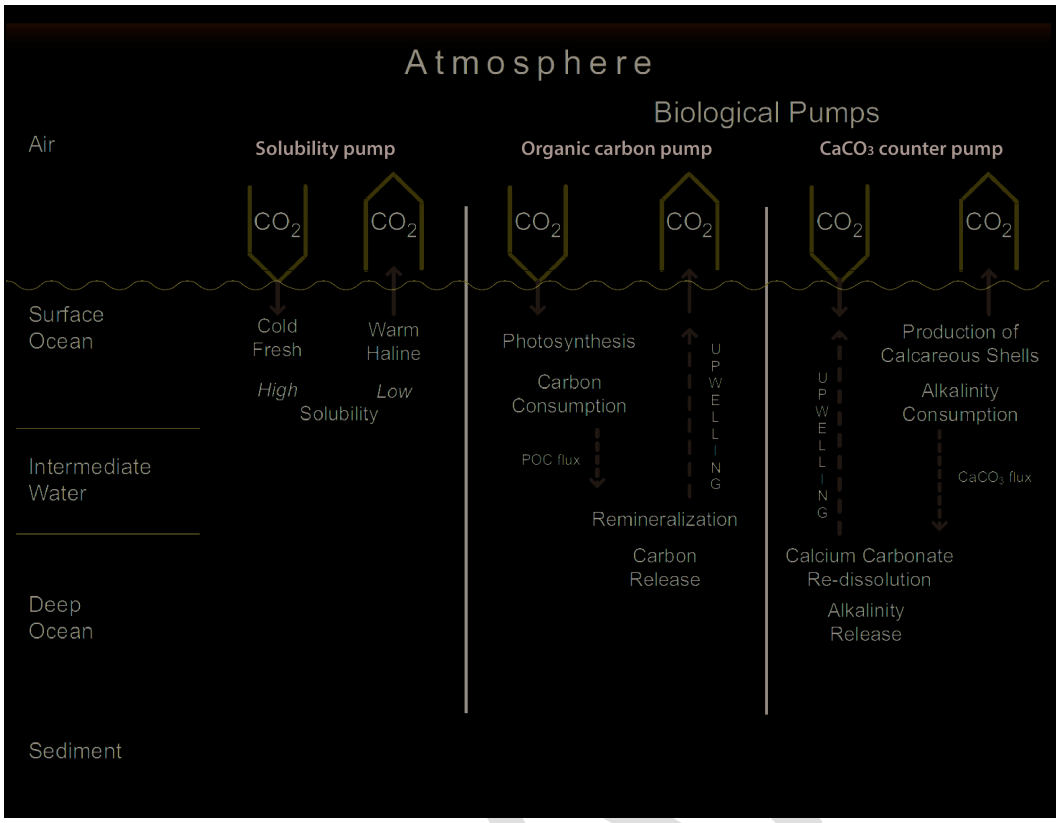

Figure 43 *The major marine carbon pumps through which the oceanic sources as well as sinks for atmospheric CO_2 are governed (following Denman et al., 2007; Heinze et al., 1991).*

With these four measurements, one covers at least one element of the various "oceanic carbon pumps", the physical-chemical "solubility pump", the "organic carbon pump", and the "CaCO3 counter pump" (*Volk and Hoffert, 1985*; Figure 43).

4.2 Description/source of data sets

Relevant Earth Observations data-sets have be exploited and reprocessed to build compatible arctic data-sets for the ECVs of the marine carbon cycle (oceanic and atmospheric pCO_2 as well as ocean colour/primary productivity). In detail, for oceanic pCO_2 the comprehensive data-sets SOCAT and LDEO have been combined leading to 796666 point observations north of 60° latitude in the period 1972-2011. Observations of atmospheric CO_2 were collected from the GLOBALVIEW-CO2 data integration project comprising 8 measurement stations north of 60° latitude with continuous extended records of CO_2 in the period 1979-2011. Monthly Primary Production fields were retrieved from the sensors MODIS and SeaWiFs. The data-product is available for different kinds of chlorophyll retrieving algorithms and Primary Production retrieving algorithms for the time period 1998-2010 (June-September) for the pelagic arctic area at a spatial resolution of 4 km. The MODIS sensor was furthermore utilized for the retrieval of monthly concentrations of Emilia huxleyi, coccoliths, diatomic chl and suspended inorganic carbon produces by Emilia huxleyi for the time period 2002-2010 (June-September) for the Arctic.

For the integration of the produced-data sets of pCO_2 and ocean colour/primary productivity with the biogeochemical model hindcast, the model MICOM-HAMMOC-M was deployed. It is based on the MICOM-HAMOCC version described in *Assmann et al., 2010*, but newly integrated in the NorESM framework. NorESM is a state-of-the-art Earth system model originating from the Community Climate System Model 4. It differs from the CCSM4 in the ocean component (MICOM), the ocean carbon cycle (HAMOCC) and the treatment of atmospheric chemistry, aerosol and clouds. In order to adapt MICOM-HAMOCC to NorESM, the north pole of the model was shifted from Siberia to Greenland. Moreover, the model resolution was refined, so that two model versions are now available: MICOM-HAMOCC-L (3.6° resolution) and MICOM-HAMOCC-M (1.125° resolution). Since the finer resolution is advantageous for the data-model comparison of MONARCH-A, MICOM-HAMOCC-M is deployed here. The synoptically forced coupled physical biological ocean model run is based on a spin-up integration of 800 years with a constant preindustrial atmospheric CO_2 concentration of 278 ppm, initialised with climatology-data from the World Ocean Atlas (WOA).

4.2.1 Surface-water partial pressure of CO_2 (pCO_2^{sea})

The data-set used for the model-observation comparison combines the Global Surface pCO_2 LDEO Database (*Takahashi et al., 2012***)** with the Surface Ocean Carbon Atlas (SOCAT) Database (*Pfeil et al., 2012*). Both databases are unique in terms of coverage and quantity of quality controlled observations of pCO_2/fCO_2. While the LDEO database consists of approximately 6.4 million quality controlled measurements of surface water pCO_2 made over the global oceans during 1957-2011, the SOCAT database includes fCO_2 data from more than 10 countries, producing an initial database composed of more than 1850 cruises from 1968 to 2007 with approximately 6.3 million measurements. Within the SOCAT dataset the fCO_2 measurements from an autonomous Neill underway pCO2 system onboard R/V G.O.Sars (utilised in WP3.2) are included.

For the combined SOCAT/LDEO dataset, all data north of 60°N from both SOCAT and LDEO were included. Before integrating the selected SOCAT data, the fCO_2 data from the SOCAT database were converted into pCO_2 data following the conversion formula of *Takahashi et al, 2012*. Finally the combined dataset consists of 796666 pCO_2 data points north of 60° latitude in the period 1972-2011, thereof 671278 SOCAT measurements (covering the time period 1981-2011 in the Arctic) and 125388 LDEO measurements (covering the time period 1972-2008 in the Arctic). The data was interpolated to the MICOM-HAMOCC-M grid, leading to a maximum of 46 month with observation for one grid cell within the time period 1972-2011. Figure 44 shows that this number of 46 months is an exception. While a few grid cells have data-coverage of over 20 month, most of the grid cells have data-coverage of less than 6 month and half of the oceanic arctic grid cells have no coverage at all. Due to this weak data-coverage a confident analysis of model performance and pCO_2 trends is difficult to achieve.

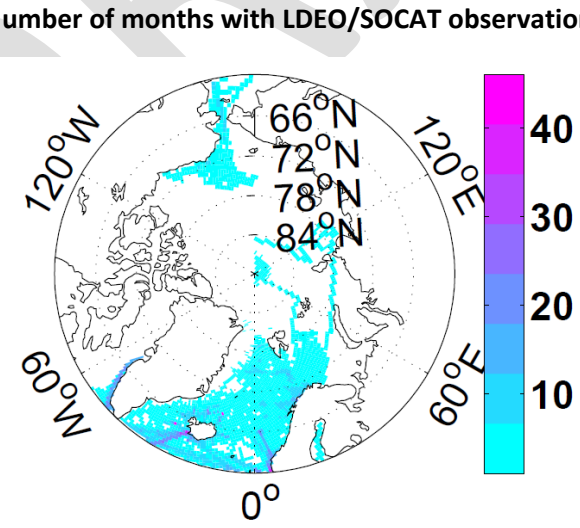

Figure 44. *Number of months with LDEO/SOCAT data-coverage per MICOM-HAMOCC-M grid-cell for the time period 1972-2011.*

Comparing the time series per grid point with the data-product it can be seen that the model reproduces the temporal behavior of the data well south of 66°N, between 60°W and 30°E with good correlations and moderate biases (Figure 45). In the areas between 30°E and 145°E and between

180°W and 150°W the data/model comparison shows large biases and mixed correlations. Both areas are characterized by sparse and only very recent observations (starting 1999) leading to a large uncertainty in the initialization of the model. The mixed correlations but moderate biases in the area north of 66°N, between 60°W and 30°E can be explained by the differences in the annual cycles of model and data. Here, the pCO_2 concentration of the model has its low point in June and increases afterwards, while the pCO_2-data shows low points in both June and August and only afterwards an increasing pCO_2 concentration (Figure 46). Due to the sparsity of the data north of 66°N, the data-points can highlight this negative summer feature (by having observations in months with differing model/data behavior) or ignore it (no observations in month with differing behavior), leading to grid cells with positive correlations directly next to grid cells with negative correlation (Figure 45).

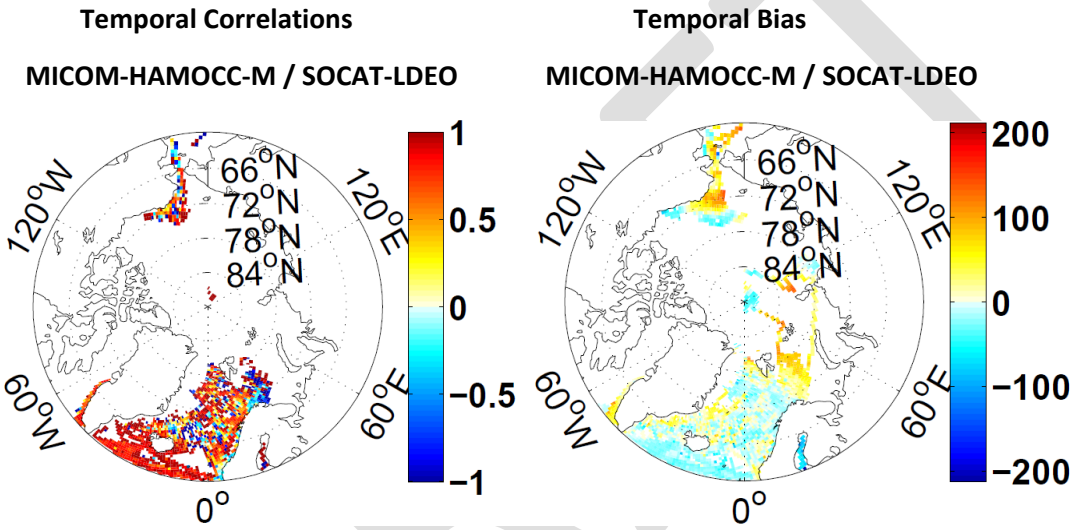

Figure 45. *Temporal Correlations (left) and Biases (right) of the pCO_2^{sea} data-model-comparison between the data-product SOCAT-LDEO and the model MICOM-HAMOCC-M for the time period 1972-2011.*

Timeseries at lon/lat: 7.89/69.07

Timeseries at lon/lat: 10.18/69.62

Timeseries at lon/lat: 1.71/66.09

Timeseries at lon/lat: 2.20/65.68

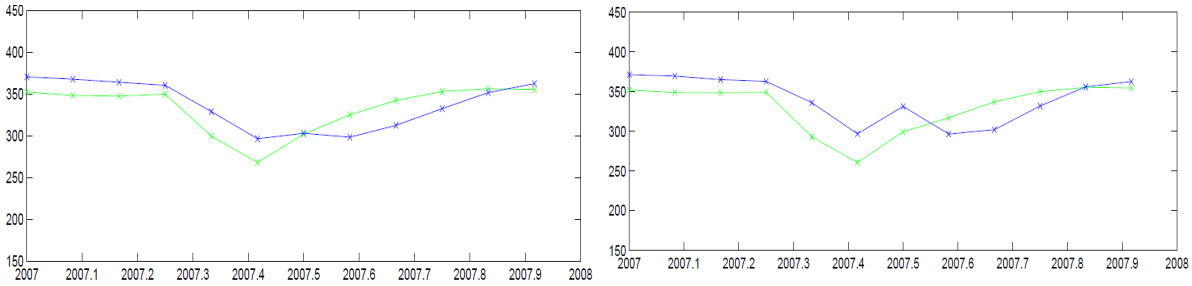

Figure 46. *Annual pCO_2^{sea} cycle of data-product SOCAT-LDEO (blue) and model MICOM-HAMMOC-M (green) for the year 2007 for four different grid points. Here, the bottom row illustrates the full annual cycles of model and data-product, while the top row illustrates how the sparsity of the data can easily lead to negative correlations (top row, left) and positive correlations (top row, right) in adjoined grid cells.*

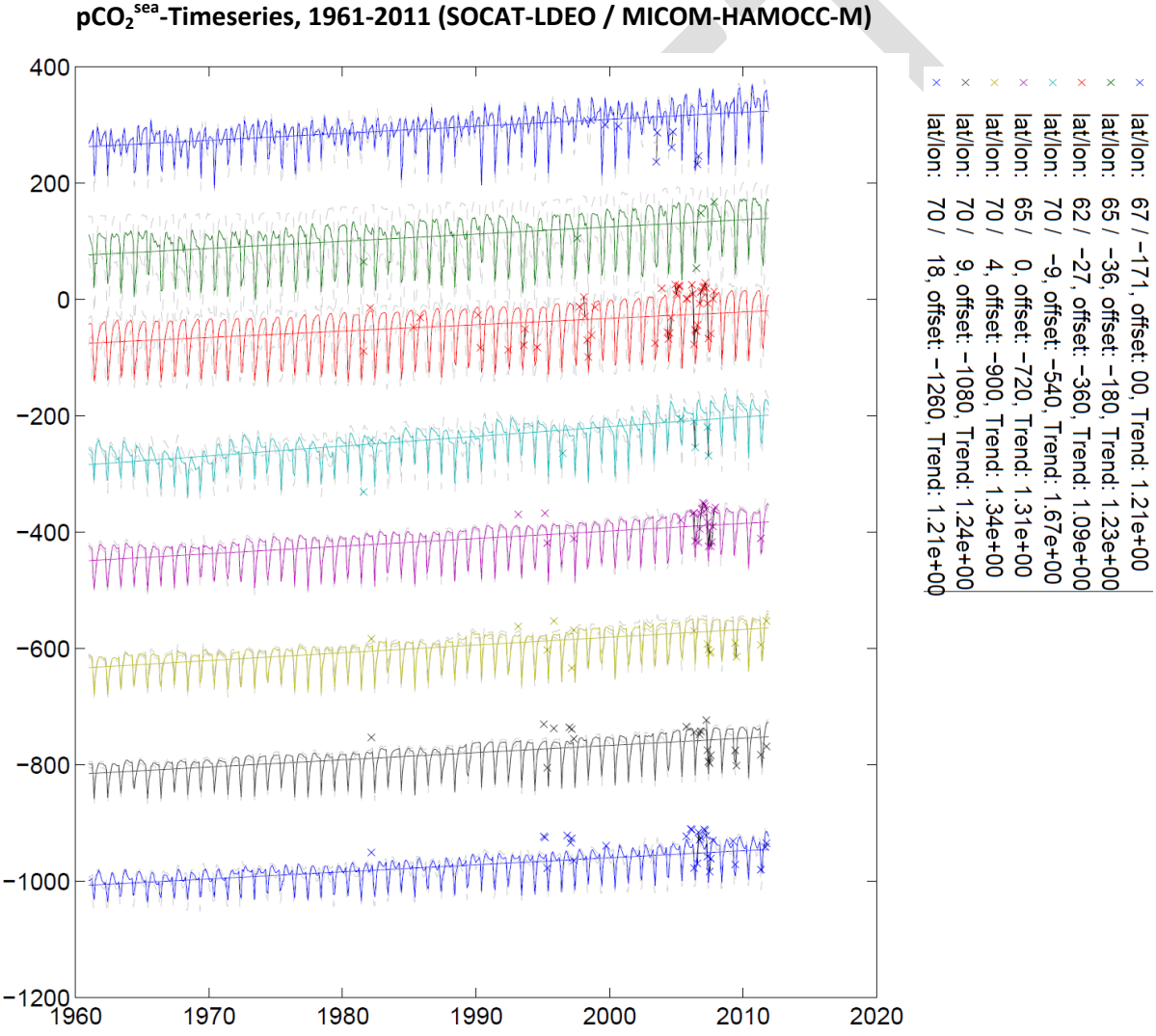

Figure 47. *Selected pCO_2^{sea} Timeseries and Trends for 1961-2011 as modelled by MICOM-HAMOCC-M (colored lines). SOCAT/LDEO-Observations are marked by colored crosses and black lines. Associated offsets and coordinates are denoted in the right panel.*

The timeseries for ocean pCO_2 at different coordinates (Figure 47) shows the consistency of the variable with a relative regular annual cycle and a positive trend for all coordinates for model and data. The complete modeled trend for the area north of 60°N is illustrated in Figure 48.

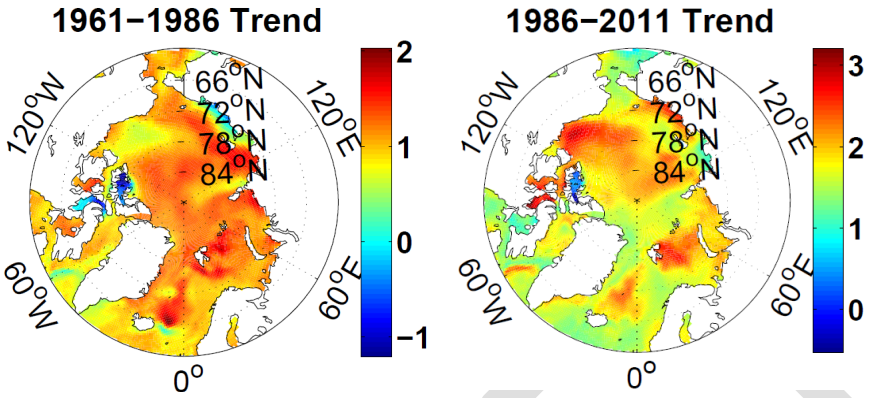

Figure 48. *pCO_2^{sea}-Trend for 1961-1986 (left panel) and for 1986-2011 (right panel) as modelled by MICOM-HAMOCC-M.*

The new combination of the SOCAT/LDEO datasets made a more comprehensive picture of pCO_2 in the Arctic possible, showing that the model MICOM-HAMOCC performs wells in the region between 60°W and 30°E. Nevertheless even the combination of LDEO/SOCAT does not give a comprehensive picture of pCO_2 in the remaining area. Here, measurements are spare and very recent (after 1999) and moreover mainly sampled in August/September. Due to this feature no full annual cycle is available, making a significant comparison impossible. Regular observations are a necessity in this area, so that trends and annual cycles can be estimated.

4.2.2 Atmospheric CO_2 partial pressure (pCO_2^{air})

Observations of atmospheric CO_2 were collected from the GLOBALVIEW-CO2 data integration project (*GLOBALVIEW-CO2, 2011*) comprising 8 measurement stations north of 60° latitude with continuous extended records of CO_2. Thereby each of the chosen measurement stations provides at least 7 years of observations with up to 32 years of observations. Their extended records comprise smoothed values as well as interpolated and extrapolated values defined for each month in the period 1979-2011 leading to 384 months covered with extended records for each station and hence 3072 data points. Combining the extended records of atmospheric CO2 with atmospheric pressure and water vapor pressure, atmospheric pCO_2 can be estimated. Since there are no continuously observed water vapor fields, the water vapor has to be calculated from SOCAT-values of salinity and temperature (here, SOCAT is the data-product of choice since atmospheric pressure is not included in the LDEO database). Due to the sparsity of the data it is very difficult to achieve a confident estimate for water vapor pressure and atmospheric pressure at the coordinates of the measurement stations, especially for the whole period 1979-2011. As a first approximation, it is here therefore assumed that atmospheric pCO2 equals the atmospheric CO2 concentration. This approach is consistent with the forcing of the model which utilizes the same approximation.

Looking at the statistics of the data/model-comparison, the forcing of the model produces the temporal behavior of the data-product well with correlations better than 0.8 and biases less than 10 ppm (in absolute value) for every station. Nevertheless, illustration of the monthly biases of the spatial distribution (Figure 49) shows that the amplitude of the annual cycle of the model is in general smaller than the amplitude of the data product. The scatter plots for February and August confirm this finding (Figure 49). Besides this difference in amplitude there is very good agreement between spatial distribution of data product and model with correlations better than 0.96.

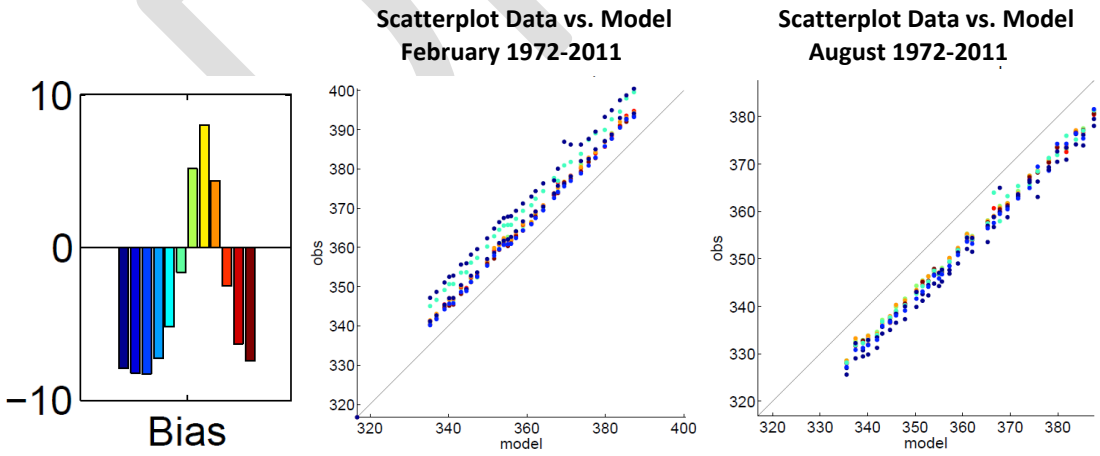

Figure 49. *Monthly pCO_2^{atm} Bias of the spatial distribution for data product/model forcing for 1972-2011 (left panel) and pCO_2^{atm} Scatterplots of data vs model for February (middle panel) and August (right panel) for 1972-2011. Bias and Scatterplots confirm that the amplitude of the annual cycle of the model forcing is smaller than the one of the data-product.*

Comparing the timeseries of the selected measurement stations to the model forcing (Figure 50) it can be seen that the variable pCO_2^{atm} has a relative regular annual cycle and a positive trend for all coordinates for model and data. Due to face that each grid point of the model uses the same forcing, the trend from 1961-2011 is 1.47 ppm at every grid point. This positive linear trend for the time period 1961-2011 is only an approximation for the development of pCO_2^{atm}. The actual gradient is weaker in the first years (associated to a linear trend of 1.176 ppm for 1961-1986) and stronger in the last years (associated to a linear trend of 1.72 ppm for 1986-2011) showing the accelerated increase rate of pCO_2^{atm}.

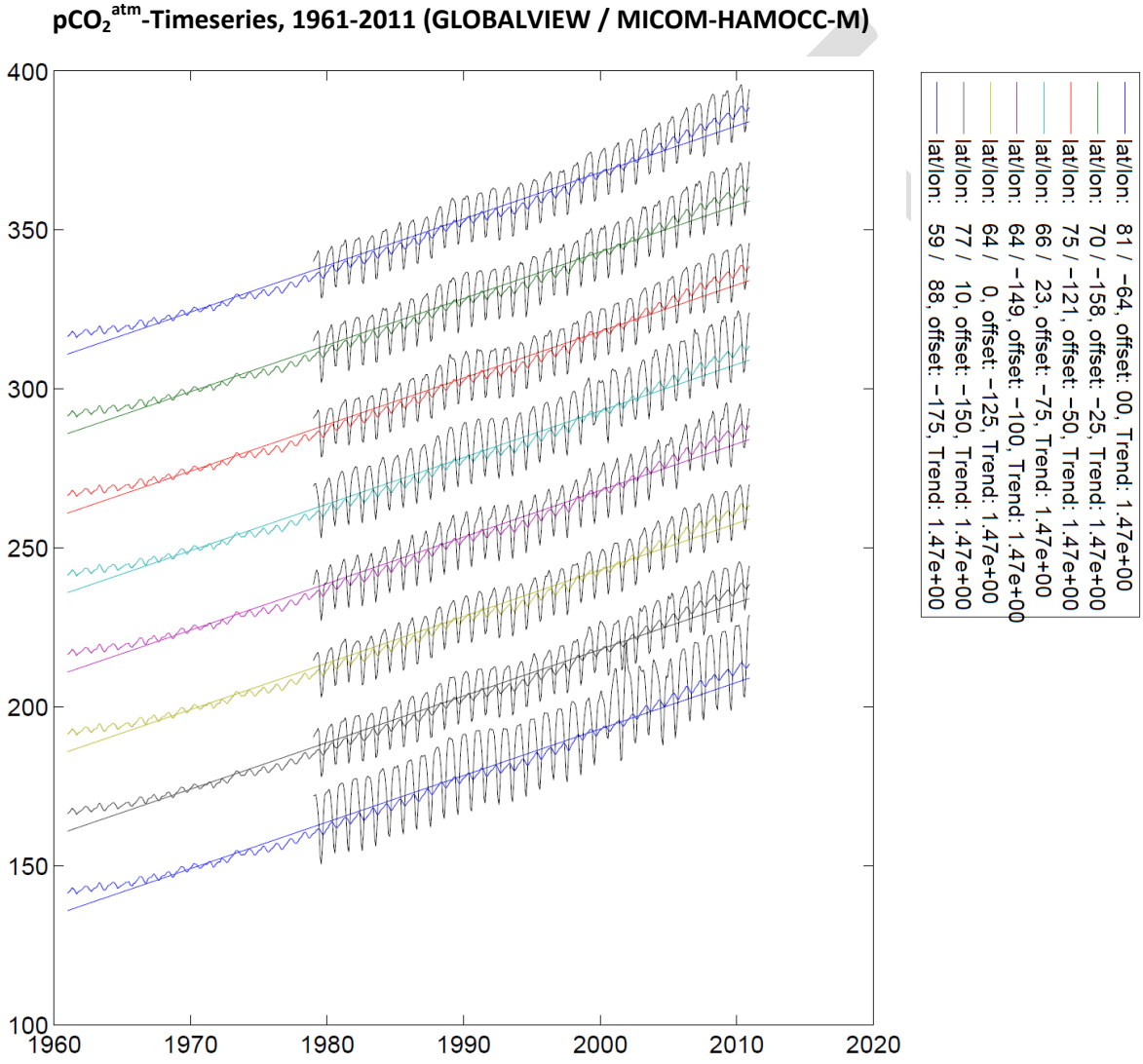

Figure 50: *Selected pCO_2^{atm} Timeseries and Trends for 1961-2011 as modelled by MICOM-HAMOCC-M (colored lines). Extended GLOBALVIEW-records are marked by black lines. Associated offsets and coordinates are denoted in the right panel.*

For a relatively uniform variable like CO_2^{atm}, the GLOBALVIEW-CO_2 dataset shows in an impressive way that continuous measurements at a fixed coordinate are by far more important than a large amount of widespread observations. The 8 measurement stations of CO_2^{atm} give a comprehensive picture of the development of CO_2^{atm} for the period of 1979-2011.

4.2.3 Primary Production

Monthly Primary Production fields were retrieved from the sensors MODIS and SeaWiFs. For both sensors, 3 color data sources were investigated, retrieved with either the standard NASA OC3/4 retrieval algorithm (spatial resolution: 4km for MODIS and 9km for SeaWiFS) or the NASA GSM retrieval algorithm (spatial resolution: 4km for MODIS and 9km for SeaWiFS) or the NASA GSM algorithm combined with a procedure of cloudiness partial removal from the Oregon State University data (spatial resolution: 9km). Furthermore, three different algorithms for the retrieval of Primary Production were tested for the Arctic Basin, namely the algorithms of *Behrenfeld et al., 1997*, *Behrenfeld et al., 2005,* and *Marra et al., 2003*. Since the combination of the retrieval from the Oregan State University together with the Behrenfeld algorithm showed the best results for the Primary Production retrieval (in comparison with shipborne Primary Production measurements at stations across the Arctic Basin, see *Petrenko et al., 2012*), the associated dataset from the SeaWiFs sensor is utilized for the data/model comparison. This dataset is available for the time period 1998-2010 (June-September) leading to a maximum of 48 month with observation for one MICOM-HAMOCC-M grid cell. Smaller numbers of observation-months are resulting from cloudiness and ice cover (*Petrenko et al., 2013;* see Figure 51). Since ice cover of model and data-product differ, all grid points which show different ice-cover than the data-product are taken out of the comparison for the respective point in time.

Number of months with observations of Primary Production

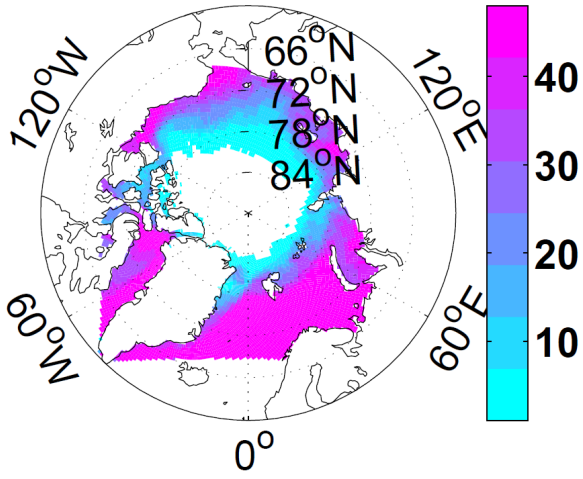

Figure 51. *Number of months with SeaWiFs-Primary Production data-coverage per MICOM-HAMOCC-M grid-cell for the time period 1998-2010.*

Looking at the correlations of the temporal comparison per grid point (Figure 52) it can be seen that the model reproduces the temporal behavior of Primary Production well. Correlations of exactly 1.0 or -1.0 are due to the sparsity of the data. Biases are as well moderate except for relatively high biases at the northern Greenland coast and the Russian coast section at the Barents Sea. Nevertheless, monthly correlations and bias are only moderate showing that the model is able to produce the general temporal behavior, but not the monthly trend. Furthermore, it becomes apparent that the model is not able to produce the annual peak of Primary Production in coastal regions in August/September. Selected timeseries for different coordinates confirm that the model

produces the general behavior of Primary Production well, but is not able to reproduce monthly trends (Figure 53). The timeseries show furthermore that the annual cycle of Primary Production is irregular in both range and form. For relatively short timescales like the period 1998-2010, it is therefore very likely that the calculated linear trend is governed by just a few extreme values which are not representative for a general trend in Primary Production. The relatively low values of the modeled trends for the time period 1961-2011 (Figure 54) support this thesis. No significant trend can be confirmed for Primary Production in the Arctic within the last 50 years.

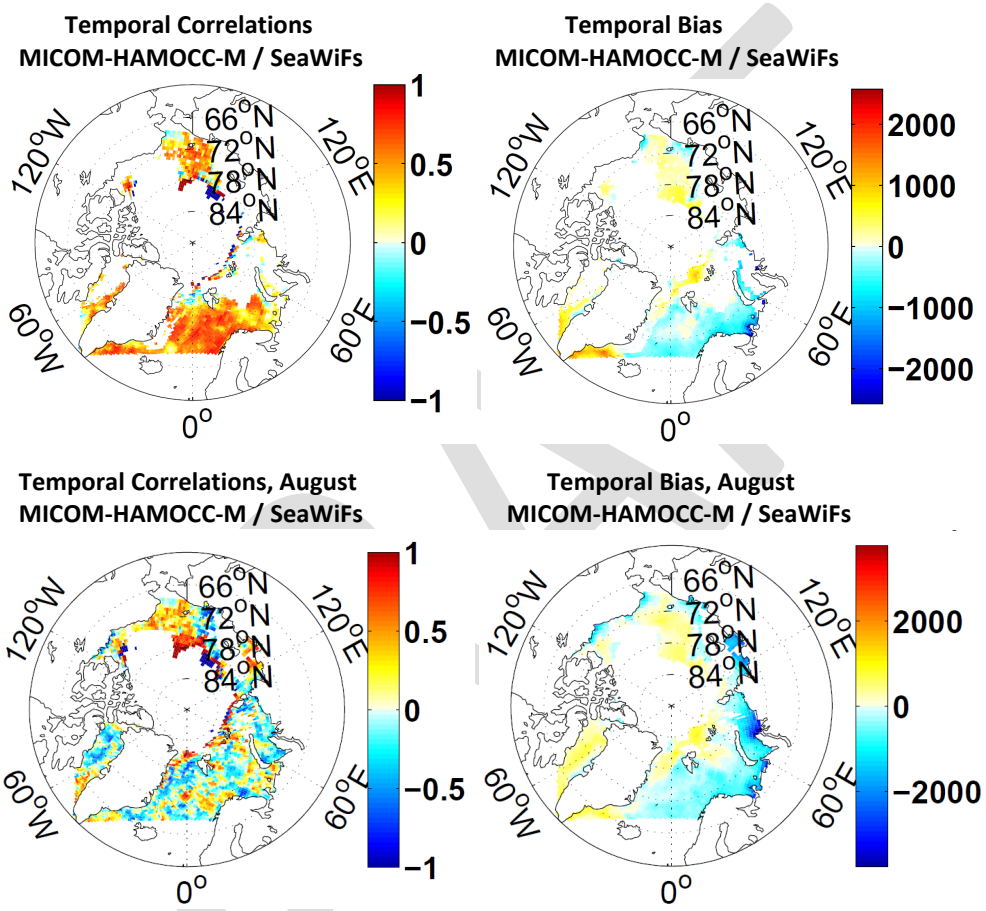

Figure 52. *Temporal Primary Production Correlations (left) and Biases (right) of the data-model-comparison between the data-product SeaWiFs and the model MICOM-HAMOCC-M for the time period 1998-2010. Depicted are both Correlations and Biases for the whole time period (top row) as well as Correlations and Biases for only the month August (bottom row).*

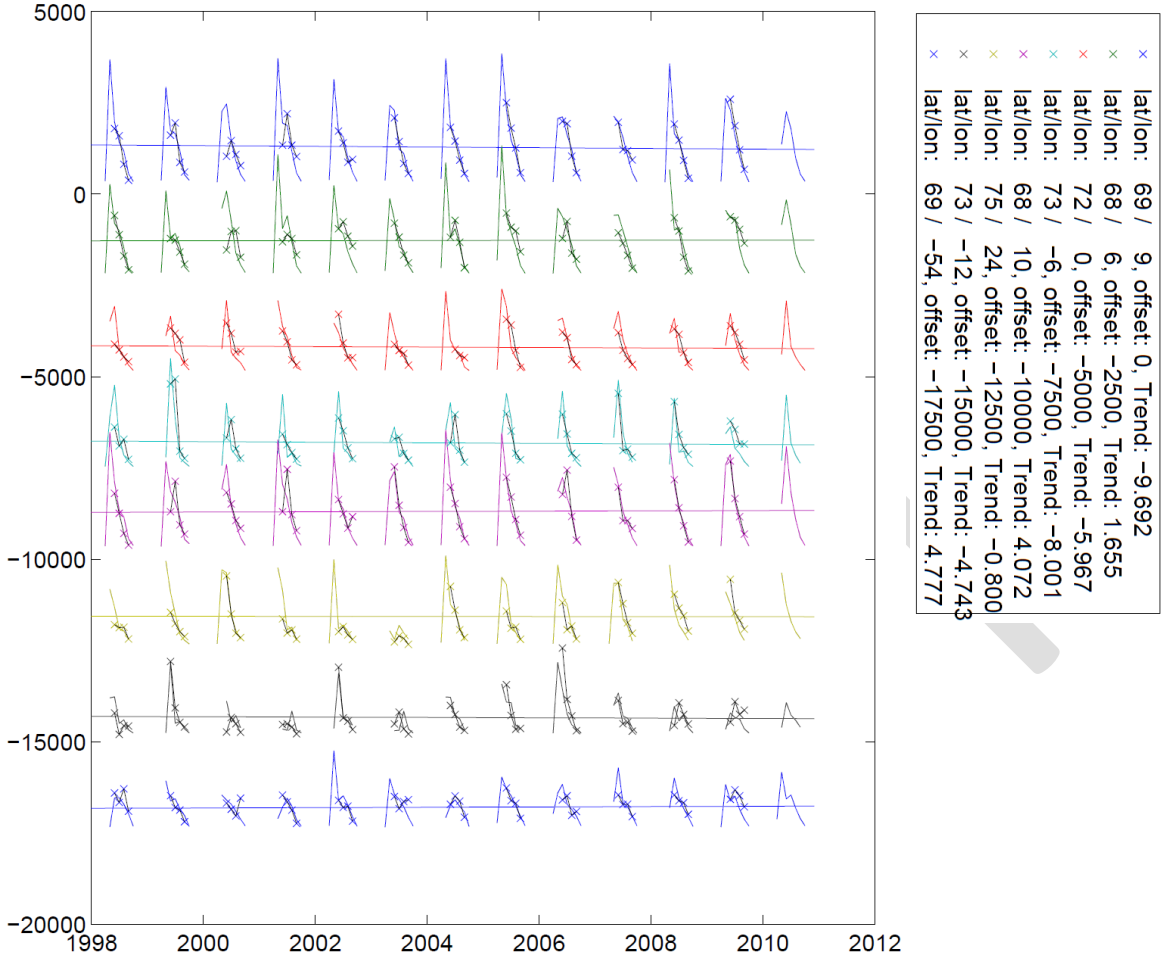

Figure 53. *Primary Production: Selected Timeseries and Trends for 1998-2010 as modelled by MICOM-HAMOCC-M (colored lines). SeaWiFs-Observations are marked by colored crosses and black lines. Associated offsets and coordinates are denoted in the right panel.*

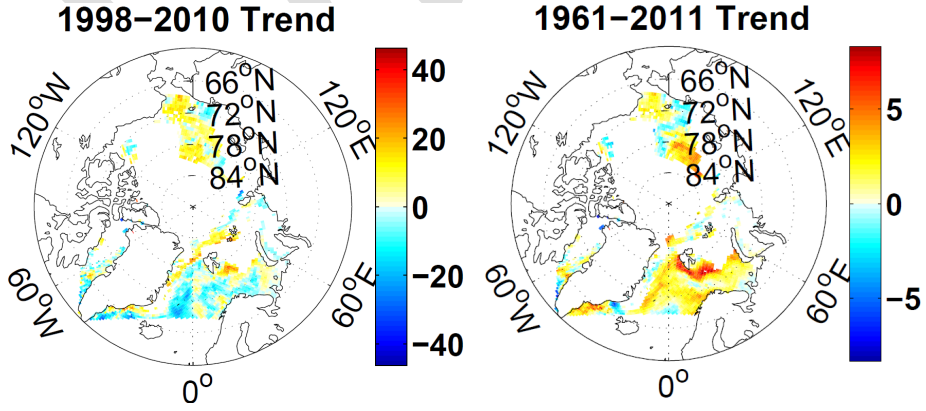

Figure 54. *Primary Production-Trend for 1961-2011 (left panel) and for 1998-2011 (right panel) as modelled by MICOM-HAMOCC-M.*

Suspended Calcium Carbonate. Apart from the retrieval of Primary Production, the MODIS sensor was utilized for the retrieval of monthly concentrations of Emilia huxleyi, coccoliths, diatomic chl and suspended inorganic carbon produced by Emilia huxleyi for the time period 2002-2010 (June-September) for the Arctic. For this purpose, a modified BOREALI algorithm has been employed for areas of Emilia huxleyi blooms (*Korosov et al., 2009; Petrenko et al., 2013*). The retrieved suspended inorganic carbon was compared to the suspended Calcium Carbonate of MICOM-HAMOCC-M. The 5364922 observations were interpolated to the MICOM-HAMOCC-M grid leading to a maximum of 34 month with observation for one MICOM-HAMOCC-M grid cell. Smaller numbers of observation-months are resulting from cloudiness and ice cover (Figure 55). Since ice cover of model and data-product differ, all grid points which show different ice-cover than the data-product are taken out of the comparison for the respective point in time.

Number of months with observations of Suspended Inorganic Carbon

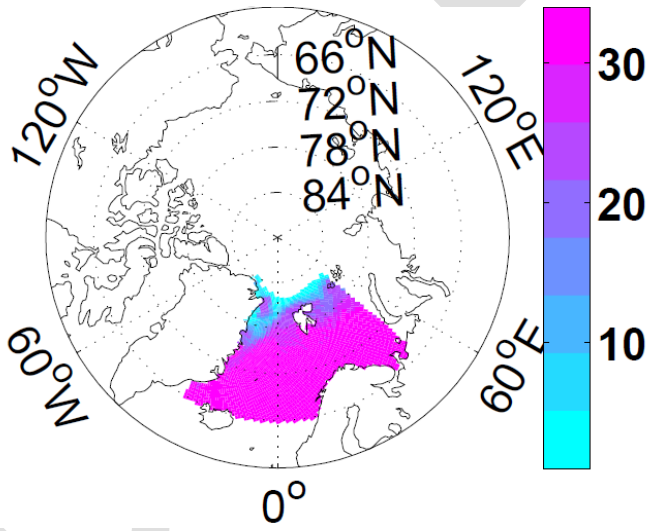

Figure 55. *Number of months with MODIS-Suspended Inorganic Carbon data-coverage per MICOM-HAMOCC-M grid-cell for the time period 2002-2010.*

The results of the comparison between data-product and model show poor correlations for both spatial and temporal distributions (Table 1and Figure 56). These poor correlations are due to the fact that the non-zero concentrations of the data-product appear mainly in coastal regions (specifically north of Norway) while the non-zero concentrations of the model appear all over the GIN-seas and the Barents Sea (Figure 57). Furthermore the data-product has a peak in concentrations in August for most of the data-points, but the model output has a peak in concentrations in June (Figure 58). Finally the model shows a regular annual cycle in both form and magnitude while form and magnitude of the annual cycle of the data-product are varying a lot (Figure 58).

Spatial Correlations MICOM-HAMOCC-M / MODIS

Month	June	July	August	September
Correlation	-0.069	-0.026	-0.102	-0.129

Table 1. *Spatial Correlations of the data-model-comparison between the data-product of Suspended Inorganic Carbon from MODIS and $CaCO_3$ of MICOM-HAMOCC-M for the time period 2002-2010.*

Temporal Correlations,

MICOM-HAMOCC-M / MODIS

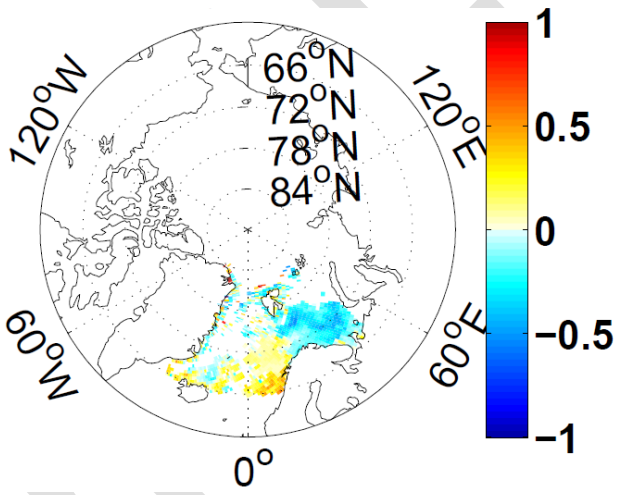

Figure 56. *Temporal Correlations of the data-model-comparison between the data-product MODIS and the model MICOM-HAMOCC-M for the time period 2002-2010.*

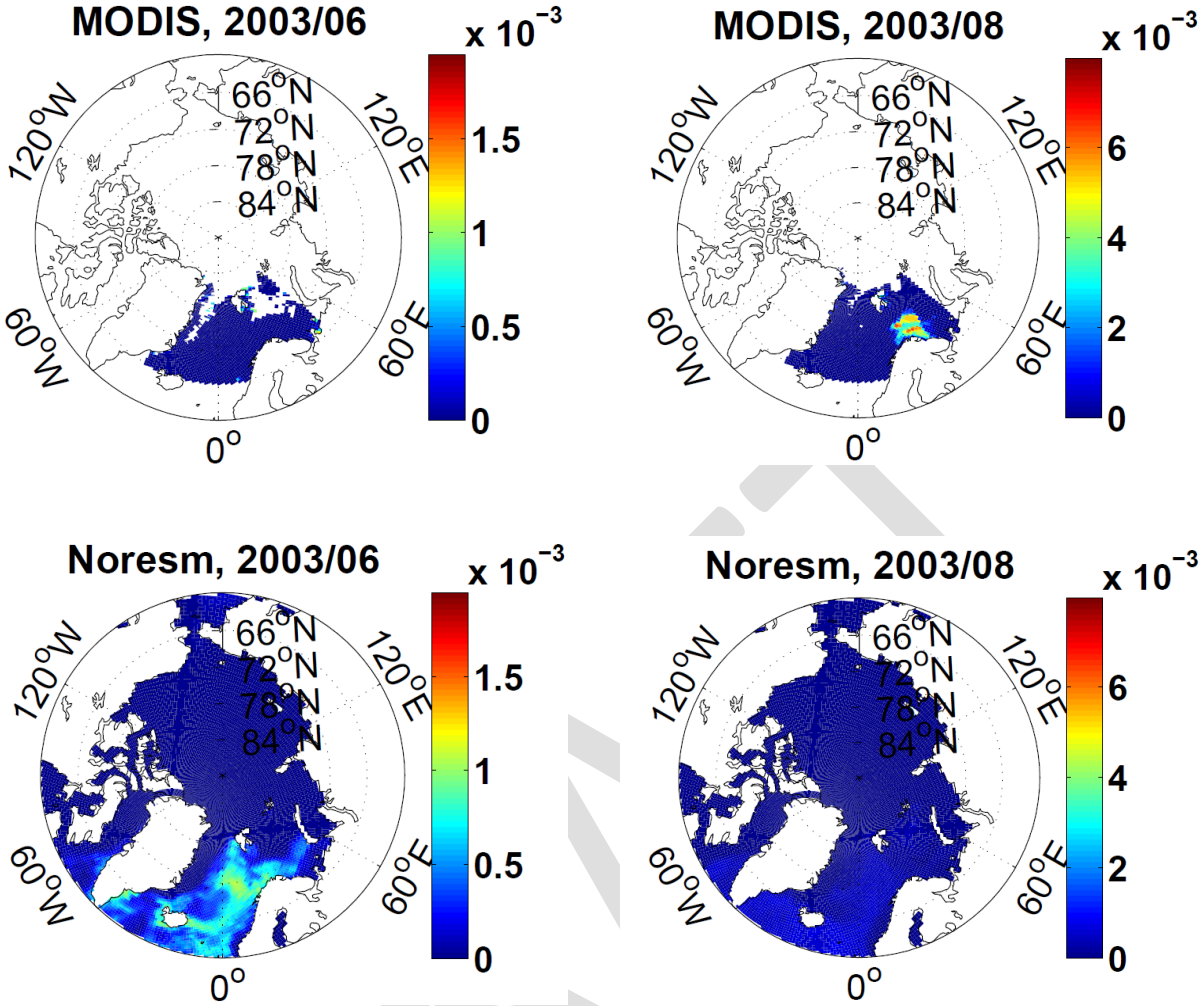

Figure 57. *Suspended Inorganic Carbon concentrations retrieved from MODIS (top row) and $CaCO_3$ concentrations of MICOM-HAMOCC-M (bottom row) for June 2003 (left panels) and August 2006 (right panels).*

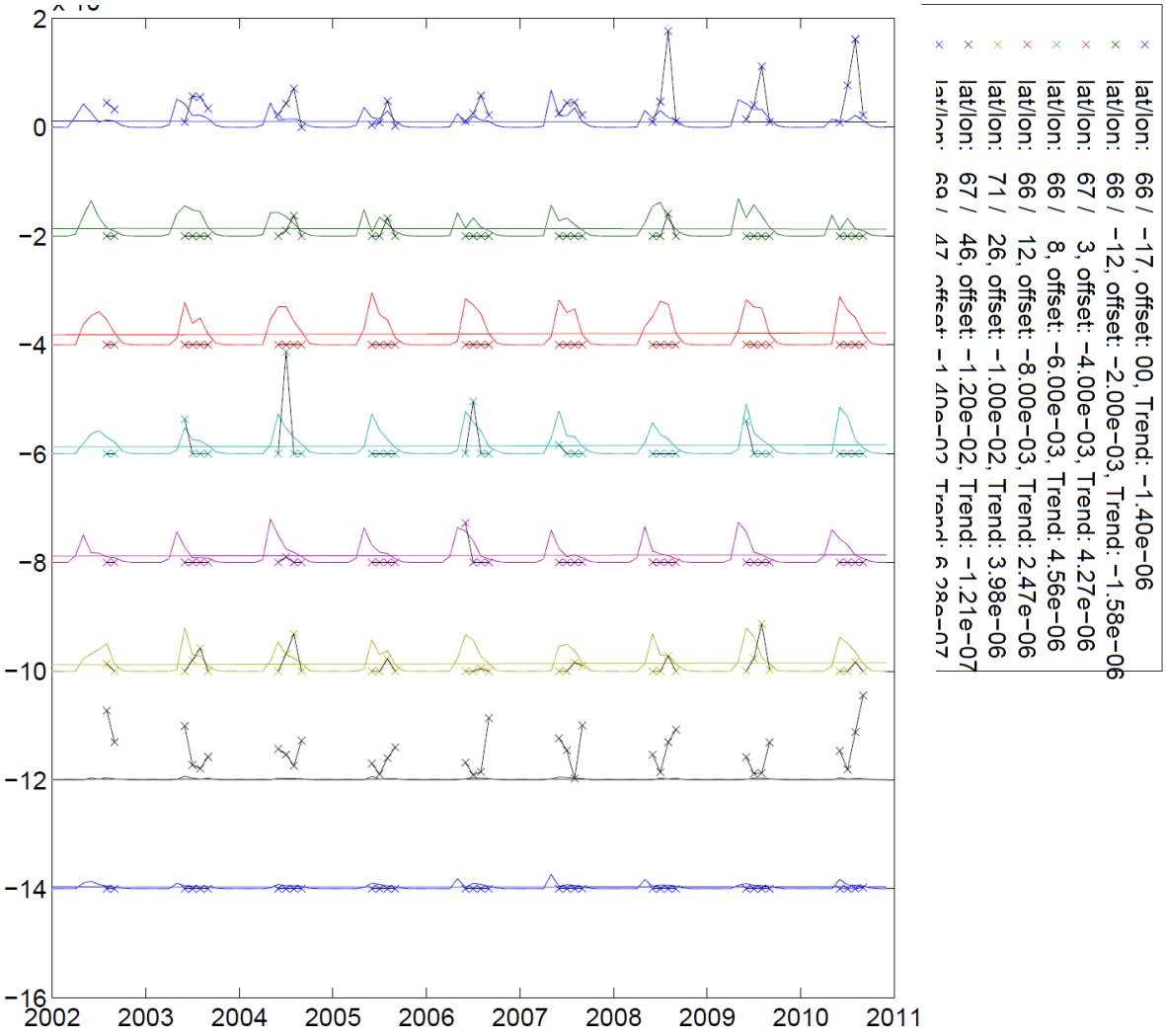

Figure 58. *Selected Timeseries and Trends for 2002-2010 as modelled by MICOM-HAMOCC-M (colored lines). MODIS-Observations are marked by colored crosses and black lines. Associated offsets and coordinates are denoted in the right panel.*

The comparison of concentrations of suspended $CaCO_3$ in the surface ocean from shell material belonging to the species Emiliania huxleyi (i.e. the available data-product) and the modelled tracer "suspended $CaCO_3$" is to be considered with care: The model includes all shell material of $CaCO_3$ forming organisms in one tracer (coccolithophoridae-shells, forminifera-shells, and also aragonitic shells - though the later are not explicitly accounted for in the model in general) and all formation of $CaCO_3$ shells is lumped together into an export flux of particulate inorganic carbon. Suspended $CaCO_3$ can re-enter the surface boxes of the model through circulation and mixing. Therefore, one can get at best a semi-quantitative hint on whether the model works through the observed data in our case. Nevertheless, this is some progress as one traditionally does not have any reliable information on biogenic $CaCO_3$ available in the upper ocean from observations. For a more straightforward comparison between model and observations, observation based estimates of export production rates of $CaCO_3$ would be needed.

5 Synthesis

5.1 Highlights of relevant ECVs

The time series and products of the 11 relevant ECVs have then been assessed and synthesized with respect to mutual forcing and feedback mechanisms associated with changes in terrestrial carbon and water fluxes, sea level and ocean circulation and the marine carbon cycle in the high latitude and Arctic regions. They are available at the MONARCH-A web portal (monarch-a.nersc.no), either directly or linked to other existing data repositories. Some highlights of the findings regarding the ECVs are provided below:

Snow Cover

- Clear indication of a decrease in snow cover extent during spring and earlier snow disappearance for the majority of northern latitudes for the period 1989-2009 from both observations and models. This agrees with recent studies [e.g. *Derksen and Brown*, 2012]. However, over this period, snow cover extent and the dates of snow appearance remain largely unchanged during autumn.

- The last 30 years of Globsnow data show varying trends in snow water equivalent (SWE) in different parts of the boreal region; nonetheless, for the period 1989-2009, areas of significant decrease in SWE dominate northern latitudes and spatially correlate with regions exhibiting earlier snow disappearance dates. This raises the question of whether reduced spring snow extent and earlier disappearance of snow is mainly a consequence of decreases in snowfall. However, reductions in SWE over the past 20 years average only 3-4%, but the dates of snow disappearance have shifted by about a month. This suggests that other factors have contributed, most likely the increase in air temperature observed over northern latitudes.

- By using transect field data collected in the former Soviet Union from 1966 to 1996 [*Krenke*, 2004] the SWE retrieval of Globsnow was evaluated, and was found to capture not only the magnitude of SWE in the region but also the seasonal and inter-annual variation observed in the field data. Globsnow was therefore used to produce trends of SWE for 1980-1996, and these were compared with trends produced by land surface models over the same period. All models captured the major trends observed in northern latitudes over that period, mainly a significant negative trend in Europe and a positive one in central Siberia. However, the inter-annual variation observed in Globsnow was described correctly only by one model, JULES.

River Discharge

- Detailed comparison between the Global River Data Center (GRDC) and model runoff is carried out for the Fraser, Yenesei and Ob basins. GRDC data shows that the Fraser decadal mean runoff decreased between the 1990s and the 1970s, while for the Yenesei it increased, and for the Ob it was stable but with significant inter-annual variability. The model captures the trend in the Fraser but less well in the Yenesei, while it tracks the variability on the Ob very well. However, it shows greater inter-annual variability than the data.

Permafrost

- The permafrost temperature is observed to be increasing at most sites where we have long records, but there are only a few such sites, so instead focus is set on active layer depth (ALD), the permafrost parameter with the best available spatial distribution and temporal duration of data. The ALD has tended to increase in the Russian sub-arctic zone, Mongolia and China over the last decade(s). The strongest trends have been observed in the Russian European North and Chukotka. Different parts of Alaska and Canada exhibit different trends. Increases in ALD are observed at sites in the interior, but both increasing and decreasing trends have been detected in areas close to the ocean. Drawing general conclusions from these data is hampered by the sparse, non-uniform spatial sampling of the observations and the fact that ALD has substantial spatial variability, since it depends on soil composition and very different values of ALD can be measured at points several kilometers apart. The trends in ALD observed at these sites can also be different.

Ice Sheet Mass Balance

- Spatial–temporal variability and changes of Greenland ice sheet elevation from 1992 to 2010 are analyzed from merged ERS-1, ERS-2 and Envisat satellite radar altimeter data. A methodology for determining inter-satellite biases was developed and applied, in order to merge measurements from these different satellites and to create continuous and consistent time series of ice sheet elevations. An average elevation change rate of 1.9±0.3 cm/year from 1992 to 2010 over 81% of the Greenland ice sheet area.

- Surface height changes for the Greenland Ice Sheet were also estimated based on NASA's laser altimetry satellite mission ICESat giving a distinct thinning of the ice sheet along the southeast and west coasts, and a smaller but consistent thickening in the interior part of the ice sheet. This is in agreement with the trends derived from ERS/ENVISAT.

- The GRACE estimate of the total mass changes for the entire ICESat period (October 2003-March 2008) is -204 +/- 21 Gt/yr. In comparison, the conversion of the ICESat heights into mass changes using firn densification and snow density models, results in a larger estimate of -240 +/- 28 Gt/yr.

Sea Level

- On average over the 60-year time span (1950-2009), we find a positive Arctic Coastal Mean Sea Level (CMSL) trend of 1.62 +/- 0.11 mm/yr (after correcting for GIA and IB). The results indicate that between 1950 and the mid-to-late 1990s, Arctic CMSL was mostly driven by internal climate modes, in particular the AO, possibly through changes in wind-stress and associated ocean circulation (although quantitative analyses of the latter effects remain to be performed), as well as ocean mass changes. Since the mid-to-late 1990s, Arctic CMSL shows a marked rise of 4.07 +/- 0.65 mm/yr.

- In order to generate a new dataset suitable to study sea level variability and trend in the Arctic Ocean, satellite altimetry data from the T/P, ERS-1, ERS-2, GFO, Envisat, Jason-1 and Jason-2 missions have been reprocessed to reduce uncertainties associated with presence of sea ice, tidal influences, uneven sampling and lack of spatial coverage. The improvements concern: (1) the mean sea surface; (2) the ocean tide model; (3) the regional multi-mission merging; (4)

the sea level grid computation using the objective analysis approach. These improvements lead to a much larger availability of the sea level data in the Arctic region.

- Model results clearly show that in the North Atlantic, Nordic Seas and coastal zones of Norway and even Russia, significant changes also affected sea level as of mid-to-late 1990s, in agreement with other recently reported changes in Arctic climate during the last 1-2 decades (i.e., Serreze and Barry, 2011). This period (last 15 years) may represent a transition in the Earth system evolution as recently suggested by Peltier and Lutchke (2009) and Roy and Peltier (2011). The results also show an increase of the ocean mass component along the Norwegian coast, at least partly explained by the recent acceleration in land ice loss as reported by numerous recent studies.

Sea Ice Volume

- Sea ice freeboard heights and dynamic topography of the Arctic Ocean observed from ICESat altietry 2003-2008 have been updated on a spatial resolution 0.1°x0.2°. The sea ice freeboard heights show good spatial correlation between the distribution of first year ice and multiyear ice observed by QuikSCAT scatterometer data. Overall, a decrease in the Arctic Ocean mean freeboard heights of approximately 10-15 cm is observed since the beginning of the ICESat observations in 2003.

Sea Ice Drift

- Sea ice drift from sea ice models have been compared to observations from satellite and in situ buoys and drift station measurements over the last 30-50 years.

- Sea ice extent estimates from evaluated ocean multi-model reanalyses as well as from remote sensing data have been intercompared and assessed. Dramatic reduction in summer sea ice extend have been encountered in the last decade with the record minimum sea ice extent in September 2012.

Ocean Current

- The GOCE based MDT shape and spatial pattern representing the mean from 1993-2009 for the North Atlantic, Nordic Seas and the Arctic Ocean show elevation changes from the high in the Arctic Ocean to the low in the sub-polar gyre in the North Atlantic reaching about 0.9 m. The regional shape of the MDT with the orientation of the dominant slopes in the different sub-domains reveals the presence of the circulation pathways in: (i) the sub-polar gyre south of Greenland; (ii) the inflow of Atlantic Water respectively between Iceland and the Faroe Islands and between the Faroe and Shetland Islands; (iii) the continuous northward flowing Atlantic Water towards the Arctic Ocean; (iv) the southward flowing East Greenland Current; (v) the Beaufort Gyre; and (vi) the transpolar drift in the Arctic Ocean.

- Model/data intercomparison of the MDT show that there is a large spread among models.

CO2 Partial Pressure

- The investigation of surface-water CO2 partial pressure, atmospheric CO2 partial pressure, primary production, and suspended calcium carbonate showed that both the oceanic and the

atmospheric CO2 partial pressure are very consistent variables which have a very regular annual cycle and a very similar behaviour all over the Arctic. In contrast, both primary production and suspended calcium carbonate show an irregular annual cycle in both range and form varying over the Arctic.

Ocean Colour

- The correlations of the temporal comparison per grid point reveal that the model reproduces the temporal behavior of Primary Production well. Biases are as well moderate except for relatively high biases at the northern Greenland coast and the Russian coast section at the Barents Sea. Nevertheless, monthly correlations and bias are less good/moderate showing that the model is able to produce the general temporal behavior, but not the monthly trend. Furthermore, it becomes apparent that the model is not able to produce the annual peak of Primary Production in coastal regions in August/September.

- Comparison between observed and modelled suspended inorganic carbon show poor correlations for both spatial and temporal distributions, most likely due to the fact that the non-zero concentrations of the data-product appear mainly in coastal regions (specifically north of Norway) while the non-zero concentrations of the model appear all over the GIN-seas and the Barents Sea. Furthermore the data-product has a peak in concentrations in August for most of the data-points, but the model output has a peak in concentrations in June. Finally the model shows a regular annual cycle in both form and magnitude while form and magnitude of the annual cycle of the data-product are varying a lot.

Near Surface Wind

- It is found that satellite-derived wind products have a higher spatial resolution, and has much better performance with regard to detection of strong (storm) wind patterns. However, the model wind is also a first requirement and a constraint for the satellite-based wind retrieval procedure. A comparison between several wind products shows that, although the remotely sensed winds are assimilated in ERA Interim, the weather model cannot adequately resolve the small-scale (100-200 km) storm tracks and corresponding wind speeds. QuikSCAT, CERSAT/IFREMER blend and PO.DAAC blend seem to be quite successful in storm detection, whereas ASCAT and ERAI fail in detection of the wind speeds exceeding 20 m/s.

The monarch-a.nersc.no web portal will be the entry point for users to find and download these data.

5.2 Land processes

Models provide the most effective means of synthesizing the land variables, since they not only contain most of these variables, but inherently contain the interactions between them through the processes embodied in the models. This is illustrated by the system diagram in Figure 59, which shows how variables considered in this report contribute to the carbon and water cycles, and how they contribute in the models.

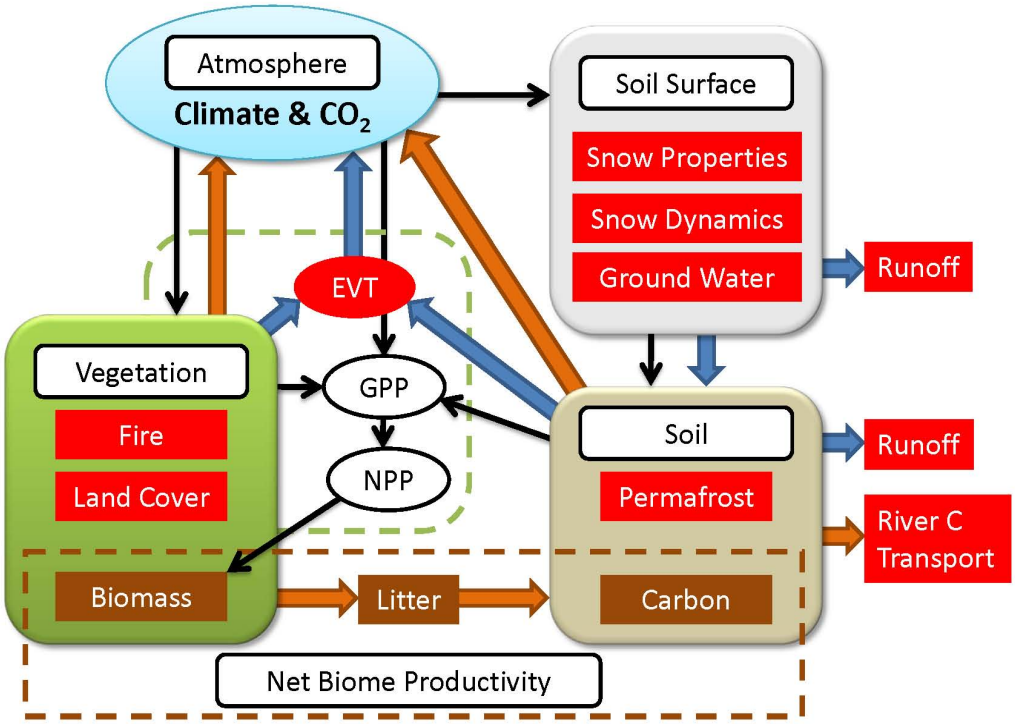

Figure 59. *System diagram illustrating how models integrate processes and variables in representing the carbon and water cycles.*

Hence model analysis and model runs have been used to answer the following questions:

1. Do the models exhibit the observed trends (or lack of them) for the ECVs considered, both globally and regionally?
2. What effects do these trends or their absence have on the carbon and water balances?

Note that these questions are not considered for the surface water and fire ECVs. Surface water is not represented in the models, and fire is omitted for two reasons:

(a) the data series is too short to investigate trends
(b) the disparity between models and data is so great that investigation of trends using the models would not be meaningful.

Model-data comparisons of decadal trends in snow variables: The results presented in Sections 2.2.1 and 2.2.2 clearly indicate a decrease in snow cover extent during spring and earlier snow disappearance for the majority of northern latitudes for the period 1989-2009; this agrees with recent studies [e.g. *Derksen and Brown*, 2012]. However, over this period, snow cover extent and the dates of snow appearance remain largely unchanged during autumn. The last 30 years of Globsnow data show varying trends in SWE in different parts of the boreal region; nonetheless, for the period 1989-2009, areas of significant decrease in SWE dominate northern latitudes and spatially correlate with regions exhibiting earlier snow disappearance dates. This raises the question of whether reduced spring snow extent and earlier disappearance of snow is mainly a consequence of decreases in snowfall. However, reductions in SWE over the past 20 years average only 3-4%, but the dates of snow disappearance have shifted by about a month. This suggests that other factors have contributed, most likely the increase in air temperature observed over northern latitudes (Figure 14).

By using transect field data collected in the former Soviet Union from 1966 to 1996 [*Krenke*, 2004] the SWE retrieval of Globsnow was evaluated, and was found to capture not only the magnitude of SWE in the region but also the seasonal and inter-annual variation observed in the field data. Globsnow was therefore used to produce trends of SWE for 1980-1996, and these were compared with trends produced by land surface models over the same period. All models captured the major trends observed in northern latitudes over that period, mainly a significant negative trend in Europe and a positive one in central Siberia (Figure 60). However, the inter-annual variation observed in Globsnow was described correctly only by one model, JULES.

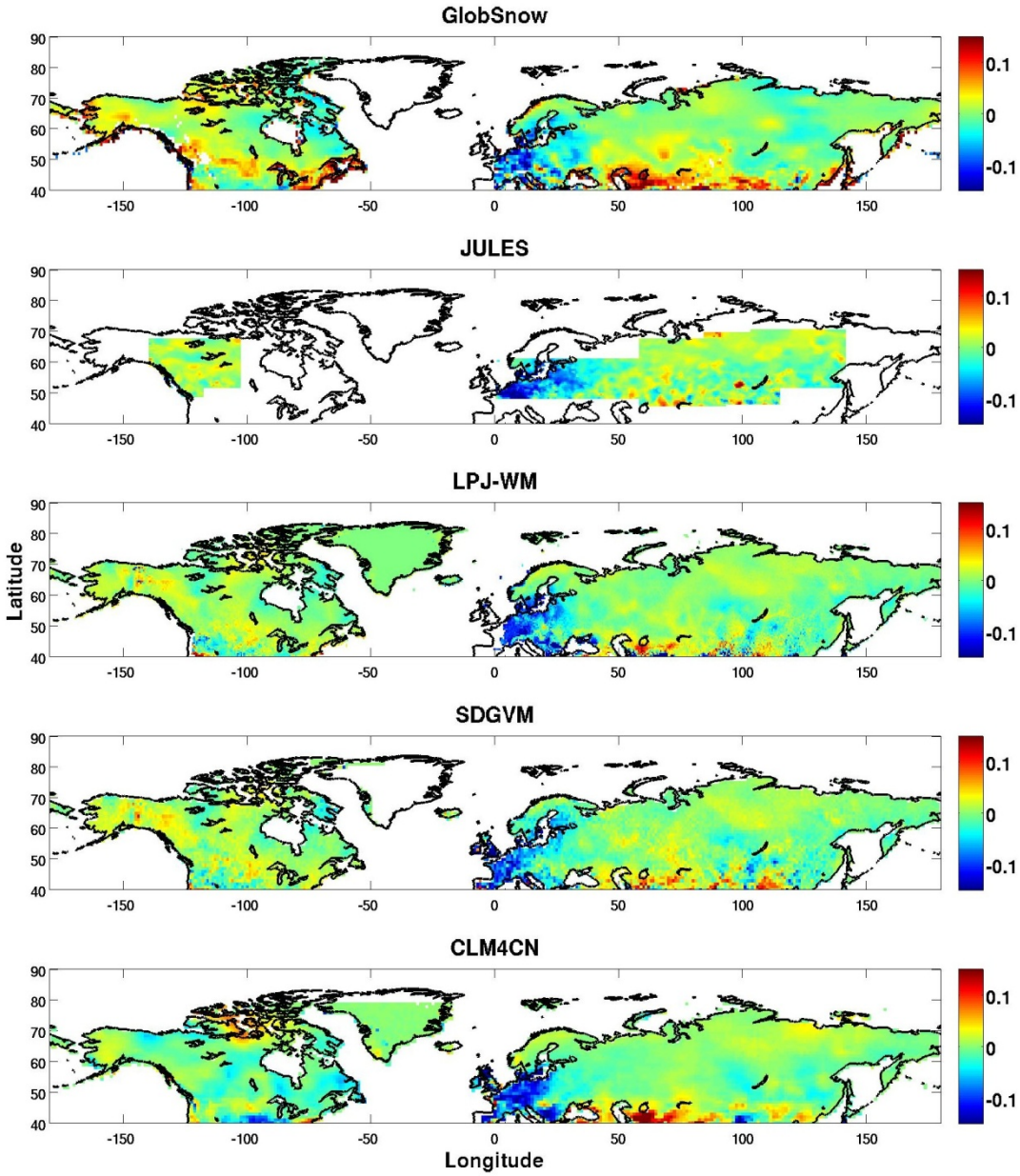

Figure 60. *Trends of SWE over the period 1980-1996 for GlobSnow and 4 land surface models. The statistic illustrated is the ratio of the annual rate of change of the maximum SWE divided by the mean value of the maximum SWE over the same period.*

The pan-boreal water balance: Driving the Sheffield Dynamic Global Vegetation Model (SDGVM) with the CRU data set produces a gradual increase in pan-boreal runoff of ~10% up until 2000 followed by a decrease to 2006 (Figure 61). A longer time series would be required for both climate data and runoff observations to determine whether the modeled drop in runoff after 2000 is significant.

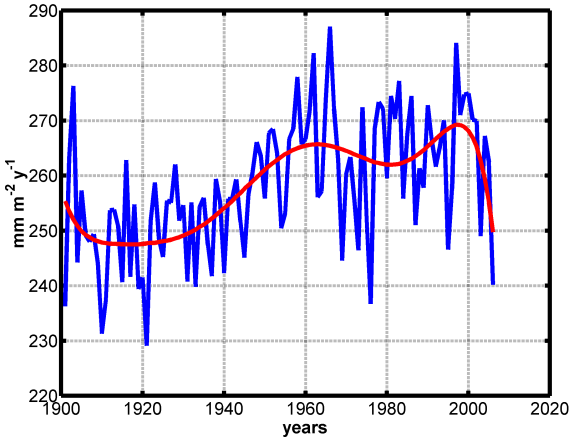

Figure 61. *Mean annual pan-boreal runoff for the period 1900-2005 for latitudes above 50° N as calculated by the SDGVM driven by the CRU climate dataset. Note that the y-axis is not scaled to zero.*

These overall trends mask significant differences between basins, mainly driven by precipitation, as indicated by the spatial patterns of mean runoff difference between the 1990s and 1970s shown for both GRDC data and SDGVM calculations for several large high-latitude basins in Figure 62. The model and data agree on the sign of the trends except in the Ob, where GRDC shows little change while SDGVM indicates increased runoff. Greater decreases in runoff are given by the model than the data in the Mackenzie and Lena basins.

A more detailed comparison between GRDC and model runoff is given in Figure 63 for the Fraser, Yenisei and Ob basins. GRDC data shows that the Fraser decadal mean runoff decreased between the 1990s and the 1970s, while for the Yenisei it increased, and for the Ob it was stable but with significant inter-annual variability. The model captures the trend in the Fraser but less well in the Yenisei, and it tracks the variability on the Ob very well. However, it shows greater inter-annual variability than the data, and this may be the cause of the apparent difference between the data and model seen in Figure 62 for the Ob.

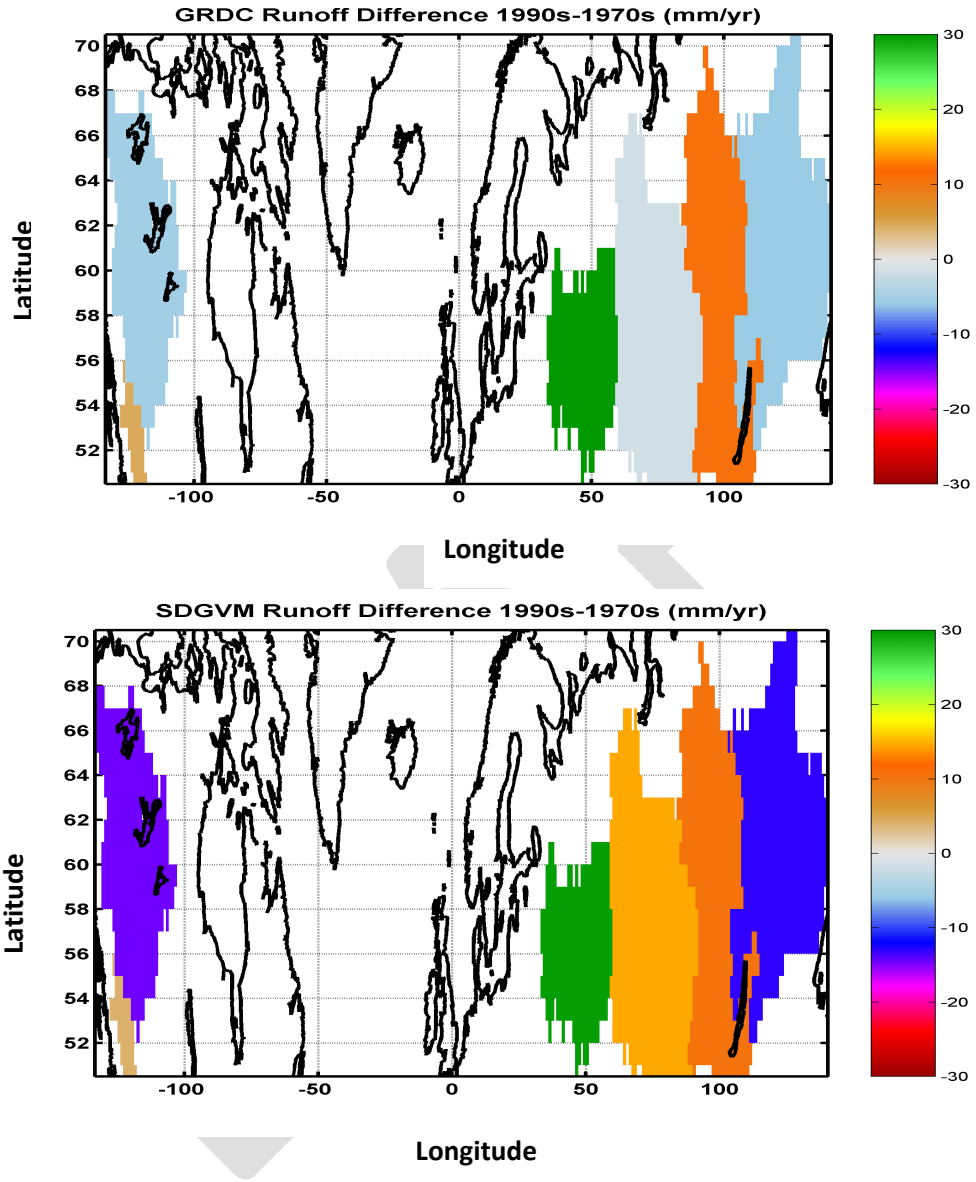

Figure 62. *Differences between the mean annual runoff [mm/yr] in the 1990s and the 1970s for several large high latitude basins derived from the GRDC data and as calculated by the SDGVM.*

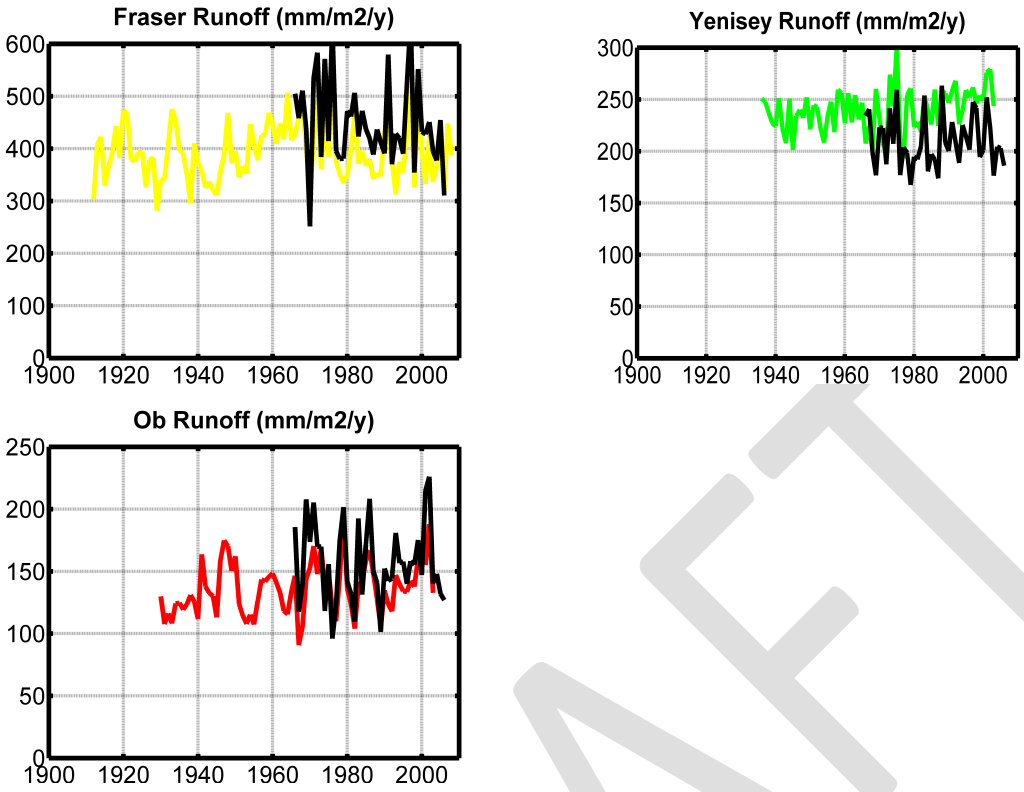

Figure 63. *GRDC runoff data (colours) with SDGVM modeled runoff (1966-2006) shown in black.*

Discussion: There are strong connections between fire, permafrost, biomass, land cover and net carbon balance (Net Biome Production), as analysed in Kantzas et al. (2013). Figure 64 is taken from this paper and shows the mean annual magnitude of all the fluxes making up the carbon balance over the period 1981-2006 for latitudes northward of 50° N. NPP, NEP and NBP indicate Net Primary Production, Net Ecosystem Production and Net Biome Production, and R_h is heterotrophic (soil) respiration, as calculated by three state-of-the-art Dynamic Vegetation Models. The fluxes are related by NEP = NPP - R_h and NBP = NEP – Fire. It can be seen that fire is a very significant contributor to the net carbon balance, but models differ considerably as regards both its absolute magnitude and its magnitude relative to NBP.

The available time series of data on carbon cycle processes, especially fire, are at present too short to provide statistically significant evidence of trends over the last few decades, particularly since the area burnt by boreal fires exhibits large inter-annual variability. The models all exhibit much too small temporal and spatial variability in burned area compared to the satellite record, so the current model representation of fire in models is clearly inadequate. This casts doubt on their ability to estimate other important processes, such as the dynamics of permafrost. Since fire is a very significant factor in determining the magnitude and even the sign of the net carbon flux at high latitudes, the model-based estimates of the net carbon flux must therefore be considered as provisional. This is a deficiency that needs to be urgently considered with respect to the present and future capacity and design of the observing system

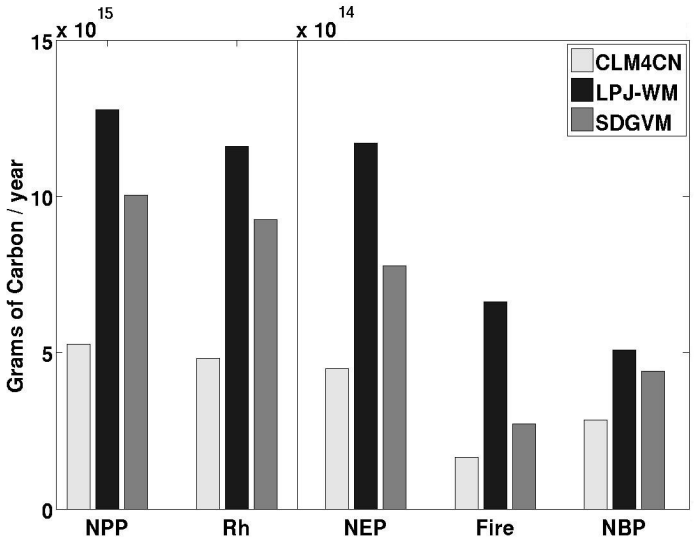

Figure 64. *Pan-boreal estimates of mean annual NPP, R_h, NEP, fire emissions and NBP for the CLM4CN, LPJ-WM and SDGVM models for the period 1981-2006 and latitudes northward of 50° N. NPP and R_h are given in units of PgC yr^{-1}, while the scale for the other three fluxes is an order of magnitude less.*

For the water balance the situation is much better, with long time series of both high quality satellite-derived estimates of Snow Water Equivalent and runoff data for all the major high latitude basins. Models and data are in broad agreement, so that the data can be interpreted in terms of processes. In addition, model-data and model-model differences can be explained in terms of driving data (especially precipitation) and differences in model representations and parameterisations.

5.3 Ocean circulation and sea surface height

Our model results show (Figure 42d), that there is increase in curl of surface ocean currents in BGR, and one of possible reasons for this is lesser SIC and SIT. After the mid of 1990s episodes of September SIC decrease and strengthening of surface current curl coincide, while for SIT correlation is not well established. The relative role of changes in ice properties and atmospheric characteristics for ocean currents variability should be further investigated.

As mentioned before, faster and more “anticyclonic” currents in the BGR lead to accumulation of freshwater in the upper part of the water column. Model simulations indicate (Figure 42e) that since the middle of the 1990s there is steady increase of freshwater content in BRG, accelerated after 2005. This increase is observed from direct oceanographic measurements, and is also indicated by satellite SSH data. A schematic representation of the processes, that potentially affect changes of the SSH in the BGR is shown in Figure 65. Reprocessed data of sea level anomalies let us investigate, at least to some extent, variability of SSH in BRG. Sea ice cover prevents satellites from getting sufficient amount of information during winter time, so only yearly mean values are shown. Both model and data agree (Figure 42f) on large positive SSH trend since the mid 1990s. The model results also indicate that this trend is the largest one since at least 1970. It is possible, that the ocean in the BGR experiences some sort of a shift in its state during about the last 15 years. This shift involves both sea

ice and the upper ocean. Whether the same shift is observed for the whole Arctic Ocean is not clear, but there are also considerable changes in other regions of the Arctic Ocean, and in the North Atlantic

Recent warming of the Arctic region has been reported by Karcher et al. (2003) and Polyakov et al. (2005). These studies observed significant changes in temperature of the Arctic and Nordic Seas during the 1990s. Rigor and Wallace (2004) showed that areal coverage of multi-year sea ice decreased even during 1989-90 when the AO was in extremely high index state. This could be explained by longer ice free periods during summer, the open ocean absorbing more heat, preventing formation of sea ice (positive feedback mechanism). Warming in the Nordic Seas reduces heat loss from the Atlantic water before it enters the Arctic Ocean, with warmer Atlantic water propagating into the Arctic region. Carton et al. (2011) investigated the interannual/decadal variability of Atlantic water in the Nordic and adjacent seas. Their analysis shows a succession of four multi-year warm events occurring in the region between 1950 and 2009 (i.e., the same time span as in the present study), the last reported warm event began in the late 1990s and persisted for nearly a decade. Our results clearly show that in the North Atlantic, Nordic Seas and coastal zones of Norway and even Russia, significant changes also affected sea level as of mid-to-late 1990s, in agreement with other recently reported changes in Arctic climate since 1-2 decades (i.e., Serreze and Barry, 2011). This period (last 15 years) may represent a transition in the Earth system evolution as recently suggested by Peltier and Lutchke (2009) and Roy and Peltier (2011). Finally our results also show an increase of the ocean mass component along the Norwegian coast, at least partly explained by the recent acceleration in land ice loss as reported by numerous recent studies.

As one can see from the above discussion, SSH is an important integral parameter, that reflects changes in many characteristics of the system. It is therefore important to continue and improve its observational record. In order to understand the relative contributions of different processes and their interaction it is also important to observe or provide model estimates of additional quantities, such as freshwater content.

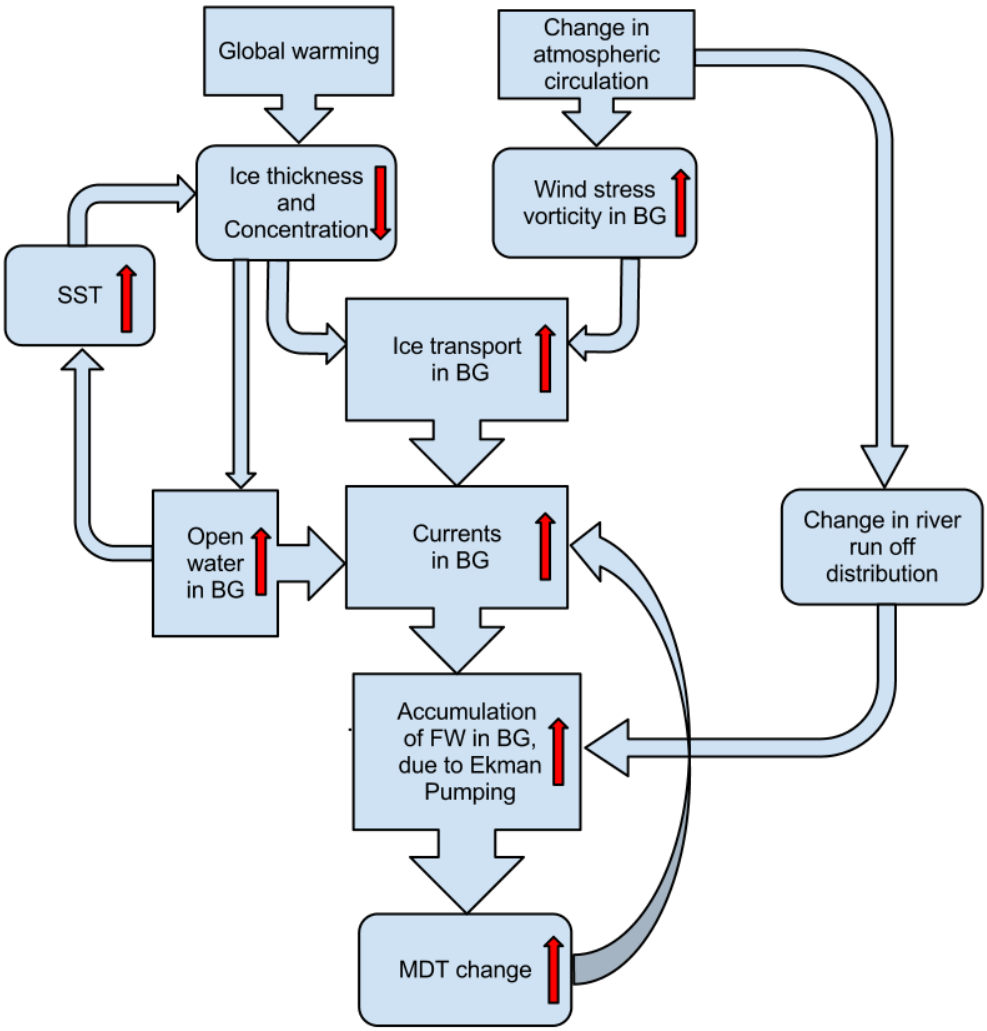

Figure 65. *Schematic representation of changes and feedbacks in Beaufort Gyre Region.*

5.4 The marine carbon cycle

The investigation of surface-water CO_2 partial pressure, atmospheric CO_2 partial pressure, primary production, and suspended calcium carbonate showed that both the oceanic and the atmospheric CO_2 partial pressure are very consistent variables which have a very regular annual cycle and a very similar behaviour all over the Arctic. In contrast, both primary production and suspended calcium carbonate show an irregular annual cycle in both range and form varying over the Arctic.

While a few well distributed measurement stations with monthly observations are sufficient to get a comprehensive picture for consistent ECVs, it is relatively difficult and costly to get a comprehensive picture of non-consistent ECVs. Here, widespread measurements for at least 40 years are needed to capture both different regional behavior (e.g. coastal versus non-coastal behavior) and their trends (for relatively short timescales it is very likely that the calculated linear trend is governed by just a few extreme values which are not representative for a general trend in the ECV).

Unfortunately the provided data-sets of the non-consistent ECVs primary production and calcium carbonate production cover both relatively short time-scales, so it was neither possible to confidently validate the model nor to determine significant trends. Nevertheless are the delivered comprehensive Arctic datasets of both calcium carbonate and primary production a preciosity since there is traditionally not much reliable information for both variables. The collected information allows for a first data-model comparison. It is highly important that the sensor-retrievals for both variables are continued in the following years so that a confident analysis with a determination of significant trends is hopefully possible.

The datasets for the consistent ECVs oceanic and atmospheric pCO_2 are by far more comprehensive and allow for a more confident data-model comparison (for oceanic pCO_2 at least within the region between 60°W and 30°E). The measurement stations of atmospheric CO_2 providing effectively a good characterization of CO_2 with continuous measurement on a few, well distributed locations. A similar measurement network would be desirable for oceanic pCO_2. Still the LDEO/SOCAT database allows for confident statements about the trends of pCO_2^{sea} in the region between 60°W and 30°E. Here, the model MICOM-HAMOCC-M calculates an increasing trend that accelerates with time (Figure 66). The trend for 1961-1986 varies here from 0.2 ppm to 2.0 ppm, while the trend for 1986-2011 varies from 1.25 ppm to 2.6 ppm. Meanwhile the trend of pCO_2^{atm} is 1.176 ppm for 1961-1986 and 1.72 ppm for 1986-2011. In comparison, the trend of pCO_2^{sea} is increasing quite rapidly, especially for high latitudes. At some grid points the trend of pCO_2^{sea} is even higher than the trend of pCO_2^{atm} leading to a decreasing CO_2 uptake.

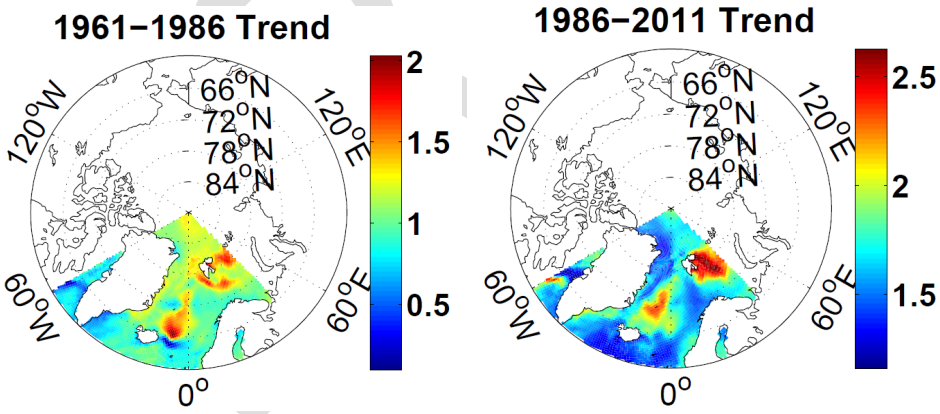

Figure 66. *pCO_2^{sea}-Trend for 1961-1986 (left panel) and for 1986-2011 (right panel) as modelled by MICOM-HAMOCC-M.*

5.5 Synthesis of interaction and mutual feedback across/between the carbon cycle, the ocean circulation and the land processes

The three first distinct themes studied in MONARCH-A, notably: - changes in terrestrial carbon and water fluxes; - changes in sea level and ocean circulation; - and changes in marine carbon cycle are indeed strongly interrelated and interacting as part of the complex multidisciplinary functionality of the Earth system as suggested in Figure 67. As such several of the Essential Climate Variables (ECVs) display seasonal and interannual variations that are mutually influenced (e.g. reinforced or damped) at a broad range of spatial scales. In the following some of the interdisciplinary processes and their mutual feedbacks connected with these ECVs investigated in the MONARCH-A project are further discussed according to the water cycle, sea level and marine carbon cycle.

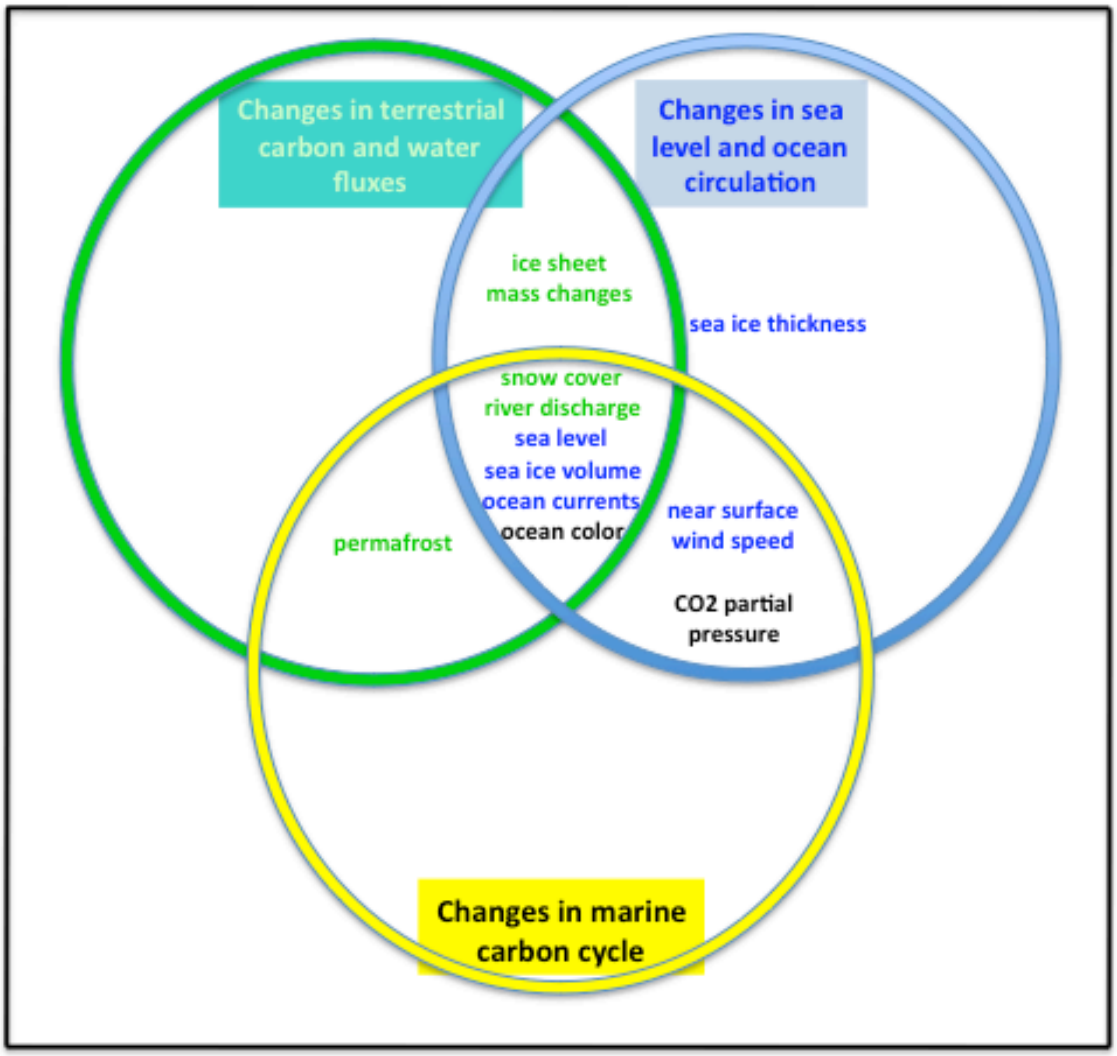

Figure 67. *Schematic illustration of the intersections and interactions between the three major research themes addressed in the MONARCH-A project. The location of the ECVs inside the different intersections of the three themes signals their cross-disciplinary interactions and feedback.*

High latitude and Arctic regional water cycle: This encapsulates processes and dynamics in the biosphere, the cryosphere, the atmosphere (not addressed in this MONARCH-A project) and the hydrosphere as well as complementary and mutual cross–sphere interactions and feedbacks. Regarding the two former spheres the changes in snow cover and snow water equivalent, river discharges, permafrost extent and ice sheet and glacier elevations are all features of the water cycle with its distinct seasonal to annual variability. Moreover, for the hydrosphere the gradual retreat in sea ice concentration, extent and volume indirectly influence the water cycle through changes in the ocean-atmosphere fluxes (e.g. evaporation and sensible heat) that, in turn, might enhance the regional precipitation. Monitoring and prediction of the water cycle at high latitude and Arctic region may seem simple but, in contrary, it is extremely challenging as weak and strong changes, interactions and mutual feedback between the ECVs occur over a broad range of temporal and spatial scales that is not properly incorporated into the design and operation of the observing system. In result, we lack process understanding. Combined with model deficiencies in spatial resolution and reliable parameterizations the predictive skill of the water cycle is also rather limited.

The sea level budget: The increasing area of open water in the Arctic Ocean and the sub Arctic-seas in the presence of a decline in the sea ice extent alter the upper layer hydrographic conditions and hence the steric height contribution to sea level change. Moreover, changes in the mean and variable freshwater runoff from the biopshere and the cryosphere (including meltwater from permafrost areas) lead to a freshening of the ocean surface layer and a sea level change. The presence of sea ice further complicates the retrieval of the mean sea surface from satellite altimetry. In particular thin ice with equivalent ice freeboard height ranging up to about 10 cm poses a great challenge to be precisely measured. In view of the rather tiny signal of the mean global annual trend in sea level rise of about 2-3 mm/year the accuracy of the correction of the altimeter surface height measurement to the sea ice freeboard signal is therefore highly demanding. Lack of adequate validation limits the ability to quantify the accuracy of this correction and hence the uncertainty in the mean sea surface determination in the permanent sea ice covered interior Arctic Ocean. Changes in the transport of heat with the ocean currents from the North Atlantic to the Arctic Ocean may also change the steric height contribution to changes in the mean regional sea level. Finally, the mass loss associated with melting ice sheets also lead to glacial isostatic adjustment (GIA) that must be corrected before the corresponding regional seasonal to decadal sea level budget can be accurately closed.

The marine carbon cycle. The high latitude seasonal land vegetation cycle (influenced by changes in the snow cover and SWE) influences the atmospheric CO_2 concentration and its seasonal cycle, while the influence of the ocean seasonality on the atmospheric CO_2 record is fairly small in high latitude and Arctic waters. The atmospheric CO2 record at Point Barrow, Alaska, USA (Keeling et al., 2008) shows a fairly strong seasonal amplitude slowly increasing (e.g., Wu and Lynch, 2000) with time pointing towards a gradual intensifying of the spring-growth/autumn-degradation pattern of the terrestrial biomass (supporting evidence for an increase in CO_2 fertilization for land plants). This pattern could lead to a (very slight) bias towards reduced oceanic uptake of CO_2 during the ice free months (when also the atmospheric CO_2 is minimal). However, this effect will probably be smaller than other errors in present ocean biogeochemical circulation models although it could indicate that ocean biogeochemistry in the high latitude and Arctic Ocean may be less affected by rising CO_2

(apart from the severe impact due to ocean acidification). Further investigations are needed to verify this hypothesis.

The river discharges and their concentration of carbon, nutrients and other dissolved inorganic and organic matter (e.g. alkalinity) also modify the biological carbon pump and the inorganic solubility pump. If more nutrients than carbon are released, then under assumption of stable "Redfield ratios", a net drawdown of the CO_2 partial pressure could be the consequence and vice versa. At present, the oceanic data base of nutrients and carbon is not sufficient to reveal such potential modifications. The remotely sensed primary production record (through ocean color and chlorophyll estimates) may allow documenting such changes along the coastal zones and continental margin over time provided the separation of chlorophyll from dissolved organic matter can be obtained with satisfactory accuracy. Overall, a quantification of the respective forcing and feedback mechanisms and their change over time are not yet feasible largely due to lack of sustainable observations providing long time series.

For the linkage between ocean physical processes and the marine carbon cycle, a number of additional processes need to be considered. Phytoplankton blooms, specifically under development of more permanently ice-free areas in the Arctic could potentially accelerate warming and hence melting processes if the biomass in the euphotic layer of the ocean indeed would absorb radiation and this contribute to warming. Changes in temperature and salinity (due to both advection and convection) also influence directly the solubility of CO_2 (worse under warming) and buffer capacity (better under warming). These partially compensating effects can in principle be fairly well established (e.g. Tjiputra et al., 2010a), if sufficient time series data are available. However, the combined action of reducing sea ice coverage, surface warming, potential changes in freshwater supply from land, and changing inflows from the Atlantic (Barents Sea, Fram Strait) and Pacific (Bering Strait) and related synergistic effects on ocean carbon cycling are difficult to predict. In order to establish respective changes unambiguously from observations, a seasonal coverage of sea surface pCO_2 measurements in concert with remotely sensed primary production rates would be needed. It is not yet established what the net effect of sea ice growth and melting is on ocean carbon cycling, potentially sea ice formation can result in out-gassing of CO_2 from the ocean (Miller et al., 2011). Whether this temporary release is compensated for by other effects during the seasonal cycle is not established, although it appears that the primary production in the Arctic shelf seas have increased as a result of decline in the sea ice extent (Petrenko et al., 2013) potentially favoring a stronger biological pump.

Implication for the Observing System. The MONARCH-A project has revealed deficiency in the in-situ observing system for the high latitude and Arctic region. In combination with multidisciplinary satellite observations its therefore necessary to develop and sustain the system in order to advance the process understanding, cross-disciplinary interaction and mutual feedbacks. Only via the implementation and operation of a regionally and globally balanced observing system will it be possible to consistently monitor the state and variability of the Earth System.

Terrestrial carbon and water fluxes: Reliable estimate of the seasonal and decadal changes in snow water equivalent (SEW) relies on accurate observations of the ***snow cover*** extent, snow depth and

snow density. Whereas satellites are giving very good observations of the snow cover measurements of snow thickness and density are scattered and irregular in time. As such the accuracy of the estimation of the SWE can be questioned. The in-situ observing capacity should therefore improve in order to have more precise figures for the SWE and hence its contribution to ***river discharges***. Likewise is the need to secure sustainable in-situ observations of ***permafrost*** and its contribution to river discharges at adequate temporal and spatial resolution. Proper estimation of the meltwater fluxes from the Greenland ***Ice Sheet*** to the Arctic Ocean is also challenging as in-situ observations are limited and we can only rely on coarse resolution observations of mass changes from satellite. Another major challenge regarding river discharges is also the fluxes of carbon, nutrients, dissolved inorganic and organic matter, and other natural and man-made substances to the shelf seas. As long as the in-situ observations are insufficient we are faced with a major challenge to properly characterize the biogeochemical state and its interaction with the physical state of the ocean. This, in turn, implies knowledge gaps both regarding the marine carbon cycle and the marine ecosystem functionality.

Sea level and ocean circulation: ***Sea ice thickness*** and freeboard height needs to be precisely measured from in-situ observation system with sufficient spatial coverage across all seasons to complement and validate satellite observations (Cryosat, SMOS) as well as forced coupled ocean-sea ice models and coupled climate models. This will yield improved correction of the sea ice freeboard signal for reconstruction of the mean sea surface and ***sea level*** change with known uncertainties from altimetry as well as more reliable estimate of changes in the ***sea ice volume*** in both the Arctic Ocean and its export through the Fram Strait. The in-situ observations should also ensure measurements of the sea ice deformation field occurring under different atmospheric conditions and at different seasons in order to gain better quantitative understanding of the mechanical behavior of sea ice and, in turn, more reliable parameterization of sea ice rheology in models. Advances in the knowledge of the state and variability of the hydrographic conditions and ***ocean currents*** in the Arctic Ocean at seasonal time scales and mesoscale spatial resolution are moreover needed to quantify the thermohaline circulation and the Atlantic Meriodional Overturning Circulation (AMOC) with known uncertainties as well as to validate forced and coupled models and improve reanalyses.

Marine carbon cycle: The effect of increased absorption of CO_2 by the ocean with the consequence of a chemical state shift towards lower pH and lower carbonate saturation ("ocean acidification") can have short and longer-term consequences for marine ecosystems (e.g., Riebesell et al., 2007; Müller et al., 2010; Büdenbender et al., 2012), though also acclimation effects have been recorded (e.g., Form and Riebesell, 2012). Sustainable monitoring of the ocean carbon cycle in the Arctic surface layer is therefore essential. Next to observations of ***surface ocean pCO_2***, ***ocean color*** and primary production of organic carbon, and suspended CaCO3 material (as done in MONARCH-A), the measurement of other state variables would be needed (such as the carbonate ion concentration). Moreover it would be desirable to have time series of calcite and aragonite production available. A further issue is the potentially advanced released of CH4 from gas hydrates around the Arctic Ocean continental margin. The stability of these hydrates is determined among other factors by the ocean temperature and the ambient pressure. A warming of seawater could potentially release the methane stored in the hydrates (Biastoch et al., 2011) and hence contribute to ocean acidification. Sustainable observations of methane release to the ocean is therefore urgently needed and should

be complemented to include systematic measurement of ***permafrost*** change with sufficient spatial coverage.

In order to best possible predict changes in high latitude seawater pH and carbonate ion concentration, respective benchmark values from observations for marine carbon cycling are highly desirable. For this purpose, total dissolved inorganic carbon (DIC) and alkalinity (Alk) would be needed. Biogeochemical tracers such as DIC, Alk, nutrients, and oxygen can also be used to validate flow fields of the ocean and can provide valuable additional constraints for oceanic physical state estimation. However, due to the overall not very high biological production rates, a statistical significant Alk signal in the Arctic ocean would probably require several decades of measurements in order to show a large scale increase in Alk (due to less uptake of CO_3^{2-} ions by organisms), whereas a corresponding signal in the tropical Pacific may be a better early warning indicator (Ilyina et al., 2009).

6. References

Arino, O., S. Casadio, and D. Serpe (2012), Global night-time fire season timing and fire count trends using the ATSR instrument series, *Remote Sens Environ*, *116*, 226-238, doi: 10.1016/j.rse.2011.05.025.

Chang, A. T. C., Foster, J. L., & Hall, D. K. (1987). Nimbus-7 SMMR derived global snow cover parameters. *Annals of Glaciology*, 9,39 44.

Derksen, C., and R. Brown (2012), Spring snow cover extent reductions in the 2008-2012 period exceeding climate model projections, *Geophys Res Lett*, *39*, doi: Artn L19504, doi: 10.1029/2012gl053387.

Giglio, L., J. T. Randerson, G. R. van der Werf, P. S. Kasibhatla, G. J. Collatz, D. C. Morton, and R. S. DeFries (2010), Assessing variability and long-term trends in burned area by merging multiple satellite fire products, *Biogeosciences*, *7*(3), 1171-1186.

Kantzas, E.P., M. Lomas & S. Quegan (2013), Fire at high latitudes: data-model comparisons and their consequences, *Global Biogeochem. Cycles*, under review.

Kasischke, E. S., N. L. Christensen, and B. J. Stocks (1995), Fire, Global Warming, and the Carbon Balance of Boreal Forests, *Ecol Appl*, *5*(2), 437-451.

Krezek-Hanes, C. C., F. Ahern, A. Cantin, and M. D. Flannigan (2011), *Trends in large fires in Canada, 1959-2007*, Canadian Councils of Resource Ministers, Ottawa.

Picard G, Quegan S, Delbart N, Lomas MR, Woodward FI & Le Toan T (2005), Bud-burst modelling in Siberia and its impact on quantification of the carbon budget, *Global Change Biology* **12**, 2164-2176.

Stocks, B. J., et al. (1998), Climate change and forest fire potential in Russian and Canadian boreal forests, *Climatic Change*, *38*(1), 1-13.

Takala, M., K. Luojus, J. Pulliainen, C. Derksen, J. Lemmetyinen, J. P. Karna, J. Koskinen, and B. Bojkov (2011), Estimating northern hemisphere snow water equivalent for climate research through assimilation of space-borne radiometer data and ground-based measurements, *Remote Sens Environ*, *115*(12), 3517-3529, doi: 10.1016/j.rse.2011.08.014.

Aagaard, K., J.H. Swift, and E.C. Carmack (1985): Thermohaline circulation in the Arctic Mediterranean seas, *Journal of Geophysical Research – Oceans*, 90(NC3), 4833-4846.

ACIA (2005): *Arctic Climate Impact Assessment,* Cambridge University Press, 1042 pp.

Arino, O., S. Casadio, and D. Serpe (2012), Global night-time fire season timing and fire count trends using the ATSR instrument series, *Remote Sens Environ*, *116*, 226-238, doi: 10.1016/j.rse.2011.05.025.

Assmann, K.M., M. Bentsen, J. Segschneider, and C. Heinze (2010): An isopycnic ocean carbon cycle model, *Geoscientific Model Development,* 3, 143–167, www.geosci-model-dev.net/3/143/2010/

Barletta V.R., L. Sandberg Sørensen and R. Forsberg (2012), "Variability of mass changes at basin scale for Greenland and Antarctica", The Cryosphere Discuss., 6, 3397-3446, doi: 10.5194/tcd-6-3397-2012

Behrenfeld, M. and P. Falkowski (1997): *Photosynthetic rates derived from satellite-based chlorophyll concentration,* Limnol. Oceanogr. 42(1): 1-20.

Behrenfeld, M., E. Boss, D. A. Siegel, and M. S. Donald (2005): *Carbon-based ocean productivity and phytoplankton physiology from space*, Global Biogeochemical Cycles. 19(GB1006), doi: 10.1029/2004GB002299.

Bentamy A, Girard-Ardhuin F, Maksimovich E, Piollé JF, Chapron B, 2013. D2.5.3: Assessment of using high resolution satellite based wind field observations, Monarch-A deliverable no. 2.5.3

Biastoch, A., T. Treude, L. H. Rüpke, U. Riebesell, C. Roth, E.B. Burwicz, W. Park, M. Latif, C.W. Böning, G. Madec, and K. Wallmann (2011): Rising Arctic Ocean temperatures cause gas hydrate destabilization and ocean acidification, *Geophys. Res. Letters*, 38, L08602.

Broecker, W.S., and T.-H. Peng (1982): *Tracers in the sea*, ELDGIO Press, Lamont-Doherty Geological Observatory, Columbia University, Palisades, New York, 690 p.

Büdenbender, J., U. Riebesell, and A. Form (2012): Calcification of the Arctic coralline red algae *Lithothamnion glaciale* in response to elevated CO2, *Mar. Ecol. Progr. Ser.,* 441, 79-87.

Caldeira, K., and M.E. Wickett (2003): Anthropogenic carbon and ocean pH, *Nature*, 425, p. 365.

Chang, A. T. C., Foster, J. L., & Hall, D. K. (1987). Nimbus-7 SMMR derived global snow cover parameters. *Annals of Glaciology*, 9,39 44.

Ciais, P., A.J. Dolman, R. Dargaville, L. Barrie, A. Bombelli, J. Butler, P. Canadell, P., and T. Moriyama (2010): Geo Carbon Strategy, Geo Secretariat Geneva,/FAO, Rome, 48 pp.

Comiso, J. C., 2002: A rapidly declining Arctic perennial ice cover. Geophys. Res. Lett., 29, 1956, doi:10.1029/2002GL015650.

Denman, K.L., G. Brasseur, A. Chidthaisong, P. Ciais, P.M. Cox, R.E. Dickinson, D. Hauglustaine, C. Heinze, E. Holland, D. Jacob, U. Lohmann, S. Ramachandran, P.L. da Silva Dias, S.C. Wofsy, and X. Zhang (2007): Couplings Between Changes in the Climate System and Biogeochemistry. In: *Climate Change 2007: The Physical Science Basis. Contribution of Working Group I to the Fourth Assessment Report of the Intergovernmental Panel on Climate Change* [Solomon, S., D. Qin, M. Manning, Z. Chen, M. Marquis, K.B. Averyt, M.Tignor und H.L. Miller (eds.)]. Cambridge University Press, Cambridge, United Kingdom und New York, NY, USA, p. 499-587.

Derksen, C., and R. Brown (2012), Spring snow cover extent reductions in the 2008-2012 period exceeding climate model projections, *Geophys Res Lett*, *39*, doi: Artn L19504, doi: 10.1029/2012gl053387.

Doble, M. J., Skourup, H., Wadhams, P., and Geiger, C. (2011). The relation between sea ice surface elevation and draft: Results from high-resolution mapping by co-incident AUV sonar and airborne scanning laser. JGR Oceans, 2011JC007076, in press

Form. A.U., and U. Riebesell (2012): Acclimation to ocean acidification during long-term CO2 exposure in the cold-water coral *Lophelia pertusa, Global Change Biology,* 18, 843–853.

Forsberg, R, V. R. Barletta, L. S. Sørensen: **Monarch-A D2.3.3** Gridded time series of GRACE-based Greenland mass changes, September 2011

Friedlingstein, P., P. Cox, R. Betts, L. Bopp,W. van Bloh, V. Brovkin, P. Cadule, S. Doney,M. Eby, I. Fung, G. Bala, J. John, C. Jones, F. Joos, T. Kato, M. Kawamiya,W. Knorr, K. Lindsay, D. Matthews, T. raddatz, P. Tayner, C. Reick, E. Roeckner, K.-G. Schnitzler, R. Schnur, K. Strassmann, A.J. Weaver, C. Yoshikawa, and N. Zeng (2006): ClimateCarbon Cycle Feedback Analysis: Results from the C4MIP Model Intercomparison, *J. Climate*, 19, 3337-3353.

Giglio, L., J. T. Randerson, G. R. van der Werf, P. S. Kasibhatla, G. J. Collatz, D. C. Morton, and R. S. DeFries (2010), Assessing variability and long-term trends in burned area by merging multiple satellite fire products, *Biogeosciences*, *7*(3), 1171-1186.

GLOBALVIEW-CO2 (2011): Cooperative Atmospheric Data Integration Project - Carbon Dioxide. CD-ROM, NOAA ESRL, Boulder, Colorado [Also available on Internet via anonymous FTP to ftp.cmdl.noaa.gov, Path: ccg/co2/GLOBALVIEW].

Gattuso, J.-P., and L. Hansson, eds. (2011): *Ocean Acidification*, Oxford University Press, 326 p.

Gregory JM, Stott PA, Cresswell DJ, Rayner NA, Gordon C, Sexton DMH (2002) Recent and futurechanges in arctic sea ice simulated by the HadCM3 AOGCM. Geophys Res Lett 29(24):28–28–4, DOI10.1029/2001GL014575

Guinotte, J.M., and V.J. Fabry (2008): Ocean Acidification and Its Potential Effects on Marine Ecosystems, *Annals of the New York Academy of Sciences,* 1134, 320–342.

Hakkinen, S., Proshutinsky, A., Ashik, I., 2008. Sea ice drift in the arctic since the 1950s. Geophysical Research Letters 35, L19704+. URL http://dx.doi.org/10.1029/2008GL034791

Heinze, C., E. Maier-Reimer, and K. Winn (1991): Glacial pCO2 reduction by the World Ocean - experiments with the Hamburg Carbon Cycle Model, *Paleoceanography*, 6, 395-430.

Henry, O, P. Prandi, W. Llovel, A. Cazenave, S. Jevrejeva, D. Stammer, B. Meyssignac, N. Koldunov, 2012, Tide gauge-based sea level variations since 1950 along the Norwegian and Russian coasts of the Arctic Ocean; Contribution of the steric component, Journal of Geophysical Research, vol.117, c06023, doi:10.1029/2011JC007706, 2012.

Holmes, M.A., J.W. McClelland, B.J. Peterson, S.E. Tank, E. Bulygina, T.I. Eglinton, V.V. Gordeev,

Gurtovaya, T.J., P.A. Raymond, D.J. Repeta, R. Staples, R.G. Striegl, A.V. Zhulidov, and S.A. Zimov (2012): Seasonal and Annual Fluxes of Nutrients and Organic Matter from Large Rivers to the Arctic Ocean and Surrounding Seas, *Estuaries and Coasts*, 35, 369–382.

Ilyina, T., R.E. Zeebe, E. Maier-Reimer, and C. Heinze (2009): Early detection of ocean acidification effects on marine calcification, *Global Biogeochemical Cycles*, 23, GB1008, 11 pp.

IPCC (2007): *Climate Change 2007: The Physical Science Basis. Contribution of Working Group I to the Fourth Assessment Report of the Intergovernmental Panel on Climate Change* [Solomon, S., D. Qin, M. Manning, Z. Chen, M. Marquis, K.B. Averyt, M. Tignor and H.L. Miller (eds.)]. Cambridge University Press, Cambridge, United Kingdom and New York, NY, USA, 996 pp.

Ivanov Vladimir V., Vladimir A. Alexeev, Irina Repina, Nikolay V. Koldunov, and Alexander Smirnov, "Tracing Atlantic Water Signature in the Arctic Sea Ice Cover East of Svalbard," Advances in Meteorology, vol. 2012, Article ID 201818, 11 pages, 2012. doi:10.1155/2012/201818

Ivanov V. V., V. Alexeev, T. Alexeeva, N. V. Koldunov, I. Repina, A. Smirnov, "Arctic sea ice becoming seasonal?", review paper, accepted by *Issledovanie Zemli iz Kosmosa*, 2013 (in Russian).

Jeansson, E., A. Olsen, T. Eldevik, I. Skjelvan, A.M. Omar, S.K. Lauvset, J. E. Ø. Nilsen, R.G.J. Bellerby, T. Johannessen, and E. Falck (2011): The Nordic Seas carbon budget: Sources, sinks, and uncertainties, *Global Biogeochemical Cycles*, 25, GB4010.

Johannessen, J.A., R. P. Raj, J. E. Ø. Nilsen, T. Pripp, P. Knudsen, F. Counillon, D. Stammer, L. Bertino, O.B. Andersen, N. Serra and N. Koldunov, (2013) Toward improved estimation of the dynamic topography and ocean circulation in the high latitude and Arctic Ocean, Submitted to Earth´s Hydrological Cycle, Springer .

Kaleschke, L., Tian-Kunze, X., Maaß, N., Mäkynen, M., Drusch, M., Mar. 2012. Sea ice thickness retrieval from SMOS brightness temperatures during the arctic freeze-up period. Geophysical Research Letters 39 (5). URL http://dx.doi.org/10.1029/2012GL050916

Kantzas, E.P., M. Lomas & S. Quegan (2013), Fire at high latitudes: data-model comparisons and their consequences, *Global Biogeochem. Cycles*, under review.

Kasischke, E. S., N. L. Christensen, and B. J. Stocks (1995), Fire, Global Warming, and the Carbon Balance of Boreal Forests, *Ecol Appl*, *5*(2), 437-451.

Keeling, R.F., S.C. Piper, A.F. Bollenbacher and J.S. Walker (2008): Atmospheric CO2 records from sites in the SIO air sampling network. In *Trends: A Compendium of Data on Global Change*, Carbon Dioxide Information Analysis Center, Oak Ridge National Laboratory, U.S. Department of Energy, Oak Ridge, Tenn., U.S.A., http://cdiac.ornl.gov/trends/co2/sio-bar.html.

Khvorostovsky K. Merging and analysis of elevation time series over Greenland ice sheet from satellite radar altimetry. 2012, *IEEE Trans. Geosc. Remote Sens*., vol., 50, 1.

Khvorostovsky, K, **Monarch-A D2.3.1** Time series of satellite altimetry height changes of the Greenland ice sheet, year since 1992 expressed as height change grids, September 2011

Korosov, A., D. Pozdnyakov, A. Folkestad, L. Pettersson, K. Sorensen, and R. Shuchman (2009): *Semi-empirical Algorithm for the Retrieval of Ecology-relevant Water Constituents in Various Aquatic Environments*, Algorithms, 2, pp. 470-497. doi:10.3390/a2010470.

Krezek-Hanes, C. C., F. Ahern, A. Cantin, and M. D. Flannigan (2011), *Trends in large fires in Canada, 1959-2007*, Canadian Councils of Resource Ministers, Ottawa.

Kwok R, Rothrock DA (2009) Decline in Arctic sea ice thickness from submarine and ICESat records: 1958–2008. Geophysical Research Letters 36(15):L15,501+, DOI 10.1029/2009GL039035

Kwok, R., Cunningham, G. F., Wensnahan, M., Rigor, I., Zwally, H. J., and Yi, D.: Thinning and volume loss of the Arctic Ocean sea ice cover: 2003–2008, J. Geophys. Res., 114, C07005, doi:10.1029/2009JC005312, 2009.

Laxon, S. W., Giles, K. A., Ridout, A. L., Wingham, D. J., Willatt, R., Cullen, R., Kwok, R., Schweiger, A., Zhang, J., Haas, C., Hendricks, S., Krishfield, R., Kurtz, N., Farrell, S., Davidson, M., Jan. 2013. CryoSat-2 estimates of arctic sea ice thickness and volume. Geophys. Res. Lett., n/a. URL http://dx.doi.org/10.1002/grl.50193

Loeng, H. et al. (2005): Marine Systems, in: *Arctic Climate Impact Assessment*, Cambridge University Press, 454-538.

Lundberg, L., and P.M. Haugan (1996): A Nordic Seas-Arctic Ocean carbon budget from volume flows and inorganic carbon data, *Global Biogeochemical Cycles*, 10, 3, 493-510.

Manizza, M., C. Le Quéré, A.J. Watson, and E.T. Buitenhuis (2005): Bio-optical feedbacks among phytoplankton, upper ocean physics and sea-ice in a global model, *Geophysical Research Letters*, 32, L05603, doi:10.1029/2004GL020778, 4 p.

Marra, J., C. Ho, C. Trees (2003): *An Alternative Algorithm for the Calculation of Primary Productivity from Remote Sensing Data,* LDEO Technical Report, #LDEO-2003-1, National Aeronautics and Space Administration Publ. 27 p.

Maslanik, J. A., C. Fowler, J. Stroeve, S. Drobot, J. Zwally, D. Yi, and W. Emery (2007), A younger, thinner Arctic ice cover: Increased potential for rapid, extensive sea-ice loss, Geophys. Res. Lett., 34, L24501, doi:10.1029/2007GL032043.

Maslanik J, Stroeve 615 J, Fowler C, EmeryW(2011) Distribution and trends in arctic sea ice age through spring 2011. Geophysical Research Letters 38(13):L13,502+, DOI 10.1029/2011GL047735

McPhee, M. G., Proshutinsky, A., Morison, J. H., Steele, M., Alkire, M. B., May 2009. Rapid change in freshwater content of the arctic ocean. Geophysical Research Letters 36 (10), L10602+. URL http://dx.doi.org/10.1029/2009GL037525

Meier, W. N., Stroeve, J., Barrett, A., and Fetterer, F.: A simple approach to providing a more consistent Arctic sea ice extent time series from the 1950s to present, The Cryosphere, 6, 1359-1368, doi:10.5194/tc-6-1359-2012, 2012.

Meyssignac, B., W. Llovel, M. Becker and A. Cazenave, An assessment of two dimensional past sea level reconstructions over 1950-2009 based on tide gauge data and different input sea level grids, Surveys in Geophysics, vol.33, p.945-972, doi:10.1007/s10712-011-9171-x, 2012.

Mienert, J., M. Vanneste, H. Haflidason, and S. Bünz (2010): Norwegian margin outer shelf cracking: a consequence of climate-induced gas hydrate dissociation? *Int. J. Earth. Sci. (Geol Rundsch),* 99 (Suppl 1): S207–S225.

Mikaloff Fletcher, S.E., N. Gruber, A.R. Jacobson, S.C. Doney, S. Dutkiewicz, M. Gerber, M. Follows, F. Joos, K. Lindsay, D. Menemenlis, A. Mouchet, S.A. Müller, and J. L. Sarmiento (2006): Inverse estimates of

anthropogenic CO2 uptake, transport, and storage by the ocean, *Global Biogeochemical Cycles*, 20, GB2002.

Milkov, A.V. (2004): Global estimates of hydrate-bound gas in marine sediments: how much is really out there? *Earth-Science Reviews*, 66, 183–197.

Miller, L.A., G. Carnat, B.G.T. Else, N. Sutherland, and T.N. Papakyriakou (2011): Carbonate system evolution at the Arctic Ocean surface during autumn freeze-up, *J. Geophys. Res.,* 116, C00G04.

Morison, J., Kwok, R., Peralta-Ferriz, C., Alkire, M., Rigor, I., Andersen, R., Steele, M., Jan. 2012. Changing arctic ocean freshwater pathways. Nature 481 (7379), 66-70. URL http://dx.doi.org/10.1038/nature10705

Müller, M.N., K.G. Schulz, and U. Riebesell (2010): Effects of long-term high CO2 exposure on two species of coccolithophores, Biogeosciences, 7(3), 1109-1116.

Nghiem, S. V., I. G. Rigor, D. K. Perovich, P. Clemente-Colón, J. W. Weatherly, and G. Neumann (2007), Rapid reduction of Arctic perennial sea ice, Geophys. Res. Lett., 34, L19504, doi:10.1029/2007GL031138.

Nilsen, J. E. Ø., H. Hatun, K. A. Mork, and H. Valdimarsson (2008), The NISE Data Set. *Technical Report 08-01*, Faroese Fisheries Laboratory, Box 3051, Torshavn, Faroe Islands.

Notz D, Marotzke J (2012) Observations reveal external driver for arctic sea-ice retreat. Geophysical Research Letters 39(8):L08,502+, DOI 10.1029/2012GL051094

Nøst, O. A., and P. E. Isachsen (2003), The large-scale time-mean ocean circulation in the Nordic Seas and Arctic Ocean estimated from simplified dynamics, J. Mar. Res., 61, 175– 210

O'Connor, F.M., O. Boucher, N. Gedney, C.D. Jones, G.A. Folberth, R. Coppell, P. Friedlingstein, W.J. Collins, J. Chappellaz, J. Ridley, and C.E. Johnson (2010) Possible role of wetlands, permafrost, and methane hydrates in the methane cycle under future climate change, a review, *Reviews of Geophysics*, 48, RG4005, 1-33.

Orr, J.C., V.J. Fabry, O. Aumont, L. Bopp, S.C. Doney, R.A. Feely, A. Gnanadesikan, N. Gruber, A. Ishida, F. Joos, R.M. Key, K. Lindsay, E.Maier-Reimer, R.Matear, P. Monfray, A. Mouchet, R.G. Najjar, G.-K. Plattner, K.B. Rodgers, C.L. Sabine, J.L. Sarmiento, R. Schlitzer, R.D. Slater, I.J. Totterdell, M.-F. Weirig, Y. Yamanaka, and A. Yool (2005): Anthropogenic ocean acidification over the twenty-first century and its impact on calcifying organisms, Nature, 437, 681-686.

Petrenko, D., Zabolotskikh, E., Pozdnyakov, D., and Karlin, L. (2012): Assessment of the adequacy of algorithms of the retrieval of primary production in the Arctic from satellite ocean colour data, *Scientific transactions of the Russian Hydrometeorological University*, 24, 137-162.

Petrenko, D., Pozdnyakov, D., Johannessen, J., Counillon, F., and Sychev, V. (2013): Satellite derived multi-year trend in primary production in the Arctic Ocean, *International Journal of Remote Sensing*, 3903-3937, doi:10.1080/01431161.2012.762698.

Petrenko, D., Zabolotsikh, E., Pozdnyakov, D., Counillon, F., and Karlin, L. (2013): Interannual variations of and trend in the production of inorganic carbon by coccolithophores in the Arctic during 2002-2010 as observed from space, *Earth research from space*, in press.

Pfeil, B., A. Olsen, D.C.E. Bakker et al. (2012): *A uniform, quality controlled, Surface Ocean CO2 Atlas (SOCAT),* submitted to Earth System Science Data (see *Earth Syst. Sci. Data Discuss*., 5, 735-780.

Picard G, Quegan S, Delbart N, Lomas MR, Woodward FI & Le Toan T (2005), Bud-burst modelling in Siberia and its impact on quantification of the carbon budget, *Global Change Biology* **12**, 2164-2176.

Prandi, P, M. Ablain, A. Cazenave and N. Picot, 2012, A new estimation of mean sea level in the Arctic Ocean from satellite altimetry, Marine Geodesy, vol.35, p61-81, doi:10.1080/01490419.2012.718222, 2012.

Proshutinsky, A., Krishfield, R., Timmermans, M.-L., Toole, J., Carmack, E., McLaughlin, F., Williams, W. J., Zimmermann, S., Itoh, M., Shimada, K., Jun. 2009. Beaufort gyre freshwater reservoir: State and

variability from observations. Journal of Geophysical Research 114 (C1), C00A10+. URL http://dx.doi.org/10.1029/2008JC005104

Raupach, M.R., G. Marland, P. Ciais, C. Le Quéré, J.G. Canadell, G. Klepper, C.B. Field (2007): Global and regional drivers of accelerating CO2 emissions, *Proceedings of the National Academy of Sciences of the United States of America,* 104(24), 10288-10293.

Raven, J., K. Caldeira, H. Elderfield, O. Hoegh-Guldberg, P. Liss, U. Riebesell, J. Shepherd, C. Turley, A. Watson, R. Heap, R. Banes, and R. Quinn (2005): Ocean acidification due to increasing atmospheric carbon dioxide Policy document 12/05, The Royal Society, London, ISBN 0 85403 617 2, 60 pp.

Riebesell, U., K.G. Schulz, R.G.J. Bellerby, M. Botros, P. Fritsche, M. Meyerhöfer, C. Neill, G. Nondal, A. Oschlies, J.Wohlers, and E. Zöllner (2007): Enhanced biological carbon consumption in a high CO2 ocean, *Nature*, 450(7169), 545-548.

Richter, K., J. E. Ø. Nilsen and H. Drange (2012), Contributions to sea level variability along the Norwegian coast for 1960–2010, J. Geophys. Res. 117, C05038, doi:10.1029/2011JC007826

Richter, K., R. Riva, and H. Drange (2013), Impact of self-attraction and loading effects induced by shelf mass loading on projected regional seal level rise, Geophys. Res. Lett. 40, doi:10.1002/grl.50265

Ruhl, H.A., M. André, L. Beranzoli , M.N. Çağtay, A. Colaço, M. Cannat, J.J. Dañobeitia, P. Favali, L. Géli, M. Gillooly, J. Greinert, P.O.J. Hall, R. Huber, J. Karstensen, R.S. Lampitt, K.E. Larkin, V. Lykousis, J. Mienert, J.M. Miranda, R. Person, I.G. Priede, I. Puillat, L. Thomsen, C. Waldmann (2011): Societal need for improved understanding of climate change, anthropogenic impacts, and geo-hazard warning drive development of ocean observatories in European Seas, *Progress in Oceanography*, 91, 1–33.

Sabine, C.L., R.A. Feely, N. Gruber, R.M. Kee, K. Lee, J.L. Bullister, R. Wanninkhof, C.S. Wong, D.W.R. Wallace, B. Tilbrook, F.J. Millero, T.-H. Peng, A. Kozyr, T. Ono, and A. Ríos (2004): The oceanic sink for anthropogenic CO2, *Science*, 305, 367-371.

Sarmiento, J.L., and N. Gruber (2006): *Ocean biogeochemical dynamics*, Princeton University Press, USA, 503 pp.

Skourup, H. (2010). A study of Arctic sea ice freeboard heights, gravity anomalies and dynamic topography from ICESat measurements. PhD Thesis, University of Copenhagen

Skourup, H, I. Einarsson, L. S. Sørensen, R. Forsberg, L. Stenseng, S. Hendricks, V. Helm, M. Davidson: ESA CryoVEx 2011 airborne campaign for CryoSat-2 calibration and validation. Oral presentation at American Geophysical Union (AGU) fall meeting, San Francisco, California, USA. December 5-9, 2011

Spreen, G., Kwok, R., Menemenlis, D., Oct. 2011. Trends in arctic sea ice drift and role of wind forcing: 1992–2009. Geophysical Research Letters 38 (19), L19501+. URL http://dx.doi.org/10.1029/2011GL048970

Steinacher, M., F. Joos, T.L. Frölicher, L. Bopp, P. Cadule, V. Cocco, S.C. Doney, M. Gehlen, K. Lindsay, J.K.Moore, B. Schneider, and J. Segschneider (2010): Projected 21st century decrease in marine productivity: a multi-model analysis, *Biogeosciences,* 7, 979-1005.

Steinacher, M., F. Joos, T.L. Frölicher, G.-K. Plattner, and S.C. Doney (2009): Imminent ocean acidification in the Arctic projected with the NCAR global coupled carbon cycle-climate model, *Biogeosciences*, 6, 515-533

Stocks, B. J., et al. (1998), Climate change and forest fire potential in Russian and Canadian boreal forests, *Climatic Change*, *38*(1), 1-13.

Søiland, H., M. D. Prater, and T. Rossby (2008), Rigid topographic control of currents in the Nordic Seas, Geophys. Res. Lett., 35, L18607, doi:10.1029/2008GL034846Vihma, T., Tisler, P., Uotila, P., Jan. 2012. Atmospheric forcing on the drift of arctic sea ice in 1989–2009. Geophysical Research Letters 39 (2), L02501+.URL http://dx.doi.org/10.1029/2011GL050118

Sørensen, LS, R. Forsberg, S. B. Simonsen, V. R. Barletta, H. Skourup: Changes of the Greenland Ice Sheet from ICESat, CryoSat and GRACE. Oral presentation at American Geophysical Union (AGU) fall meeting, San Francisco, California, USA. December 5-9, 2011

Sørensen, LS: **Monarch-A D2.3.2** Grid of ICESat height changes, average trend 2003-2008, September 2011

Takahashi, T., S.C. Sutherland, and A. Kozyr (2012): *Global Ocean Surface Water Partial Pressure of CO_2 Database: Measurements Performed During 1957-2011 (Version 2011)*, ORNL/CDIAC-160, NDP-088(V2011), Carbon Dioxide Information Analysis Center, Oak Ridge National Laboratory, U.S. Department of Energy, Oak Ridge, Tennessee, doi: 10.3334/CDIAC/OTG.NDP088(V2011).

Takala, M., K. Luojus, J. Pulliainen, C. Derksen, J. Lemmetyinen, J. P. Karna, J. Koskinen, and B. Bojkov (2011), Estimating northern hemisphere snow water equivalent for climate research through assimilation of space-borne radiometer data and ground-based measurements, *Remote Sens Environ*, *115*(12), 3517-3529, doi: 10.1016/j.rse.2011.08.014Tjiputra, J.F., K. Assmann, M. Bentsen, I. Bethke, O.H. Otterå, C. Sturm, and C. Heinze (2010a): Bergen earth system model (BCM-C): Model description and regional climate-carbon cycle feedbacks assessment, Geoscientific Model Development, 3, 123–141.

Tjiputra, J.F., K. Assmann, and C. Heinze (2010b): Anthropogenic carbon dynamics in the changing ocean, *Ocean Science,* 6(3), 605-614.

Vinnikov KY, Robock A, Stouffer RJ, Walsh JE, Parkinson CL, Cavalieri DJ, Mitchell JFB, Garrett D, Zakharov VF (1999) Global warming and northern hemisphere sea ice extent. Science 286(5446):1934–1937, DOI 10.1126/science.286.5446.1934

Volk, T., and M.I. Hoffert (1985): Ocean carbon pumps: Analysis of relative strengths and efficiencies in ocean-driven atmospheric CO2 changes, in: The Carbon cycle and atmospheric CO2: Natural variations Archean to present, E.T. Sundquist and W.S. Broecker, eds., *Geophysical Monograph* 32, Americam Geophysical Union, 99-110.

Weiss, R.F. (1974): Carbon dioxide in water and seawater: The solubility of a non-ideal gas, *Marine Chemistry*, 2, 203-215.

Wetzel, P., E. Maier-Reimer, M. Botzet, J. Jungclaus, N. Keenlyside, and M. Latif (2006): Effects of ocean biology on the penetrative radiation in a coupled climate model, *Journal of Climate*, 19(16), 3973-3987.

Walsh, J. E., Chapman, W. L., Jan. 2001. 20th-century sea-ice variations from observational data. Annals of Glaciology, 444-448.

Wu, W., and A.H. Lynch (2000): Response of the seasonal carbon cycle in high latitudes to climate anomalies, *J. Geophys. Res.,* 105, NO. D18, 22,897-22,908.

Zachos, J.C., U. Röhl, S.A. Schellenberg, A. Sluijs, D.A. Hodell, D.C. Kelly, E. Thomas, M. Nicolo, I. Raffi, L. J. Lourens, H. McCarren, and D. Kroon (2005): Rapid Acidification of the Ocean During the Paleocene-Eocene Thermal Maximum, *Science*, 308, 1611-1615.

Zakharova E.A., Kouraev A.V., Remy F., Zemtsov V.A., Kirpotin S.N. Seasonal variability of the Western Siberia wetlands from satellite radar altimetry. Journal of Hydrology, 2013 (submitted)

END OF DOCUMENT